

© Copyright 2018

Sarah Schanz

Strath terrace formation: the influence of rock type, climate, and humans

Sarah Schanz

A dissertation

submitted in partial fulfillment of the  
requirements for the degree of

Doctor of Philosophy

University of Washington

2018

Reading Committee:

David Montgomery, Chair

Brian Collins

Alison Duvall

Program Authorized to Offer Degree:

Earth and Space Sciences

University of Washington

**Abstract**

Strath terrace formation: the influence of rock type, climate, and humans

Sarah Schanz

Chair of the Supervisory Committee:  
Dr. David R Montgomery  
Department of Earth and Space Sciences

Strath terraces record cycles of bedrock river incision and planation, and thus reflect how mountainous landscapes evolved in response to changing climate, tectonics, rock type, and other forcings. Previous work has used strath terrace age and geometry to back-calculate uplift rates and sediment production, but tends to focus on long wavelength rock uplift rates or marine isotope stage glaciation and so neglects short term (<10 ky) terrace formation. Here, I investigate the role of rock type and structure, interglacial climate, and human action on terrace formation using field studies and literature reviews with a focus on Holocene terraces. Through field mapping, terrace dating, and geospatial analyses of the Willapa River, WA, and Nehalem River, OR, I find that rock type controls valley width and the potential for terrace formation and preservation. Slaking prone rocks erode rapidly in transport-limited conditions, and durable

bedload from the headwaters can enhance erosion rates such that an extensive 10 ky terrace and an inset 100 yr terrace formed. Following up on the 100 yr terrace, I used field mapping and terrace dating in the central Cascades, WA, to find that strath terrace formation was caused by anthropogenic wood loss ca. 100 yr ago. Loss of wood decreased sediment retention and led to river incision by exposing previously covered bedrock. Anthropogenic terrace formation through wood loss is plausibly a global phenomenon; my literature review reveals terrace formation in the late Holocene is often coincident with deforestation. However, interglacial climate fluctuations coincide with and are also likely to contribute to late Holocene terrace formation, which expands on the prevalent theory that terrace formation in response to climate is dominated by glacial-interglacial cycles. My results show that basins are more sensitive to river incision than previously recognized, and that smaller amplitude climatic forcings, as well as anthropogenic forcings, can have a large impact on the topography of fluvial systems. That impact is sensitive to the internal basin characteristics, such as rock type and structure, that set the potential for erosion and landform preservation.

# TABLE OF CONTENTS

List of Figures .....	iv
List of Tables .....	vi
Chapter 1. Introduction .....	1
1.1 Motivation for work .....	1
1.2 Research questions .....	3
1.3 Outline of dissertation .....	4
Chapter 2. Lithologic controls on valley width and strath terrace formation .....	5
2.1 Abstract .....	5
2.2 Introduction .....	6
2.3 Channel erosion .....	8
2.4 Study areas .....	10
2.4.1 Willapa River .....	10
2.4.2 Nehalem River .....	11
2.5 Methods .....	13
2.5.1 Mapping and incision rates .....	13
2.5.2 Valley width .....	14
2.5.3 Longitudinal stream characteristics .....	15
2.6 Results .....	16
2.6.1 Field mapping and observations .....	16
2.6.2 Terrace ages and incision rates .....	18

2.6.3	Valley width.....	20
2.6.4	Slope-area analysis.....	22
2.7	Discussion.....	23
2.7.1	Strath occupation time .....	23
2.7.2	Lithological control on valley width.....	25
2.8	Conclusions.....	31
Chapter 3. Multiple paths to straths: A review and reassessment of terrace genesis.....		32
3.1	Abstract.....	32
3.2	Introduction.....	33
3.3	Database compilation.....	36
3.4	Results.....	38
3.4.1	Causes of strath terrace formation .....	38
3.4.2	Constraining strath terrace age.....	46
3.4.3	Timing of strath terrace formation.....	49
3.5	Discussion.....	50
3.5.1	Global, regional, and watershed controls on terrace formation .....	50
3.5.2	Resolving potential forcings for late Holocene strath terraces .....	54
3.6	Conclusion .....	63
Chapter 4. Anthropogenic strath terrace formation caused by reduced sediment retention .....		65
4.1	Abstract.....	65
4.2	Introduction.....	66
4.3	Study site.....	69

4.4	Methods.....	70
4.4.1	Geomorphic mapping.....	70
4.4.2	Dating terrace incision .....	72
4.4.3	Mid-valley profile .....	74
4.5	T1 extent and timing .....	74
4.6	Older terraces in the study site.....	78
4.7	Possible climatic drivers of T1 formation.....	79
4.8	Anthropogenic effects on the Teanaway landscape .....	81
	Chapter 5. Concluding thoughts .....	84
	Bibliography .....	86
	Appendix A.....	98
	Appendix B .....	130
	Curriculum vitae .....	131

## LIST OF FIGURES

Figure 2.1. Location of study basins in Washington and Oregon States. ....	11
Figure 2.2. Maps of geology and terraces of the (A) Willapa and North rivers, Washington, and (B) Nehalem River, Oregon. Boxes indicate locations of closer views of terraces located in typical basalt (C, E) and sandstone reaches (D, F). ....	12
Figure 2.3. (A) Weathered siltstone cobble from the Willapa River terrace T4. (B) Siltstone and basalt cobbles in the alluvium. ....	16
Figure 2.4. (A) Talus piles accumulated on a 5-m high bank of the Willapa River, within the marine sedimentary bedrock. (B) Active weathering of subaerially exposed siltstone banks in 0.5-1.0 cm flakes. (C) Small knickpoint on Falls Creek, a tributary to the Willapa River, with basalt bedrock. (D) Basalt bank on Falls Creek. ....	18
Figure 2.5. (A) Calibrated ages for radiocarbon samples collected along the Willapa River. (B) Incision rates calculated from the median calibrated age and strath height above low flow shown against distance upstream of the estuary for the Willapa River. ....	19
Figure 2.6. Valley width and elevation as a function of distance upstream of the estuary for the (A) Nehalem and (B) South Fork Willapa rivers. ....	21
Figure 2.7. Drainage area versus valley width data for the Nehalem, Willapa, and North rivers. ....	22
Figure 2.8. Slope area plots for the (A) North River, (B) Willapa River, (C) Nehalem River, and (D) all rivers. ....	23
Figure 3.1. Illustration of the relationship between the bedrock strath and the terrace, as well as definitions of incision and planation directions. ....	36
Figure 3.2. External forcings enact channel response through a variety of pathways, eventually leading to incision or planation of a strath. ....	38
Figure 3.3. The distribution of external forcings attributed to strath formation. Numbers represent the total number of terraces in our database attributed to each forcing. ....	39
Figure 3.4. The proportion of strath terraces having (light green) and lacking (dark green) independent evidence of the assigned forcing. ....	40



Figure 3.5. Timing of strath incision (red) and planation (blue) in response to global climate ..... 42

Figure 3.6. (A) Age distribution of strath terraces in our database over the last million years. Age is binned by 1 ky. (B) Age distribution for the last 20 ky in 0.5 ky bins and colored by the ascribed forcing..... 50

Figure 3.7. Pathways from global climate forcings to channel response causing strath planation, contrasting (A) the simplified path from Fig. 2 and (B) the pathways emerging once regional and watershed controls are considered. .... 54

Figure 3.8. Locations of late Holocene unassigned strath terraces compared with locations of volcanoes active in the late Holocene and Last Glacial Maximum (LGM) ice extent..55

Figure 3.9. Ages of late Holocene terraces without an attributed forcing compared with deforestation age for each region..... 61

Figure 4.1. Locations of previously studied strath terraces in the Pacific Northwest ..... 67

Figure 4.2. Location map of the Middle and West fork Teanaway Rivers..... 68

Figure 4.3. Geomorphic maps of the West and Middle Fork Teanaway rivers with locations of dendrochronology and radiocarbon samples shown. .... 75

Figure 4.4. Schematic representation of terminology for strath (S) and terrace top (T) surfaces.. ..... 76

Figure 4.5. Mid-valley profile of current channel (black lines) and terrace treads for the Middle and West Fork Teanaway Rivers. .... 77

Figure 4.6. Timing of S1 terrace incision along the Middle and West Fork Teanaway rivers. .... 78

Figure 4.7. Full terrace sequence in the West Fork (upper) and Middle Fork (lower) Teanaway valleys. .... 79

## LIST OF TABLES

Table 2.1. Terrace heights.....	12
Table 2.2. Radiocarbon sample locations and ages .....	14
Table 2.3. Power law regression $w = bA^c$ .....	20
Table 3.4. Strath dating methods .....	47
Table 4.5. Surface height above water.....	71
Table 4.6. Locations and dates of radiocarbon samples .....	73
Table 4.7. Locations and dates of dendrochronology samples .....	73

## ACKNOWLEDGEMENTS

This thesis would not have been possible without the support of my entire committee. Perhaps unwittingly, it was Jim O'Connor who first introduced me to strath terraces on a field trip to the Owyhee River in eastern Oregon; the unknown term jotted down in my field notebook somehow became the basis of a PhD thesis that I could not have foreseen at the time. To Dave Montgomery, thank you for giving me the space to grow into a fully-fledged scientist, and for letting me take the time to pursue my teaching and service interests. Your ability to summon coherent research questions at whim has been an inspiration. To the rest of my committee, Brian Collins, Alison Duvall, and Alex Horner-Devine, thank you for encouraging me to think outside of my own hypothesis, for pushing me towards clear and accurate science writing, and for being amazing scientists and people whose enthusiasm and energy inspires me every day.

So many people before graduate school helped me along my academic path. Thank you to all of my geology professors at Western Washington University who showed me that passion and work are not separate, and invested their time and energy into a shy undergraduate. Special thanks to Bob Mitchell and Doug Clark, who pushed me along towards graduate school and first put it in my head that a PhD was a possibility. To Millie Johnson, whose Honors Calculus class challenged me to actually write about math and who has remained an inspiration in my own teaching.

The community at ESS was instrumental in keeping me sane and on task. To all the staff in ESS: your untiring support and help on problems, no matter how big or small, is greatly appreciated. To my fellow graduate students, especially my cohort and officemates, I don't think

I would have completed this thesis without you believing in me, pushing me forward, and also pushing me out to happy hour pretzels at Schultzie's.

Finally, thank you to my family, without whom this definitely would not have been possible. My parents first gave me the tools and language to begin my journey in geomorphology and have supported me ever since. My brother made sure my ego remained the right size, and was my first friend in Seattle. Trevor, who became family, I am forever grateful for all that you have done to keep me sane and fed. Thank you.

## **DEDICATION**

To all the strong women of my family, but especially,

Nana and Popo

## Chapter 1. INTRODUCTION

### 1.1 MOTIVATION FOR WORK

The style and tempo of landscape evolution is a fundamental question in geomorphology; how are external and internal forcings, such as climate, tectonics, structure, and rock type, incorporated into the landscape? A key mechanism of landscape response is the fluvial network, in which river incision and widening enacts a hillslope response and eventually affects the ridgetops. As rivers widen and incise, they form and abandon terraces whose presence and geometry offer insight to the external and internal forcings that caused landscape change (e.g., Lavé and Avouac, 2001; Limaye and Lamb, 2016).

In order to use terraces to infer how forcings have changed over time, we need to understand how those forcings affect rivers and lead to incision and widening. Previous work has related river incision to the movement of sediment; as sediment loads initially increase, abrasion of particles on the riverbed erodes rock and any exposed bedrock erodes by slaking and plucking. At higher sediment loads, erosion is shut off as an immobile alluvial cover settles (Sklar and Dietrich, 2001; Scheingross et al., 2014; Lamb et al., 2015). At a larger spatial scale, higher sediment loads lead to dynamic and laterally mobile meanders (Constantine et al., 2014) and more frequent avulsions in braided channels (Ashworth et al., 2004), thereby widening channels and floodplains. As such, higher sediment loads tend to be associated with terrace planation while lower sediment loads or a higher transport capacity are linked with river incision.

The transport capacity of sediment, as well as bedrock erosion, is set by the water discharge, slope, grain size, and rock type, as shown in the simplified equations for sediment transport and bedrock erosion, respectively:

$$Q_s \propto (\rho g h S - \tau_c^* (\rho_s - \rho_w) g D_{50})^{\frac{3}{2}} \quad (1.1)$$

$$E = K(\rho_w g Q S) \quad (1.2)$$

where  $Q_s$  is the sediment flux,  $\rho$  is the density,  $g$  is gravitational acceleration,  $S$  is water slope,  $\tau_c^*$  is the Shield's parameter,  $D_{50}$  is the median grain size,  $E$  is the amount of bedrock erosion,  $K$  is a constant related to bedrock erodibility, and  $Q$  is the water discharge. By altering the amount of water, river slope, or bedrock hardness and density, forcings such as climate, tectonics, and structure can directly modify rates of bedrock erosion or sediment transport. Additionally, forcings can change the sediment supply through increased rainfall or seismicity to induce landslides or by glacial erosion, which will control whether bedrock incision or lateral planation is favored. As forcings change—such as through glacial cycles, changing uplift rates and styles, drainage capture, or exhumation of a different rock type—the rate of sediment transport and river incision will adjust accordingly, and periods of planation and incision will result in suites of terraces reflective of the original forcing.

However, these forcings do not have an equal effect across landscapes. For example, fluvial response to global climate does not occur at the same rate or style; terraces are incised into during interglacial periods (Personius, 1995; Carcaillet et al., 2009; García and Mahan, 2014), glacial periods (Rockwell et al., 1984; Cunha et al., 2008), and the transitions between (Antoine et al., 2000; Pan et al., 2003; Wegmann and Pazzaglia, 2009). To understand how an external forcing will change a river and thus the rest of the landscape, we need to better address fluvial response to perturbation. In this thesis, I use bedrock terraces to address two over-arching questions: What internal forcings control whether a fluvial system is prone to reaction? What are the timescales at which rivers can react to external forcings?

## 1.2 RESEARCH QUESTIONS

I investigate how basin lithology affects the potential for and timing of terrace formation using a field study in Chapter 2 and a literature review in Chapter 3. In Chapter 2, I use field mapping and geospatial analysis to test how lithology affects terrace formation and preservation. I contrast terraces in an erosion-resistant basalt and erosion-prone sandstone to understand how this internal forcing of lithology, partly controlled by the underlying structures, contributes to the landscape's susceptibility to external forcings, like climate or humans. I combine these field results with a literature review done in Chapter 3 to better understand how lithologic variations affect the timing of terrace formation in response to external forcings. In particular, starting from the same global climate signal, I track when different rivers incised or planed, and the way intra-basin lithologic heterogeneities affect when the climate signal created terraces.

To understand the different timescales of river response, I examine whether external perturbation over the last 10 to 0.1 ky caused river incision and terrace formation, using the literature review from Chapter 3 and field studies in Chapter 4. Previous modeling and field studies tend to ignore or disregard interglacial climate fluctuations as a mechanism for terrace formation and instead focus on marine isotope stage glacial cycling (e.g., Hancock and Anderson, 2002; Pan et al., 2003). I review previously studied and dated strath terraces, in which most formed in the last 10 ky, to determine whether interglacial climate variability caused terrace formation in the Holocene. At a smaller timescale, in Chapter 4 I examine whether external forcings, in the form of anthropogenic wood loss, can cause a fluvial response and terrace formation in only one century. For this last study, I use geomorphic mapping to identify terraces and then dated them using a novel combination of dendrochronology and radiocarbon that allows me to place minimum and



maximum bounds on terrace formation, in contrast to the usual practice of using a single radiocarbon date.

### 1.3 OUTLINE OF DISSERTATION

My thesis work is presented in Chapters 2-4, and was originally written and published as three standalone papers in peer-reviewed journals. Chapter 2 “**Lithologic controls on strath terrace formation and preservation**” was published in April 2016 in the journal *Geomorphology*. The editors subsequently invited me and coauthors to submit a review paper, which became Chapter 3 “**Multiple paths to straths: a review and reassessment of terrace genesis**”, which was published online in March 2018 and in the July 2018 issue of *Geomorphology*. The final chapter, Chapter 4 “**Anthropogenic strath terrace formation caused by reduced sediment retention,**” is currently in preparation. All references are contained in a single bibliography at the end. Supplementary materials from Chapters 3 and 4 are found in Appendices A-B.

## Chapter 2. LITHOLOGIC CONTROLS ON VALLEY WIDTH AND STRATH TERRACE FORMATION

*Originally published in the journal Geomorphology*

Schanz, S.A., Montgomery, D.R., 2016. Lithologic controls on valley width and strath terrace formation. *Geomorphology* 258, 58–68. Doi: 10.1016/j.geomorph.2016.01.015

### 2.1 ABSTRACT

Valley width and the degree of bedrock river terrace development vary with lithology in the Willapa and Nehalem river basins, Pacific Northwest, USA. Here, we present field-based evidence for the mechanisms by which lithology controls floodplain width and bedrock terrace formation in erosion-resistant and easily friable lithologies. We mapped valley surfaces in both basins, dated straths using radiocarbon, compared valley width versus drainage area for basalt and sedimentary bedrock valleys, and constructed slope-area plots. In the friable sedimentary bedrock, valleys are 2 to 3 times wider, host flights of strath terraces, and have concavity values near 1; whereas the erosion-resistant basalt bedrock forms narrow valleys with poorly developed, localized, or no bedrock terraces and a channel steepness index half that of the friable bedrock and an average channel concavity of about 0.5. The oldest dated strath terrace on the Willapa River, T2, was active for nearly 10,000 years, from 11,265 to 2862 calibrated years before present (cal YBP), whereas the youngest terrace, T1, is Anthropocene in age and recently abandoned. Incision rates derived from terrace ages average  $0.32 \text{ mm y}^{-1}$  for T2 and  $11.47 \text{ mm y}^{-1}$  for T1. Our results indicate bedrock weathering properties influence valley width through the creation of a dense fracture network in the friable bedrock that results in high rates of lateral erosion of exposed bedrock banks. Conversely, the erosion-resistant bedrock has concavity values more typical of detachment-limited streams, has a sparse fracture network, and displays evidence for infrequent episodic block erosion

and plucking. Thus lithology plays a direct role on the rates of lateral erosion, thereby influencing valley width and the potential for strath terrace planation and preservation.

## 2.2 INTRODUCTION

Bedrock, or strath, river terraces are often used to infer rates and styles of tectonic strain (e.g., Merritts et al., 1994; Van der Woerd et al., 1998; Lavé and Avouac, 2000; Cheng et al., 2002; Wegmann and Pazzaglia, 2002; Barnard et al., 2004; Mériaux et al., 2005). A number of modeling studies have assessed the role of climatically-driven changes in sediment supply on strath terrace formation (Hancock and Anderson, 2002; Turowski et al., 2007, 2008; Yanites and Tucker, 2010), and field studies have investigated the controls on the development and preservation of strath terraces (García, 2006; Wohl, 2008; Fuller et al., 2009; Finnegan and Balco, 2013; Larson and Dorn, 2014). Strath terraces form through a combination of lateral planation and vertical incision; when rivers with an alluvial cover migrate across valley bottoms, the underlying bedrock is eroded into a planar surface called a strath (Personius et al., 1993; Wegmann and Pazzaglia, 2002; Fuller et al., 2009; Finnegan and Balco, 2013; Pazzaglia, 2013). As vertical incision rates increase, rivers entrench faster than valleys widen, and the former valley surface is abandoned as a strath terrace. Vertical incision leading to strath formation generally is hypothesized to be caused by external changes: wetter climates and lowered sediment supply (Van der Woerd et al., 1998; Wegmann and Pazzaglia, 2002, 2009; Molin et al., 2012) or lowered base level caused by sea level retreat or tectonic uplift (Merritts et al., 1994). Internal forcings such as meander cutoffs are also found to abandon strath terraces through rapid channel avulsion and the upstream propagation of internally created knickpoints (Finnegan and Dietrich, 2011).

Using observations from basins around the world with different climates, tectonics, and vegetative cover, Montgomery (2004) noted that well-developed, planed-off strath terraces were more extensive in less resistant lithologies such as sandstone and siltstone, whereas poorly developed terraces were more common in more resistant lithologies such as quartzite and basalt. Montgomery (2004) hypothesized the difference in strath prevalence relates to the erosional properties of the bedrock; rocks subject to slaking will rapidly weather when subaerially exposed in the channel banks and thus provide the rapid lateral erosion rates necessary to plane an extensive strath. Stock et al. (2005) and Collins et al. (2016) reported rapid (i.e., 1 to 100 mm y<sup>-1</sup>) historical erosion and localized development of modern strath terraces along particular river reaches flowing over less resistant lithologies experiencing slaking in Washington State and Taiwan. Lithology is also known to influence the width of bedrock channels (Montgomery and Gran, 2001; Snyder and Kammer, 2008; Wohl, 2008) and the relative rates of channel widening and lowering (Hancock et al., 2011), thereby influencing the planation of straths.

Previous research has thus far focused on the role of lithology in controlling channel width. Here we investigate the role of lithology on strath terrace formation and preservation through its influence on valley width. The valley width reflects the preservation space for strath terraces and is also indicative of a river's ability to laterally planate and form the strath. Do the same processes that control channel width also govern valley width? Specifically, we examine the effect of lithology on spatial patterns of strath terrace preservation and valley width within the Willapa River basin in southwest Washington and the Nehalem River basin in northwest Oregon (Fig. 1), where exposures of basalt and siltstone alternate along the river profiles. We analyze the influence of bedrock properties on valley width, strath terrace presence, and relative rates of vertical and lateral erosion to assess the processes of and lithologic controls on strath terrace formation.

## 2.3 CHANNEL EROSION

Lateral and vertical incision rates are set by in-channel erosion rates and processes, which in turn are dominated by bedrock lithology, sediment supply, and water discharge (Hancock and Anderson, 2002; Pazzaglia, 2013). Vertical stream channel erosion is often expressed as a function of these factors:

$$E = K S^m A^n \quad (2.3)$$

where  $E$  is the erosion rate,  $S$  is channel slope,  $A$  is drainage area as a proxy for water discharge, and  $K$ ,  $m$ , and  $n$  are empirical constants that relate to bedrock erodibility, climate, incisional processes, and drainage basin characteristics. As the drainage area and thus water discharge increases, erosion rates intensify. Sudden increases in drainage area, such as by stream capture in the headwaters, can rapidly increase the rate of vertical erosion and abandon straths (García and Mahan, 2014). Rapid changes to river slope can occur locally from tectonic offset or base level fall (Gardner, 1983; García et al., 2004) and result in upstream propagating knickpoints or locally steepened zones where erosion is enhanced. Time transgressive strath terraces are formed as a result of the upstream propagation of knickpoints (Schoenbohm et al., 2004; Harkins et al., 2007). Although knickpoints represent a transient and local change in slope, channel slope can be influenced more broadly by basin lithology and sediment supply.

Lithology affects channel slope through setting the channel erodibility. More resistant lithologies that are harder to erode require steeper channels to produce topographic equilibrium (Gilbert, 1877). For a channel with an equilibrium long profile, erosion and uplift rates will balance; thus, if an erosion resistant bedrock (low  $K$  in Eq. 2.3) and erosion susceptible bedrock (high  $K$ ) with the same drainage area and uplift rate are compared, the erosion-resistant bedrock

requires a steeper slope in order to balance the lower  $K$  value (Stock and Montgomery, 1999). In this way, steep erosion-resistant zones can persist and form long-lasting lithologic knickpoints (Cook et al., 2009).

The lithology and amount of sediment supply also influences channel slope and incision rates. In a study of actively uplifting streams in the Santa Ynez Mountains, Duvall et al. (2004) found streams in erosion-susceptible bedrock were steeper downstream of erosion-resistant bedrock reaches than in comparably sized streams where the entire basin was composed of the erosion-susceptible bedrock. They hypothesized that the transition in bedrock lithology resulted in a transport-limited system with a supply of highly durable bedload that effectively eroded and steepened the more readily eroded bedrock downstream. Abrasion-mill studies found erosion rate increases with the square of the tensile strength of the abrading material and is dependent on the supply of bedload material (Sklar and Dietrich, 2001). As bedload initially increases in supply, saltating and suspended grains are able to abrade the bedrock. However, as the supply continues to increase, the mobile bedload layer becomes shielded from bedrock by an underlying immobile bedload layer and erosion rates decline asymptotically to zero (Sklar and Dietrich, 2001; Turowski et al., 2007).

Building on previous work on channel slope, bedrock erodibility properties, and sediment supply, we investigate the formation of strath terraces in two distinct lithologies — an easily erodible siltstone and erosion-resistant basalt — through field mapping of strath terraces, radiocarbon dating to determine incision rates, valley width measurements, and longitudinal profile analysis, and we discuss the variables controlling rates of vertical and lateral erosion. In particular, we investigate how the previously discussed erosional mechanisms interact with

lithology to determine valley width and thereby the potential for strath terrace formation and preservation.

## 2.4 STUDY AREAS

### 2.4.1 *Willapa River*

The Willapa River is located in southwest Washington State and drains an area of 680 km<sup>2</sup>, flowing from the coastal Willapa Hills to Willapa Bay in the Pacific Ocean (Figs. 1, 2A). The basin has a temperate coastal maritime climate and can receive up to 3 m of precipitation per year, mainly in the form of rain (Owenby and Ezell, 1992). Pleistocene glaciation did not reach the Willapa River basin, and snow accumulation is only temporary in the highest peaks. The bedrock is composed of Eocene Crescent Formation basalt flows in the south and southwest upper watershed, and Eocene to Miocene marine sedimentary rocks in the main valley and northeast quadrant of the watershed (Walsh et al., 1987). The marine sedimentary rocks are primarily composed of the McIntosh and Lincoln Creek Formations and are a mix of siltstones, mudstones, and sandstones with conglomerate lenses. The sedimentary rocks are not heavily cemented and are easily friable when dry (Rau, 1951). The Crescent Formation basalts are fine-grained, resistant to erosion, and form pillows and block-jointed structures. The basin was logged and splash-dammed in the late 1800s (Wendler and Deschamps, 1955), and as a result the river lacks in-channel woody debris and is mostly bedrock-floored with a thin alluvial cover.

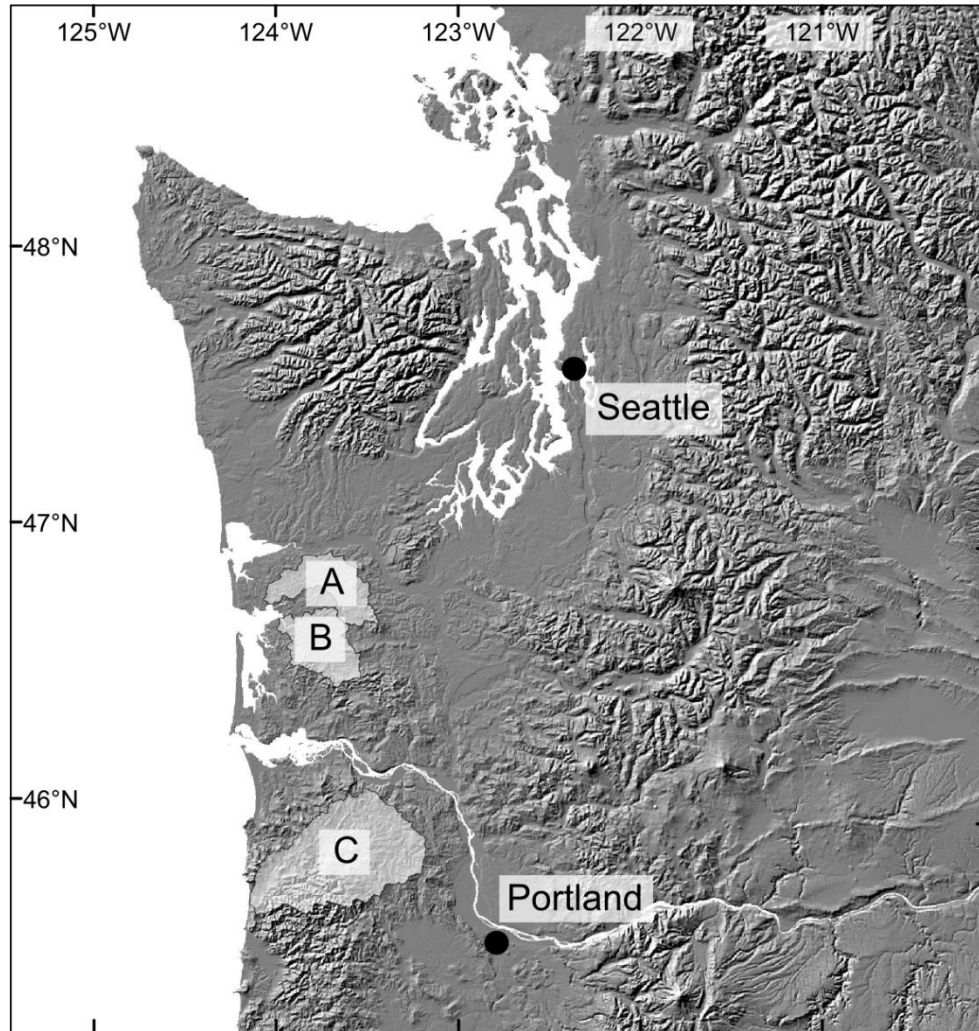


**Figure 2.1.** Location of study basins in Washington and Oregon States. A is the North River, B is the Willapa River, and C is the Nehalem River.

#### 2.4.2 *Nehalem River*

The Nehalem River is located on the north coast of Oregon and drains from the Oregon Coast Range to the Pacific Ocean, discharging into Nehalem Bay (Figs. 1, 2B). It has a drainage area of 2210 km<sup>2</sup> and an average annual rainfall of 2.9 m but can receive up to 4.5 m of rain in its headwaters (Maser, 1999). Bedrock is mostly marine sedimentary rocks of middle Miocene to late Eocene age, with late to middle Eocene basalt in the lower 50 km as well as the headwaters above river kilometer (rkm) 197. The river valley was settled and logged in the late 1800s, and log drives



and in-stream gravel mining cleared the channel of woody debris (Maser, 1999). The present channel is bedrock-floored with variable alluvial cover and lacks woody debris.

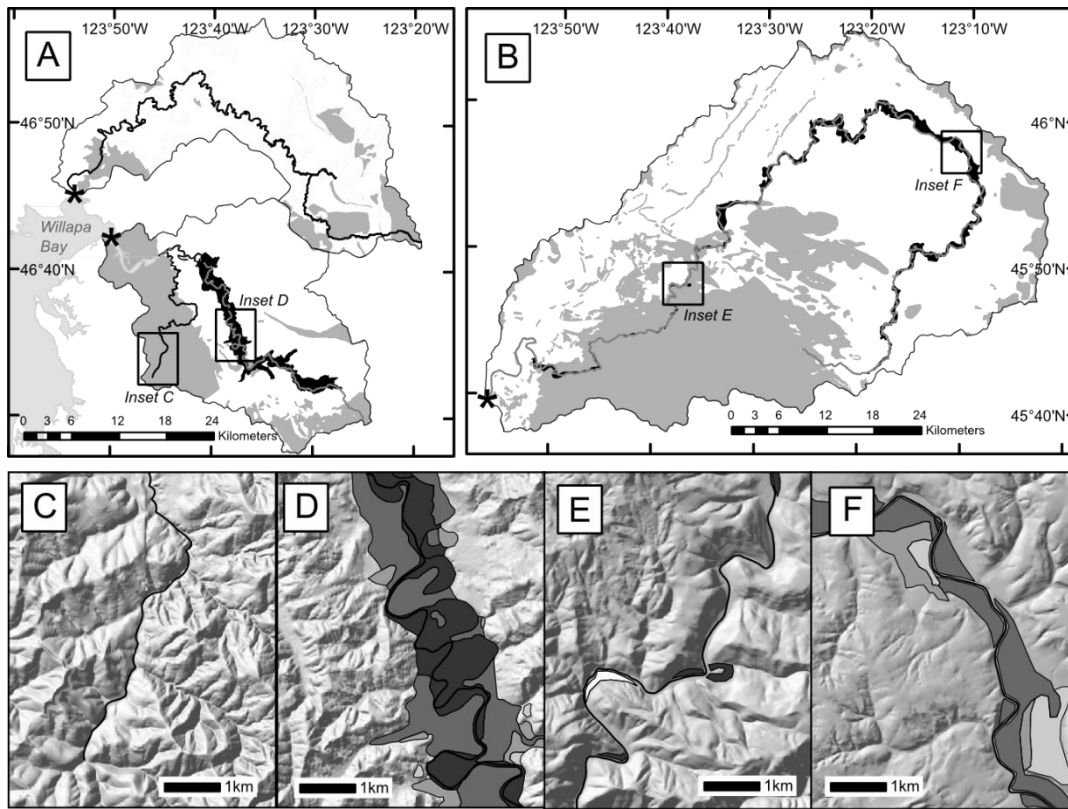


**Figure 2.2.** Maps of geology and terraces of the (A) Willapa and North rivers, Washington, and (B) Nehalem River, Oregon, with basalt bedrock in grey and siltstone in white, and the extent of mapped fluvial terraces shown in black; asterisks mark river mouths. Boxes indicate locations of closer views of terraces located in typical basalt (C, E) and sandstone reaches (D, F), with a 10-m-grid DEM hillshade background. Terraces are shaded lighter for older age. North is up for all panels.

**Table 2.1.** Terrace heights

Terrace	Elevation of terrace tread above river channel (meters)	Bedrock
Willapa T1	1-2	siltstone
Willapa T2	3-6	siltstone
Willapa T3	12-15	siltstone
Willapa T4	20-25	siltstone
Nehalem T1	<5	basalt/shale
Nehalem T2	6	shale
Nehalem T3	12	shale
Nehalem T4	30	shale
Nehalem T5	50	shale

## 2.5 METHODS

### 2.5.1 *Mapping and incision rates*

We mapped the spatial extent of terraces in the field onto 1:24,000 USGS topographic maps of the Nehalem and Willapa Rivers. Mapping of terrace surfaces on the Nehalem River was supplemented by lidar using the DOGAMI Lidar Viewer (<http://www.oregongeology.org/dogamilidarviewer/>). Terrace surfaces were differentiated based on degree of soil development, basalt weathering rind thickness, and height above the river channel. Soil development was determined by visual observation and by comparing the depth of the B horizon and degree of clay alteration in buried alluvial cobbles. Basalt clasts in the preserved terrace alluvium were broken open and the weathering rind thickness used to correlate terraces across the study area. Lastly, terrace tread height above the current river channel was used to correlate terraces; the heights are given in Table 2.1. Charcoal samples were collected from within alluvium overlying straths and dated using accelerated mass spectrometry at Direct-AMS in Seattle, Washington (Table 2.2). Radiocarbon ages were calibrated using the methods developed by Stuiver and Reimer (1993) with the software Calib Rev 7.0.2. Because of fluctuations in the global carbon reservoir over time, several radiocarbon ages contain multiple solutions when calibrated. We report all calibrated radiocarbon ages as  $2\sigma$  ranges in calibrated years before present (cal YBP) for a probability  $>0.25$ . Radiocarbon dates provide an estimate of the last time the strath was active, and incision rates obtained from these dates are minimum rates, as the true age of strath terrace abandonment could post-date the radiocarbon sample deposition. Incision rates are calculated using the midpoint of the  $2\sigma$  calibrated age BP range and the height of the strath above the low flow water surface. The riverbed is mostly bedrock with a thin alluvial cover, and we

interpret the bed fluctuations to be negligible as there is no indication of large, localized aggradation that could result in rapid changes to the riverbed elevation (Gallen et al., 2015).

**Table 2.2.** Radiocarbon sample locations and ages

Sample ID	14C age ( $\pm 1\sigma$ )	Calibrated age ( $2\sigma$ ) <sup>a</sup>	Incision rate (mm/y) <sup>b</sup>	Latitude/Longitude of sample (NAD 27)	Terrace
D-AMS 003607	68 $\pm$ 21	NA		46.5614 / -123.612	T2
D-AMS 003606	94 $\pm$ 27	23-142 (0.73) 219-264 (0.27)	31.52 10.77	46.6104 / -123.641	T1
D-AMS 011300	207 $\pm$ 24	146-189 (0.48) 268-301 (0.32)	7.58 4.46	46.6128 / -123.638	T1
D-AMS 003604	219 $\pm$ 29	145-214 (0.5) 268-307 (0.4)	8.91 5.57	46.5341 / -123.458	T1
D-AMS 005633	2918 $\pm$ 75	2862-3252	0.79	46.5562 / -123.610	T2
D-AMS 007611	5962 $\pm$ 21	6734-6809	0.30	46.5354 / -123.481	T2
D-AMS 011301	6765 $\pm$ 35	7576-7669	0.26	46.6288 / -123.697	T2
D-AMS 005631	7909 $\pm$ 45	8598-8809	0.37	46.5815 / -123.624	T2
D-AMS 005630	8896 $\pm$ 36	9904-10179	0.20	46.5352 / -123.481	T2
D-AMS 005632	8967 $\pm$ 34	10122-10227	0.13	46.5792 / -123.626	T2
D-AMS 003603	9398 $\pm$ 47	10512-10736	0.16	46.5635 / -123.566	T2
D-AMS 007612	9837 $\pm$ 27	11204-11265	0.31	46.5546 / -123.608	T2

<sup>a</sup>Years before present, calibrated based on Stuiver and Reimer (1993) using CALIB REV 7.0.1.

<sup>b</sup>Calculated using height above low flow strath and midpoint of calibrated age.

### 2.5.2 Valley width

We measured valley width as a constraint on the total lateral erosion and to characterize the space available for strath planation and preservation. To compare the influence of local lithology, we measured valley width versus upstream drainage area for locations underlain by basalt and marine sedimentary rocks. We include in this analysis data from the North River, which shares the same bedrock lithology and climate as the Willapa River and is located just north of the Willapa basin (Figs. 2.1 and 2.2). Drainage area provides a reasonable proxy for discharge, as the study basins receive comparable mean annual rainfall.

Drainage area was determined using the Hydrology toolset in ArcGIS. A 10-m-grid resolution DEM was used as the base layer, and flow accumulation was determined for each 10 x 10 m cell. The drainage area at each valley width measurement point was taken from the flow accumulation raster and converted to square kilometers.

In order to measure valley width and observe weathering behaviors in basalt and siltstone, field visits to each site were made. Heavy foliage in the tributary valleys prevented accurate field measurements of valley width, and the larger mainstem valleys were too wide to measure with our laser rangefinder. As a result, valley width was measured remotely from digital elevation models (DEMs), with field checks of valley width made where the line of sight was clear and valleys were narrow enough. Valley width was measured every 5 km along the channel for drainage areas  $>100$  km<sup>2</sup>, every 1 km for drainage areas between 10 and 100 km<sup>2</sup>, and every 100 m for drainage areas  $<10$  km<sup>2</sup>. Measurements were made using the Measure tool in ArcGIS on 1:24,000 topographic maps, avoiding tributary junctions. We then checked valley width measurements for accuracy against any available finer resolution, lidar-derived DEMs.

### 2.5.3 *Longitudinal stream characteristics*

In order to assess the effect of lithology on channel steepness in our study sites, we constructed longitudinal profiles and conducted a slope-drainage area analysis to determine the steepness index and concavity values. Longitudinal profiles for the Nehalem, North, and Willapa rivers were created using 1:24,000 topographic maps to avoid inaccurate interpolations in the 10-m DEM. The maps were digitized in ArcGIS and distances and elevations extracted manually at the intersection of the river and contour lines. Using the line segments from the longitudinal profile, the slope-drainage area plot was constructed by calculating the slope of each line segment, spanning the stream distance between contour lines and by obtaining the drainage area at the

midpoint of each line using the same process as for the valley width versus drainage area plots. A power law regression of the form  $S = k_s A^\theta$  was fit to the slope-drainage area plots, where  $k_s$  is the channel steepness index and  $\theta$  is the concavity value.

## 2.6 RESULTS

### 2.6.1 *Field mapping and observations*

Field mapping within the mainstem Willapa River identified four distinct strath terrace levels (Table 2.1, Fig. 2.2). The oldest terraces, T4 and T3, display a high degree of weathering on buried alluvial cobbles overlying the strath (Fig. 2.3A) and well-developed soil, while younger terraces T2 and T1 have little to no weathering rinds on alluvial cobbles (Fig. 2.3B) and are overlain by poorly developed soils. Five terraces were noted in the Nehalem River valley. In both basins, older terraces are preserved as unpaired and laterally discontinuous remnants, and T2 forms the main valley surface. The youngest terrace is inset into T2.

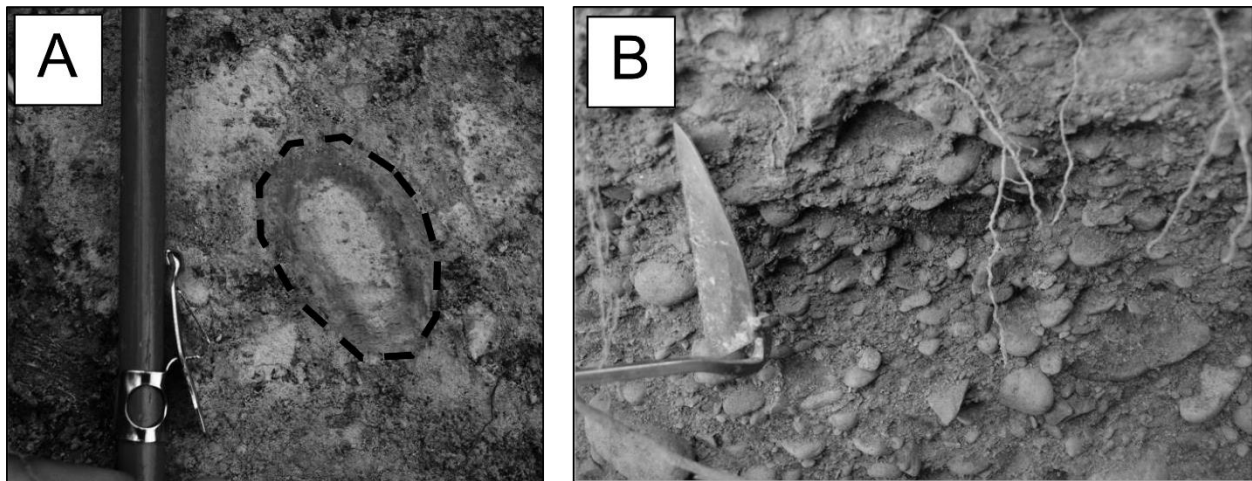


**Figure 2.3.** (A) Weathered siltstone cobble from the Willapa River terrace T4 showing weathering rind and complete alteration to clay. Dashed line shows outer limit of cobble. (B) Siltstone and basalt cobbles in the alluvium overlying the strath of terrace T2 display intact cobbles and very little to no clay alteration.

The marine sedimentary rocks in both basins displayed visible evidence of ongoing rapid physical weathering within the high and low flow channels. In the Willapa basin, large talus piles several meters high accumulate annually on the eroding banks of the river, indicating rapid physical weathering of the siltstone (Fig. 2.4A). The bedrock is heavily fractured and slaking in centimeter-sized chunks from natural wetting and drying processes. The high flow channel banks contain 1-3 m high bedrock outcrops that are wetted during winter high flows and dry during summer low flow; this subaerially exposed bedrock has a high fracture density and is easily eroded. Fractured pieces of bedrock are easily removed by hand. Spheroidal weathering around concretions within the bedrock produces 5- to 10-mm thick rinds that readily peel off within the high flow channel bounds (Fig. 2.4B). A low flow bench is common in both basins, with a deeper low flow channel incised into bedrock. Bedrock subaqueously exposed within the low flow channel is resistant to erosion and does not contain the closely spaced fracture network that has developed in the subaerially exposed siltstone.

In contrast, basalt bedrock reaches have rougher beds, with resistant blocks of bedrock forming knobs that protrude from the low flow water surface. The original fracture density of the bedrock controls channel bedforms, such as the spacing of pools and riffles (Fig. 2.4C). Notably, a secondary, weathering produced fracture system, such as observed in the marine sedimentary bedrock, has not developed. Active weathering of channel basalt is not evident, and erosion appears to concentrate along the preexisting fractures in the basalt and takes the form of large block erosion from entrainment in large floods. During field visits, the subaerial and subaqueous basalt were equally resistant to erosion and could not be dislodged by hand or hammer (Fig. 2.4D).

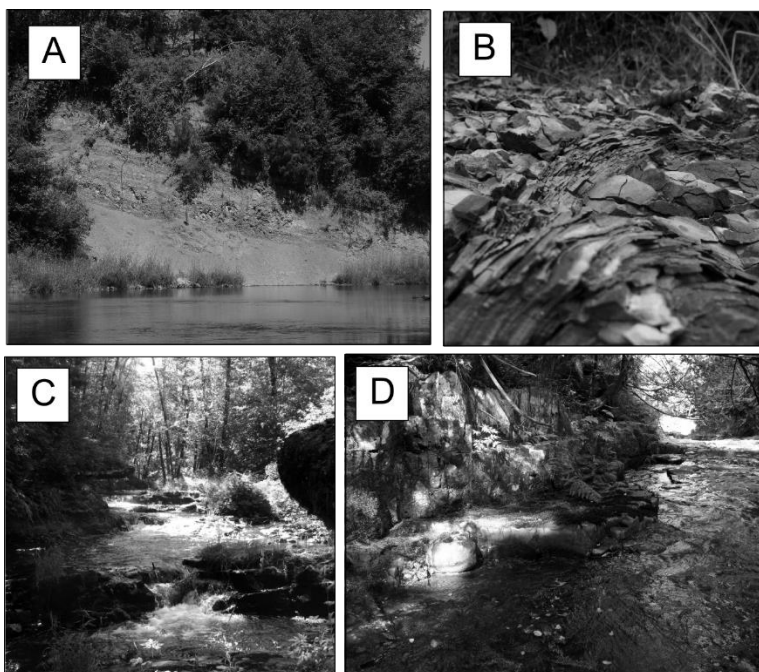


**Figure 2.4.** (A) Talus piles accumulated on a 5-m high bank of the Willapa River, within the marine sedimentary bedrock. (B) Active weathering of subaerially exposed siltstone banks in 0.5-1.0 cm flakes. Siltstone within the active channel displayed none of the exfoliation weathering that is prevalent along the exposed banks and high flow channels. (C) Small knickpoint on Falls Creek, a tributary to the Willapa River, with basalt bedrock. Preexisting fractures in the basalt control erosion and determine knickpoint spacing and location. (D) Basalt bank on Falls Creek. Bank has blocky shape determined from preexisting fractures in the basalt where erosion concentrates. Flow is to the right.

### 2.6.2 *Terrace ages and incision rates*

Radiocarbon ages are reported in Table 2.2 and Fig. 2.5A. Calibrated ages range from 23 to 307 cal YBP for T1 and from 2862 to 11,265 cal YBP for T2, a span of almost 10,000 years. Sample D-AMS 003607 is not used further in our analysis; we believe the young age of this sample is because of contamination by recent flood debris. The subdued morphology of the terrace at this site, its height 3.5 m above the river bed and within reach of recent flooding, and the developed soil cover on the terrace all support an older age for this surface.

The rate of vertical bedrock incision is an order of magnitude lower for T2 terraces (Table 2.3, Fig. 2.5B), which is expected owing to the incorporation of multiple cycles of nonincision and incision with greater terrace age (Finnegan et al., 2014). Rates vary between 0.13 and 0.79 mm y<sup>-1</sup> for T2 with a mean of 0.32 mm y<sup>-1</sup>, while T1 incision rates are between 4.46 and 31.52 mm y<sup>-1</sup> with a mean of 11.47 mm y<sup>-1</sup>. Longitudinally, T1 incision rates are highest closer to the estuary (Fig. 2.3); however, the three data points do not provide robust support for inferring a trend. Likewise, the incision rates from T2 are variable and do not show a statistically significant trend with upstream distance (Kendall's  $\tau$  of -0.098,  $p$ -value of 0.88, with a sample size of 7).

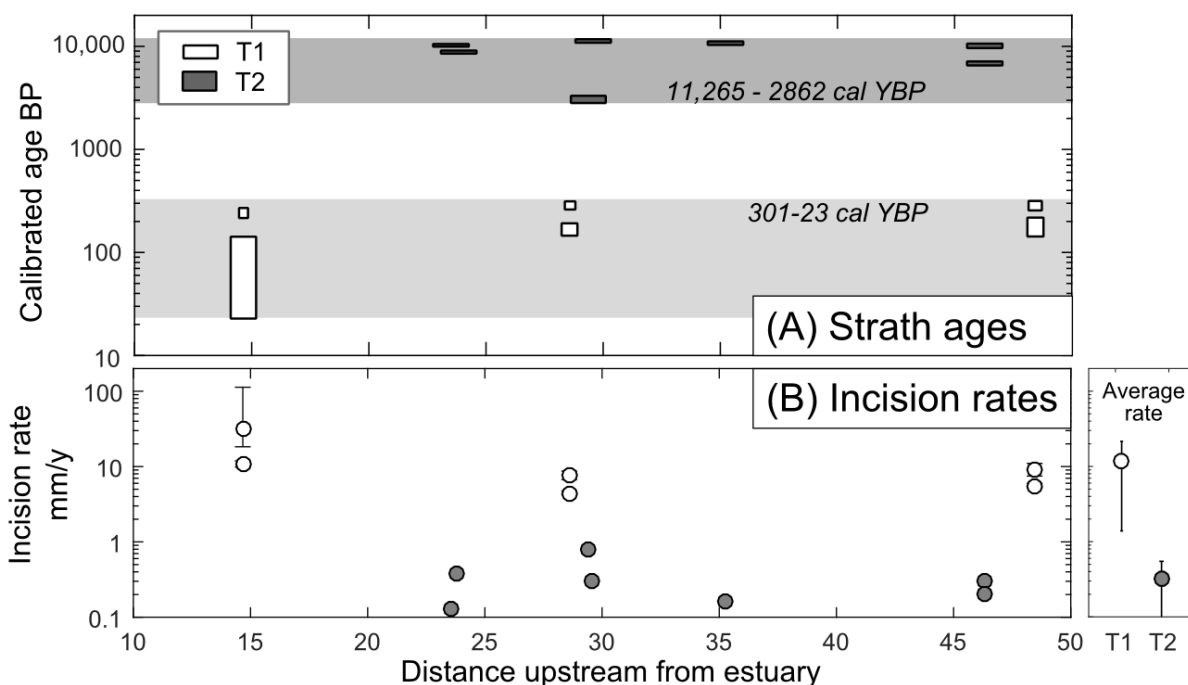


**Figure 2.5.** (A) Calibrated ages for radiocarbon samples collected along the Willapa River. Grey bars indicate the minimum range of occupation times for T2 and T1 implied by the samples. Boxes show 2 $\sigma$  range of ages, and width of boxes corresponds to the age probability for samples returning multiple calibrations with a probability >0.25. (B) Incision rates calculated from the median calibrated age and strath height above low flow shown against distance upstream of the estuary for the Willapa River. Error bars show 2 $\sigma$  range of incision rates. White circles are T1, grey circles are T2. For both plots, data is shown for all age probabilities >0.25.



**Table 2.3.** Power law regression  $w = bA^c$ 

Bedrock	b (1 $\sigma$ )	c (1 $\sigma$ )	R <sup>2</sup>
Marine sedimentary	67.1 $\pm$ 1.12	0.34 $\pm$ 0.03	0.45
Basalt	28.4 $\pm$ 1.09	0.22 $\pm$ 0.03	0.40

### 2.6.3 Valley width

Changes in valley width along the profile of the Nehalem and Willapa rivers reflect lithologic differences (Fig. 2.6). The widest valleys on the Nehalem River occur in the middle of the longitudinal profile (Fig. 2.6A), whereas the narrowest valleys are located at the farthest distance upstream from the outlet and in the reach immediately upstream of the outlet where the river is flowing through basalt. The longitudinal profile is steeper in the reaches underlain by basalt, coinciding with the narrower valleys. Profiles in the marine sedimentary rock are concave upward. In the South Fork of the Willapa River, a similar trend of narrower and steeper valleys in basalt bedrock is observed (Fig. 2.6B). Here, the valley width in basalt reaches is consistently <100 m, and a considerable widening is observed when the river encounters marine sedimentary bedrock where valley widths range from 300 to 900 m. The longitudinal profile shows abrupt breaks in slope at the transition between marine sedimentary and basalt bedrock valleys, with a concave up profile in marine sedimentary rock. The lower basalt reach is convex up, similar to the lower reach of the Nehalem River; while the upper basalt reach on the South Fork Willapa River is concave up but contains several sharp breaks in slope (e.g., at river kilometers 23 and 31).

When valley width is plotted against drainage area rather than longitudinal distance upstream, basalt and sedimentary bedrock valleys separate distinctly (Fig. 2.7). Basalt bedrock valleys are narrower than sedimentary bedrock valleys with the same drainage area. A power law least squares regression characterizes the behavior of each lithology with increasing drainage area. For both lithologies, as drainage area increases and the channel becomes larger, the valley width

also increases. However, the width of sedimentary bedrock valleys increases with drainage area by a power of  $0.34 \pm 0.03$ , while basalt valleys increase by a power of  $0.22 \pm 0.03$ , indicating that the dependence of valley width on drainage area is not the same for all rock types (Table 2.3, Fig. 2.7). Although sedimentary valleys and basalt valleys widen as drainage area increases, sedimentary valleys are 2 to 3 times wider for the same drainage area. As drainage area continues to increase, the difference in width between basalt and sedimentary valleys increases; hence the influence of lithology on valley width appears to be greater at larger drainage areas.

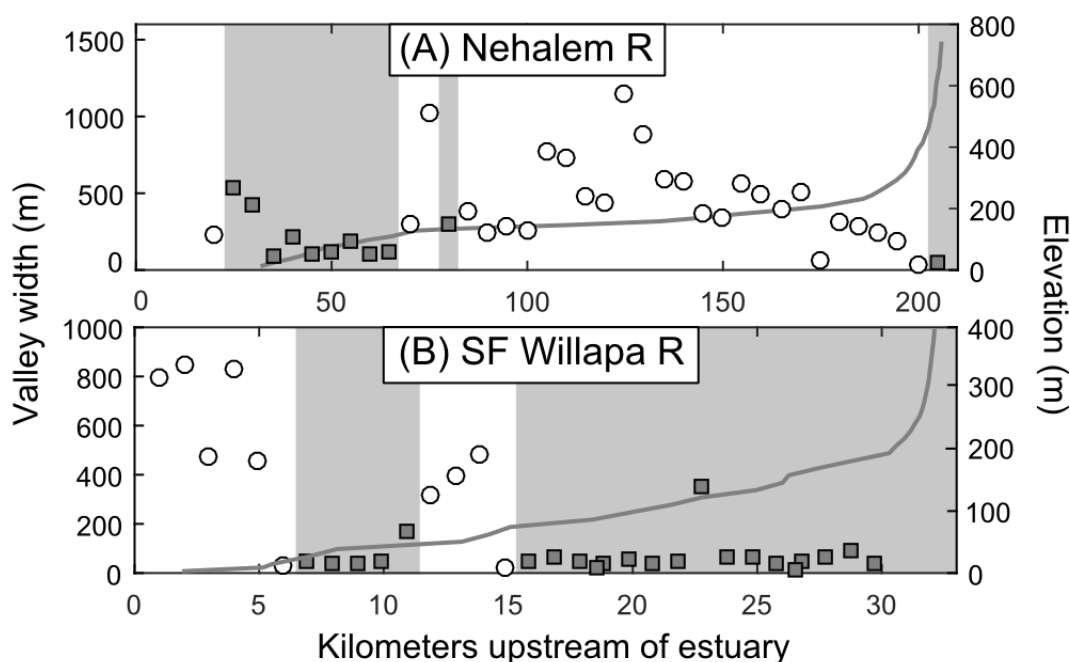


**Figure 2.6.** Valley width and elevation as a function of distance upstream of the estuary for the (A) Nehalem and (B) South Fork Willapa rivers. Grey squares indicate valley width measured in basalt bedrock while white circles show marine sedimentary bedrock. The longitudinal profile is shown in dark grey, with regions underlain by basalt indicated by the shaded background. Distance is measured in kilometers from estuary, as determined along channel centerline; valley width is measured from 1:24,000 USGS topographic maps.

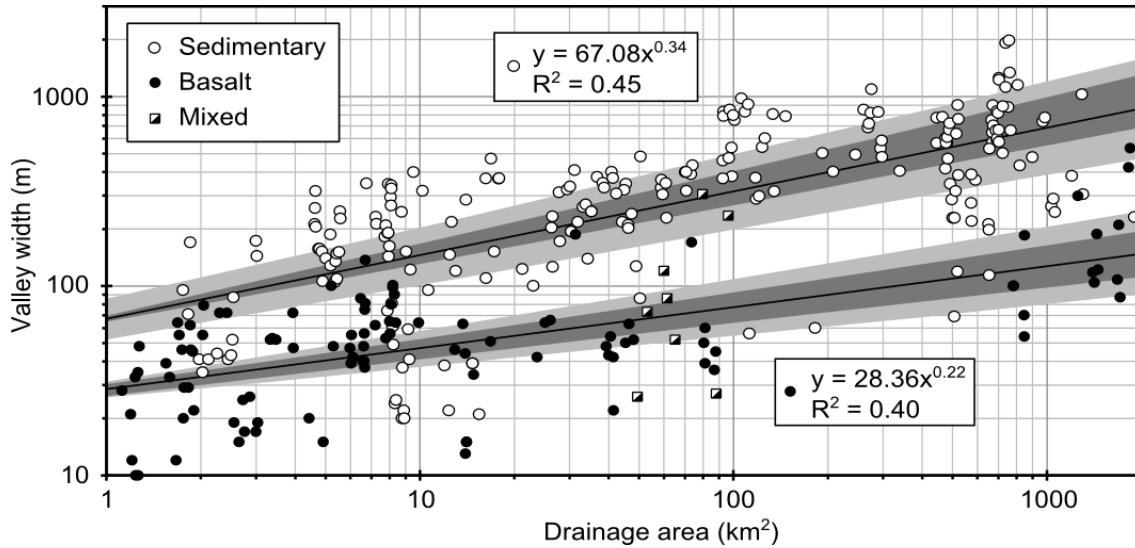


**Figure 2.7.** Drainage area versus valley width data for the Nehalem, Willapa, and North rivers. Open circles indicate marine sedimentary bedrock and closed circles denote basalt bedrock. Half-filled squares specify locations at the transition between marine sedimentary and basalt bedrock. Light grey shading shows  $2\sigma$  standard error of the power law regression and dark grey shading shows  $1\sigma$  standard error. Exponents of the regression and  $1\sigma$  errors are found in Table 3.

#### 2.6.4 Slope-area analysis

For all three basins, the concavity ( $\theta$ ) and steepness indexes ( $k_s$ ) are significantly different in basalt and sedimentary bedrock reaches (Fig. 2.8). In basalt,  $k_s$  values range from 0.07 to 0.18, while the corresponding values in sedimentary bedrock are from 0.22 to 0.32. For a given basin, the sedimentary bedrock  $k_s$  values are nearly double those in basalt. The concavity of sedimentary bedrock reaches is relatively consistent between watersheds, at 0.88, 0.94, and 0.96 for the Nehalem, North, and Willapa rivers, respectively. Concavity ranges more widely for the basalt reaches, at values of 0.42, 0.28, and 0.75 for those same rivers. When data from all three basins are combined, the  $k_s$  values are 0.27 and 0.16 and concavity values are 0.93 and 0.51 for the sedimentary and basalt bedrocks, respectively (Fig. 2.8D).

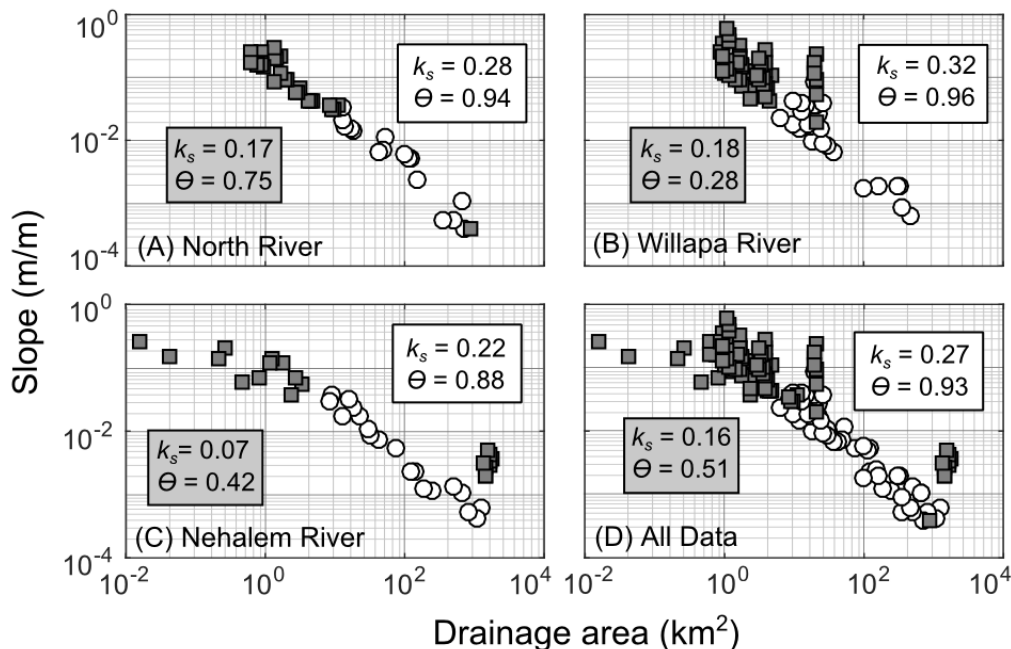


**Figure 2.8.** Slope area plots for the (A) North River, (B) Willapa River, (C) Nehalem River, and (D) all rivers. All plots are to the same scale. Grey squares are basalt bedrock and white circles represent marine sedimentary bedrock. Steepness indexes ( $k_s$ ) and concavity ( $\theta$ ) are shown in grey boxes for basalt and white boxes for the marine sedimentary bedrock.

## 2.7 DISCUSSION

### 2.7.1 *Strath occupation time*

Radiocarbon estimates of strath terrace ages span a wide range, indicating occupation of straths for extensive periods of time (Table 2.2, Fig. 2.5A). Calibrated radiocarbon ages for T2 have a range of nearly 10,000 years from 2862 to 11,265 cal YBP. This suggests T2 was an active valley floor experiencing deposition and lateral movement during most of the Holocene and, furthermore, because radiocarbon ages provide a minimum range, implies the occupation time could be even longer. The maximum duration of incision to abandon T2 interpolated from the calibrated ages is ~2500 years; this value is one-fourth of the minimum planational phase and

supports previous studies that find planation periods much longer than incisional phases (Hancock and Anderson, 2002; Wegmann and Pazzaglia, 2002; Collins et al., 2016).

The long occupation time suggested by this study and others calls for caution in evaluating incision rates, especially those obtained from a single radiocarbon sample. Although incision rates obtained from T2 seem to cluster in comparison to T1 (Fig. 2.5B), they still span nearly an order of magnitude. The range in incision rates is caused by how much of the planation phase is encapsulated in the age; a greater ratio of time spent in planation than incision results in a lower apparent incision rate owing to the Sadler effect (Finnegan et al., 2014). That inferred incision rates can vary greatly depending on sample location calls for care in using incision rates to infer rates of tectonic rock uplift. Previous authors have suggested using incision rates from terraces spanning a full glacial cycle (Wegmann and Pazzaglia, 2002) or using the lowest terrace as the reference frame to calculate incision (Gallen et al., 2015). However, if terraces can be active for up to 10,000 years, as our radiocarbon dates show, then using either of these methods without taking into account the full range of terrace occupation would still result in erroneous uplift rates.

Additionally, the relative time spans of the two terrace sets observed on the Willapa River indicates a recent shift in river incision rates. Terrace T2 is the Holocene strath terrace and was active for nearly 10,000 years before significant incision occurred to abandon it. Average incision rates are close to the long-term exhumation rates reported in the Olympic Mountains (Brandon et al., 1998). The lower terrace, T1, is much more restricted in areal extent (Fig. 2.2D) and the strath was occupied for less time, possibly up to 300 years. Incision and terrace abandonment initiated only in the last hundred years, and incision rates are much higher than short-term geodetic uplift rates that measure between 0.4 and 0.8 mm  $y^{-1}$  (Pazzaglia and Brandon, 2001). The recent abandonment of T1 falls within the Anthropocene and may well indicate an anthropogenic

influence on the landscape, which may also explain why incision rates are two orders of magnitude higher than geodetic uplift rates. Recently, Collins et al. (2016) suggested in-stream wood loss can trigger incisional periods in a river through the removal of stored accumulations of sediment once held in place by log jams; historical documents show the Willapa River was logged and cleared of wood around the time T1 incision initiated. Further evidence linking the two events is necessary, but the correlation between wood loss and incision in the Willapa River and the West Fork Teanaway River (Collins et al., 2016) suggests fluvial wood is a currently underestimated control on river incision.

### 2.7.2 *Lithological control on valley width*

Our finding that valley width, and thus strath terrace development, is controlled by lithologic variation within individual watersheds establishes that lithology is indeed a primary control on strath terrace formation, as suggested by previous work based on a compilation of studies in which straths were reported in various lithologies (Montgomery, 2004). We found little to no strath terrace development in basalt bedrock in the Willapa and Nehalem basins and multiple flights of well-developed strath terraces in sedimentary bedrock in both basins (Fig. 2.2). Observations on erosional style suggest rapid weathering by slaking is responsible for the widening and formation of straths in sedimentary bedrock. This observation is supported by measurements in similarly friable bedrock such as the Roslyn Formation in the central Cascade Range (Collins et al., 2016) and the Lincoln Creek Formation in the southern Olympic Mountains (Stock et al., 2005).

In contrast, basalt and more resistant lithologies that are not subject to weathering by slaking are slower to erode, forming narrower valleys. Concavity values in the basalt-floored streams span a broad range (Fig. 2.8), suggesting erosional mechanisms vary widely; this is likely

indicative of variations in the original fracture density that control the erosional style. These values fall nicely within the range of concavity values previously noted in a set of diverse landscapes and lithologies and imply that erosion is dependent on either shear stress or unit stream power (Tucker and Whipple, 2002). Channels eroding sedimentary bedrock, however, have very similar values of concavity because the original fracture patterns are overprinted by a new, dense, system of fractures caused by slaking. The concavity values obtained in these sedimentary basins are close to 1, a value previously only found in the Oregon Coast Range (Seidl and Dietrich, 1992). Siedl and Dietrich (1992) hypothesized streams with  $\theta \sim 1$  erode based on total stream power with a strong dependence on discharge. Tucker and Whipple (2002) later dismissed the total stream power model based on a lack of streams with  $\theta \sim 1$  and on a poor fit with modelled and observed topography. Our results indicate a  $\theta$  of 1 is not an anomalous value but perhaps a value common to streams draining easily friable sedimentary rocks, such as those in our study and that of Siedl and Dietrich (1992). Rapid slaking in these streams throughout the dry season unravels the bedrock such that sand-sized particles are produced and easily washed downstream. Thus, for these channels erosion is not dependent on stream power but instead on having a wet and dry season and a flow sufficient to transport sand-sized particles. It follows that streams draining such friable rocks would have erosion rates dependent on discharge, or drainage area in Eq. (2.3); and thus we infer that the total stream power model of Siedl and Dietrich (1992), in which  $m = n = 1$  (Eq. 2.3) and producing  $\theta \sim 1$ , is applicable to a subset of bedrock mountain rivers where the bedrock lithology is prone to rapid slaking.

Channel erosion properties appear to scale up to control the valley width in the friable sedimentary bedrock. The width of valleys increases with drainage area at a similar rate as the stream channel width in sedimentary-floored streams. Montgomery and Gran (2001) found

channel width along the sedimentary bedrock channels of the Willapa River increased with drainage area in a power law relationship where the exponent is  $0.32 \pm 0.02$ , within error of the exponent found for valley width and drainage area in the same bedrock (Table 2.3, Fig. 2.7). This suggests that erosional processes controlling channel width also apply to valley width and implies a dependence on channel width for lateral channel migration. Rearranging the equation obtained by Montgomery and Gran (2001) and the relationship between drainage area and valley width given in this study, we find that valley width is 14.4 times the channel width for all drainage areas in the sedimentary bedrock.

Hence, lateral erosion by the channel appears to scale with the original width of the channel. We suspect that this scaling reflects an indirect link between channel and valley width through meander amplitude. The relationship between meander amplitude and channel width is also linear but varies with individual channels where meander amplitude can be 2.4 to 18.6 times the channel width (Leopold et al., 1964, and references therein). Our relationship between valley width and channel width falls within that range and suggests that valley width is controlled by the meander amplitude.

The relationship between channel and valley width applies to the marine sedimentary bedrock that is prone to slaking but does not hold true for basalt bedrock where erosion is unsteady and dependent on original fracture patterns. In the following sections, we further explore the mechanisms by which lithological differences control lateral and vertical erosion and thus strath formation: channel steepness and planform, channel versus bedload lithology, and bedrock mineralogy.



### 2.7.2.1 Channel steepness and planform

As previously discussed, more resistant lithologies form steeper channels. As a result, stream power — the product of water slope, flow depth divided by width, density, and gravitational acceleration — is increased and vertical erosion enhanced. Increased vertical erosion will diminish the likelihood of long periods of lateral planation that are required to form straths; even if lateral planation is occurring, rapid vertical erosion will result in a sloped surface rather than the formation of a planar terrace (Merritts et al., 1994).

A secondary effect of steepened channels is a shift in channel planform. The Nehalem River is a meandering, single-thread channel that rapidly transitions to a much less sinuous, near straight channel where the bedrock shifts to basalt (Fig. 2.2). The South Fork Willapa River follows a similar trend as it comes in and out of the basalt and sedimentary bedrock; the basalt channels are less sinuous than the sedimentary bedrock channels. Straight planforms allow less lateral erosion and planation than braided or meandering channels, which are much more laterally mobile with continuous bank erosion and creation. Finnegan and Balco (2013) argued that braided channels are more likely to plane straths than other planforms, as the disorderly and dynamic nature of the braided channel allows it to rapidly widen a valley and erode a planar bedrock surface. If lithology exerts a first-order control on channel steepness, then channel planform will also depend on lithology, and thus the potential for planation is dependent on bedrock strength.

### 2.7.2.2 Lithologic contrasts

The volume of sediment supplied to the channel affects rates of vertical incision, but the strength of the supplied sediment will also have a considerable effect on rates of channel erosion. In the Nehalem and Willapa rivers, competent basalt bedrock is eroded in the steep hillslopes and provides long-lasting, attrition-resistant bed material. Although the Willapa River is composed of

sedimentary bedrock for tens of kilometers upstream, the dominant bedload material is basalt of cobble to gravel size. This indicates that the local bedrock is not the abrasive tool but rather that basalt bed material sourced from the headwaters is doing most of the geomorphic work. Additionally, the amount of bed material is limited owing to rapid attrition of the marine sedimentary bedrock, which makes up the majority of the basin. Any input of siltstone to the channel breaks down to sand-size particles when dry and so is rapidly transported out of the system in the next flood. As a direct result, the Nehalem and Willapa rivers are likely to remain mixed bedrock-alluvial and are unlikely to become fully alluvial unless an external sediment source is added or the retention of sediment on the riverbed is increased.

In a study of rivers draining the Oregon Coast Range, O'Connor et al. (2014) found attrition rates varied widely between different basin lithologies and was the main control on bed material transport rates and channel cover. Similarly, Duvall et al. (2004) found steeper channel reaches in erosion-susceptible rock where the bedload was comprised of erosion-resistant rock sourced upstream. Both these findings indicate the presence of competent upstream bed material combined with a mechanically weak bedrock prone to slaking results in less bed cover, steeper slopes, and thus greater incision rates. Studies in mechanically weak rock with competent bed material record rapid incision rates on the order of  $\text{cm y}^{-1}$ , much greater than background geologic erosion rates of  $1 \text{ mm y}^{-1}$  or less (Stock et al., 2005; Collins et al., 2016). Incision rates on the Willapa River are also unusually rapid for the last incision cycle, from T1 to present, while incision rates from T2 to present, which incorporate a period of nonincision, are an order of magnitude lower and are similar to long-term rock uplift rates reported by Brandon et al. (1998). Hence, as long as there is base level accommodation space, rivers such as the Nehalem and Willapa, composed of a majority of mechanically weak bedrock and a headwater source of erosion resistant

bed material, are likely to be in incisional phases. However, our radiocarbon dates indicate that this is not the case, with planation of T2 occurring for most of the Holocene and suggesting that there must be a mechanism to slow vertical incision and favor lateral widening.

If mechanically weak rock with resistant bed material is susceptible to rapid rates of erosion caused by the strength differences in the bedload and bedrock, we would expect rivers in this situation to be deeply incised with no terraces. However, rapid vertical incision creates steep bedrock banks perched above the water table and exposed to mechanical and chemical weathering processes. The marine sedimentary bedrock of the Willapa and Nehalem rivers has a high mica content and is prone to physical weathering from wetting and drying. As the bedrock banks become exposed and perched higher above the low flow channel, cycles of wetting and drying through the year mechanically loosen the bedrock (Figs. 2.4A, B). During high flows, the loosened material is rapidly transported away, resulting in up to centimeters of lateral erosion in one event (Montgomery, 2004; Stock et al., 2005; Collins et al., 2016). This process is noted not only on the Willapa and Nehalem rivers, applying to fluvial terraces, but has also been postulated to be the mechanism behind wave cut bench formation (Retallack and Roering, 2012). Collins et al. (2016) hypothesized that rapid lateral widening also occurs if a low bench of easily friable bedrock is exposed during an extreme flow event. The bench undergoes lateral and vertical erosion by slaking, as well as physical abrasion in high flows, and can erode laterally at rates of decimeters per year (Collins et al., 2016).

As rapid erosion of exposed bedrock banks proceeds, the channel widens and water flow depth as well as stream power is lowered, thus slowing rates of vertical incision. Additionally, the decrease in stream power will reduce the transport capacity of the stream and result in aggradation, further protecting the bed from erosion. The process of widening results in a negative feedback to

the incising stream that will arrest incision and turn the system toward lateral planation. Gravel deposits on top of T2 straths in the Willapa basin indicate that when the strath was active, sufficient gravel was accumulated in the channel to promote planation and slow incision. Because competent gravel supply to the system was likely as low as it is today, this indicates that the transport capacity was much lower during T2 occupation in order to accumulate gravel. This could be accomplished through a shallower slope, wider channel, or the presence of woody debris jams that partition shear stress and trap sediment. The long occupation time of T2 indicates that these conditions were stable through most of the Holocene.

## 2.8 CONCLUSIONS

Erosional properties unique to each lithology control valley width and thus the potential for strath planation and preservation, with slaking-type erosion creating valleys 2-3 times wider in marine sedimentary bedrock than in the relatively erosion-resistant basalt. Concavity values indicate basalt is eroding consistent with stream power erosion models while the sedimentary rocks of the Willapa and Nehalem basins follow a total stream power model that relies primarily on discharge as the main erosive agent. In readably friable rocks that annually slake into sand-size pieces, the total stream power model can accurately depict erosion as erosion in slaking rocks is dependent on subaerial weathering rather than fluvial abrasion or plucking. Additionally, the difference in rock strength between bedload and bedrock in the Willapa and Nehalem rivers leaves them prone to rapid vertical incision, although widening of bedrock banks from slaking can slow this process by lowering the transport capacity. Accumulations of fluvial wood during the Holocene likely kept more sediment on the channel bed, slowing incision rates and leading to more lateral movement. The loss of this wood, and associated lowered sediment retention, possibly attributed to the rapid ongoing incision that is abandoning the lowest terrace.

## Chapter 3. **MULTIPLE PATHS TO STRATHS: A REVIEW AND REASSESSMENT OF TERRACE GENESIS**

*Originally published as an invited review paper in the journal Geomorphology*

Schanz, S.A., Montgomery, D.R., Collins, B.D., Duvall, A.R., 2018. Multiple paths to straths: A review and reassessment of terrace genesis. *Geomorphology* 312, 12–23.  
<https://doi.org/10.1016/j.geomorph.2018.03.028>

### 3.1 ABSTRACT

Strath terraces, an important tool in tectonic geomorphology, have been attributed to climatic, tectonic, volcanic, and human activity, yet the pathways connecting external forcings to the channel response leading to terrace formation are highly variable and complex. To better understand variability and controls on the pathways between forcing and terrace formation, we created a comprehensive database of 421 strath terraces from peer-reviewed literature and noted the strath age and rock type, the ascribed forcing (climate, tectonics, volcanoes, or humans) or whether the cause was unasccribed, and the pathway between forcing and strath incision or planation. Study authors identify climate, tectonics, volcanoes, and humans as the forcing for 232 (55%), 20 (5%), 8 (2%), and 5 (1%) strath terraces in our compilation respectively. A forcing was not identified for the remaining 156 (37%) terraces. Strath terraces were dated using 14 different methods: 71% of terraces in our database are dated using methods, such as radiocarbon and optically stimulated luminescence, that date planation and give a maximum age of incision; 16% of terraces are dated with methods that give a minimum age of incision; and 14% use a variety of methods for which a generalization about incision age cannot be made. That the majority of terrace studies use planation ages to understand terrace formation highlights the necessity of knowing the relative timescales of incisional and planation phases, which has so far been quantified in only a handful of studies. In general, rivers in arid regions plane straths in interglacial periods when

discharge and sediment transport capacity increase, whereas temperate rivers plane in glacial or interglacial periods when sediment supply increases. Heterogeneities in rock strength between watersheds further control how sediment is produced and when straths are planed. Globally, these regional and watershed controls result in strath planation and incision during all parts of the glacial cycle. Terraces with no identified forcing in our database reach a maximum frequency during the late Holocene (4 kya-present) and could potentially be explained by regional deforestation and increased anthropogenic fire frequency, regionally active tectonics, and climate fluctuations. Deforestation and fires, by reducing the supply of wood to streams, decrease instream sediment retention and could convert alluvial channels to bedrock, thus promoting strath incision. The regional and watershed controls on strath formation highlighted in our database, as well as the possibility of anthropogenic forcings on strath terrace formation in the late Holocene, illustrate the importance of explicitly establishing the pathway between forcing and strath terrace formation in order to accurately interpret the cause of strath formation.

### 3.2 INTRODUCTION

Strath terraces are important geomorphic markers of tectonic strain, yet, to date, few meta-analyses have been conducted on the cause and timing of strath formation (e.g., Montgomery, 2004; Pazzaglia, 2013). Strath terraces form as a result of two fluvial processes: lateral planation, which bevels the strath, and vertical incision, which abandons the strath as a terrace (Fig. 3.1). Incision and planation of strath terraces are caused by adjustments to the river slope, sediment supply and caliber, and water discharge, all of which affect the transport of sediment. Lateral beveling is often associated with increased sediment loads (e.g., Bull, 1990; Personius et al., 1993; Hancock and Anderson, 2002; Wegmann and Pazzaglia, 2002). Higher sediment loads protect the

underlying bedrock from vertical incision (Sklar and Dietrich, 2001) and can promote a wider, braided morphology that enhances bedrock bank erosion through subaerial weathering (e.g., Montgomery, 2004; Finnegan and Balco, 2013). Lateral planation can also occur rapidly through subaerial bedrock weathering and erosion once low surfaces are stripped of alluvium during high magnitude flows (Collins et al., 2016) and through lateral migration of meandering channels (Merritts et al., 1994; Limaye and Lamb, 2016). Strath incision typically occurs when the transport capacity exceeds sediment supply, thereby exposing underlying bedrock to vertical erosion.

External forcings of strath terraces can be grouped into four broad categories: climate (e.g., Pan et al., 2003; Amos et al., 2007; Wegmann and Pazzaglia, 2009); tectonics (e.g., Harkins et al., 2005); volcanic activity (e.g., Ely et al., 2012; Baynes et al., 2015); and human action (e.g., Lewin et al., 1991; Carcaillet et al., 2009; Molin et al., 2012) (Fig. 3.2). Each of these forcings can cause lateral planation or vertical incision; however, all require that the landscape is undergoing a base level change, typically driven by steady rock uplift, to accommodate incision and allow terrace preservation. Global glacial cycles are the most common climatic phenomenon linked to strath terrace formation. Previous studies have related strath planation during interglacial periods (Van der Woerd et al., 1998; Fuller et al., 2009; Lewis et al., 2009) and glacial periods (Amos et al., 2007; Wegmann and Pazzaglia, 2009; Wang et al., 2015). That planation can occur in both parts of the cycle implies that fluvial response to glaciation, and perhaps other landscape perturbations, may be modulated by intermediary, regional-scale environmental variables. Additionally, the commonly held assumption that climate drives strath terrace formation in the majority of cases (e.g., Hancock and Anderson, 2002; Pan et al., 2003; Pazzaglia, 2013) has never, to our knowledge, been tested against a full data set of studied strath terraces.

With the increasing use of strath terraces in geomorphological studies, the large data set of strath ages and associated forcings now at hand allows us to reevaluate prevailing geomorphic theory on strath formation against the collected data. Here, we use an expansive compilation of previous work on strath terraces to analyze how many terraces are attributed to each forcing and the various pathways between forcing and strath formation, as well as whether terraces lacking an identified forcing can be attributed to a forcing based on their geologic history. To better interpret reported strath terrace ages, we identify the methods used to date terraces and discuss the constraints those methods place on the timing of terrace formation. We find that climate forcings are modulated by regional climate and watershed-scale characteristics, such as rock type and glacial proximity, which exert local controls on the timing and nature of fluvial response to glacial cycles. Although glacial cycles are reportedly responsible for the majority of mapped and dated strath terraces, over one-third of the terraces in our database were not associated with an identified forcing. We evaluate possible controls on late Holocene terraces, including the potential role of human-caused changes to forest structure, in-stream wood abundance, and fire regimes that affect sediment retention and river incision.



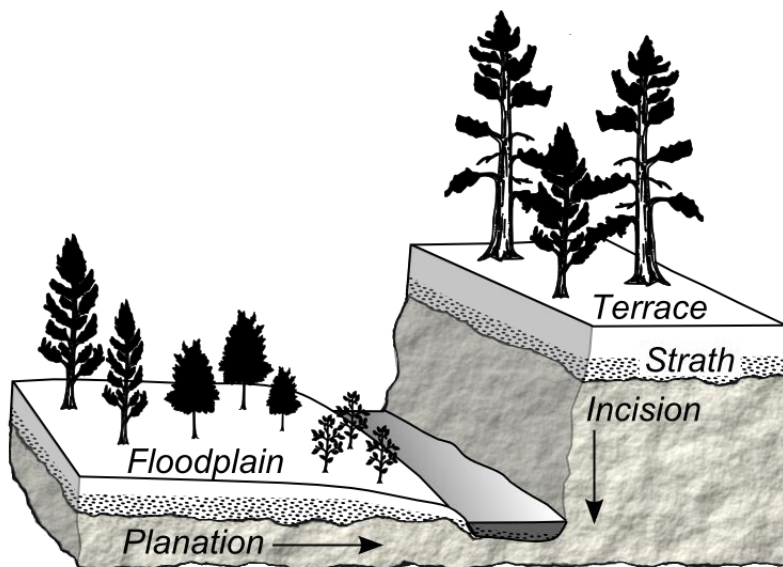


**Figure 3.1.** Illustration of the relationship between the bedrock strath and the terrace, as well as definitions of incision and planation directions. Succession of young alders (*Alnus rubra*) to older pines (*Pinus ponderosa*) on the floodplain indicates planation direction, as indicated by the arrow. Stipling represents gravel to cobble size alluvium, while white shading are floodplain sediments, generally sand to clay sized. Bedrock is shown by the rough texture.

### 3.3 DATABASE COMPILATION

To better understand how and when strath terraces form in response to climatic, tectonic, volcanic, and anthropogenic forcings, we compiled an exhaustive database of dated strath terraces from peer-reviewed publications and analyzed the reported controls on river incision and strath planation. We did not include in our compilation strath terraces lacking an age control, even if terrace formation was discussed. Using search engines and previous compilations of strath terraces (e.g., Montgomery, 2004; Finnegan et al., 2014), we gathered data for 421 dated strath terraces from 78 studies (see Appendix A). We noted the strath age, dating method, whether the age sample was collected from within terrace materials or from the terrace surface, and whether the age represents strath planation or strath incision. Ages presented in this compilation are all in calendar

years before present. For terraces that were dated multiple times, we chose the age that is closest to when the strath was incised. For example, in a suite of radiocarbon ages wherein each age represents the deposition of the dated material when the strath was an active surface, the youngest age is taken as the best estimate of the end of strath planation and beginning of strath incision. We also noted the strath terrace location, strath lithology, and the forcing mechanism attributed to strath planation and incision.

To recognize how well supported the ascribed forcing is, we noted whether each terrace had independent evidence linking strath incision or planation to the identified forcing. Independent evidence used to locally relate strath formation to a forcing included morphologic, palynologic, or isotopic data. Strath terraces lacking independent evidence were those to which a forcing was attributed based solely on age correlation.

For terraces attributed to climate, we noted whether the terrace was attributed to marine isotope stage (MIS) glacial cycles or to shorter-term climatic fluctuations. If study authors related the terrace to MIS glaciations, then we additionally noted when planation and incision occurred within the glacial cycle. To examine whether volcanism, tectonics, climate, or human actions can account for Holocene strath terraces that currently lack an identified forcing, we used data sets of active volcanoes (Smithsonian Institution, 2013), peak ground acceleration (Giardini et al., 1999), and glacial maximum ice extent (Ehlers et al., 2011), and literature reviews on Holocene climate fluctuations and deforestation age (see Appendix A for site-specific references) to compare against terrace location and age.

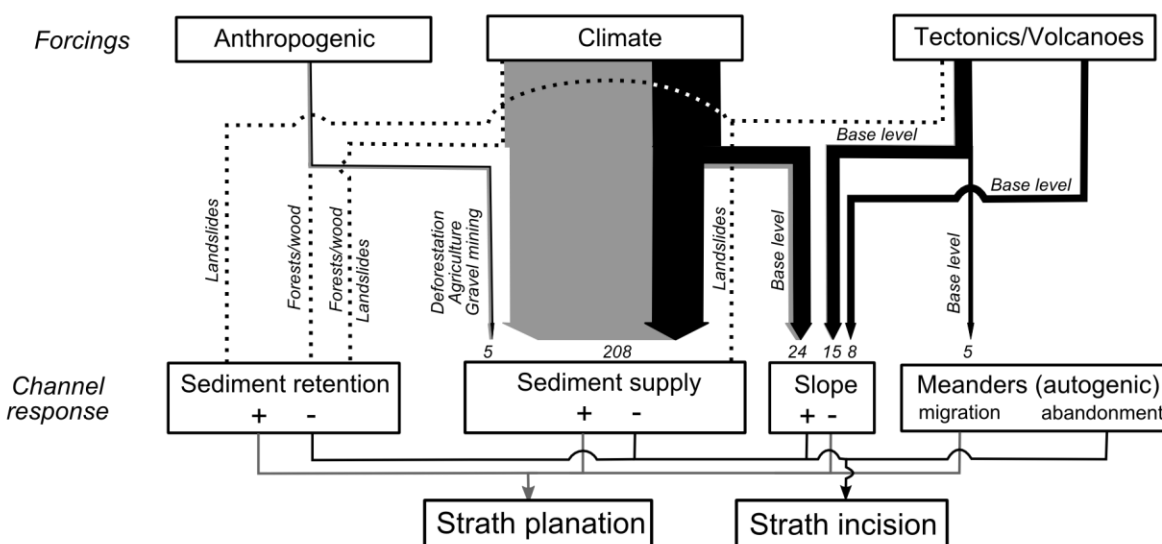


**Figure 3.2.** External forcings enact channel response through a variety of pathways, eventually leading to incision or planation of a strath. The line thickness of pathways between forcings and channel responses represent the number of strath terraces in our database attributed to that pathway, with the total above the associated channel response. Black lines represent strath terraces that had independent evidence for the ascribed forcings, while gray lines indicate that only strath age was used to assign the forcing. Dashed lines are hypothesized pathways between forcings and stream variables, as discussed in the text. Climate enacts a sediment supply response in numerous ways, which include changes in the rate of mechanical and chemical weathering, landsliding, glacial erosion, and fluvial erosion and transport (see section 3.1.1 for details).

### 3.4 RESULTS

#### 3.4.1 Causes of strath terrace formation

Of the 421 strath terraces in our compilation, 232 (55%) were attributed to climate, 20 (5%) to tectonics, 8 (2%) to volcanoes, 5 (1%) to anthropogenic activity, and 156 (37%) lacked an identified forcing (Figs. 3.2 and 3.3). Comparing forcing mechanism against the original study date showed no discernable bias in attributed forcing mechanism with time (Appendix B). Figure 3.2 shows the pathways between each external forcing and the channel response that led to strath planation and incision. The arrows connecting forcings to channel response represent the pathways taken by the 265 strath terraces in our database that were ascribed to a forcing, with thickness of

arrows showing the proportion of terraces and black or gray color indicating whether the path between forcing and channel response had or lacked independent evidence for the forcing respectively.

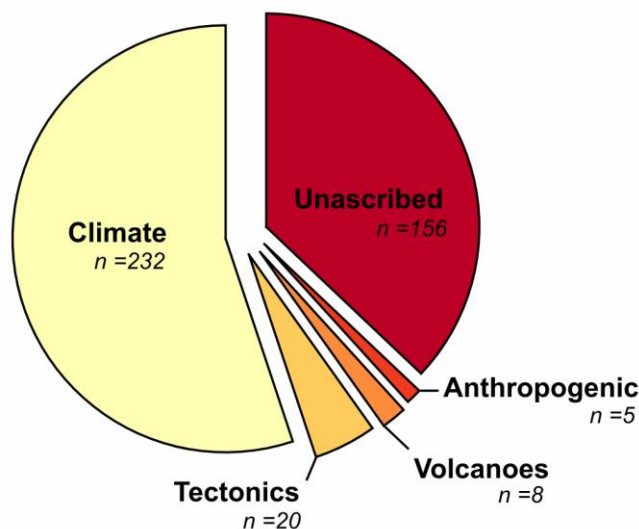


**Figure 3.3.** The distribution of external forcings attributed to strath formation. Numbers represent the total number of terraces in our database attributed to each forcing.

Of the 265 strath terraces that were assigned a forcing, under half ( $n = 103$ ) had independent evidence of the assigned forcing. Nearly all (98%) of the terraces lacking evidence were from strath terraces attributed to climate (Figs. 3.2 and 3.4). All terraces ascribed to volcanic forcings had independent evidence linking strath formation to volcanic forcings; however, these terraces are from a single study (Baynes et al., 2015). Anthropogenic strath terraces are almost evenly split between having and lacking independent evidence but come from only four studies (Lewin et al., 1991; Carcaillet et al., 2009; Wegmann and Pazzaglia, 2009; Molin et al., 2012). Strath terraces attributed to tectonic activity, from only seven studies (Appendix A), were mostly ascribed to a forcing with independent evidence, but whether this is because it is easier to find supporting evidence of tectonic forcings or if this finding reflects the small sample size is unclear. Forty-seven

studies include climatic strath terraces, and 68% of those terraces were attributed to a forcing based on age correlation alone. The greater number of studies involved, which include 232 sets of strath terraces, suggest that the high proportion of climate strath terraces lacking independent evidence of climate forcing is not caused by a skewed sample size. Rather it may be reflective of whether such evidence was available and within the scope and budget of the study.

In the following sections, we review how these four forcings influence channel response and lead to strath planation and incision. We draw from studies that used terrace age and independent secondary evidence to assign a forcing because these studies, in general, were more likely to describe the pathways and channel response between forcing and terrace formation. As indicated by Fig. 3.2, multiple pathways connect each forcing to strath terrace formation.

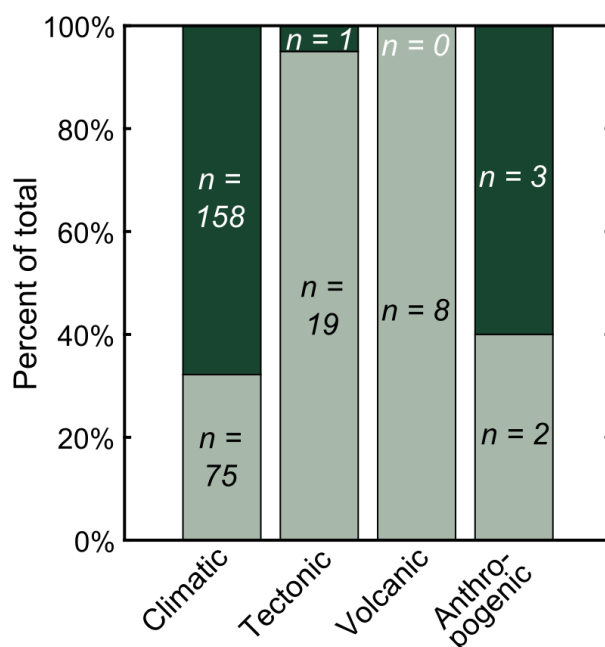


**Figure 3.4.** The proportion of strath terraces having (light green) and lacking (dark green) independent evidence of the assigned forcing. See Methods for definitions and examples of independent evidence.

#### 3.4.1.1 Climate

Strath planation is attributed most frequently to increased sediment supply during the transition from glacial to interglacial periods ( $n = 31$ ) and during glacial periods ( $n = 81$ ) (Figs. 3.2 and 3.5). In the nonglaciaded Oregon Coast Range, Personius et al. (1993) used a suite of radiocarbon ages to determine that strath planation occurred during the glacial to interglacial transition. Concurrently increased landsliding in the central Coast Range, driven by early Holocene increased storminess, was dated by Reneau et al. (1990) and likely led to the stream aggradation and strath planation documented by Personius et al. (1993). In the Bhagirathi Valley, Himalaya, cosmogenic exposure ages of strath terraces are similar to optically stimulated luminescence (OSL) ages of glacial sediment, implying that remobilization of glacial debris caused strath planation in glacial to interglacial transitions (Barnard et al., 2004). However, glacial debris in New Zealand and Italy was found to be transported earlier in the glacial cycle, causing strath planation to occur within the full glacial period (e.g., Formento-Trigilio et al., 2003; Picotti and Pazzaglia, 2008). In the nonglaciaded South Fork Eel River, California, OSL dates on terraces and pollen lake records show strath planation occurred during a wet interglacial period (Fuller et al., 2009). The wetter period likely led to more landsliding and sediment delivery to the river, leading to strath planation (Fuller et al., 2009).

Taken together, these studies demonstrate that the timing of strath planation varies with the timing of increased sediment supply which, in turn, depends on precipitation and vegetation patterns in nonglaciaded basins (Personius et al., 1993; Fuller et al., 2009) and the mobilization of glacial debris in glaciaded basins (Formento-Trigilio et al., 2003; Barnard et al., 2004; Picotti and Pazzaglia, 2008).

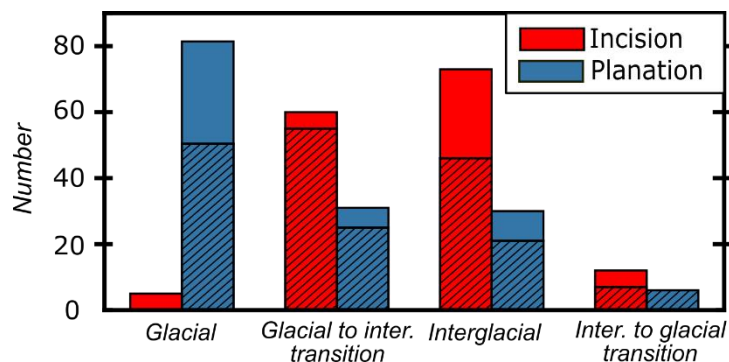


**Figure 3.5.** Timing of strath incision (red) and planation (blue) in response to global climate, subdivided into glacial periods, glacial to interglacial transitions, interglacials, and interglacial to glacial transitions. Strath terraces located in temperate regions are shown by the hatched bars, while arid regions are shown as plain bars.

Fewer studies have described strath incision during glacial cycles, and from these studies, no generalizable path is evident between MIS forcing and channel response leading to incision. While the timing of strath incision cannot be dated directly, the timing of incision can be constrained using the oldest age obtained from the next lowest terrace, giving a minimum estimate of incision time. This age, in combination with the youngest planation age of the strath terrace of interest, provides a maximum bound of the terrace formation timing. In such a manner, incision in the Oregon Coast Range was estimated to occur in the Holocene interglacial, after revegetation decreased the sediment supplied from hillslopes (Personius, 1995). In the Somme and Seine rivers, France, Antoine et al. (2000) used palynological and sedimentological data to infer that stream discharge increased during interglacial to glacial transitions but that cohesive hillslope vegetation limited the colluvial sediment input. Sediment supply remained low while transport capacity increased, enabling river incision and strath terrace formation during the transition to glacial periods (Antoine et al., 2000).

Incision can also be driven by an increase in river slope caused by climate-induced base level fall. Draining of Glacial Lake Agassiz during deglaciation decreased base level and formed

a knickpoint at the mouth of the Le Sueur River, Minnesota (Gran et al., 2013). This knickpoint propagated upstream, creating strath terraces from 13 to 1.5 kya.

In examples from Taiwan and the Himalaya, straths were planed during periods of increased sediment supply unrelated to glacial cycles because of interstadial fluctuations in monsoon strength. In Taiwan, aggradation and planation of two sets of strath terraces was correlated with periods of intensified storm activity in the middle and late Holocene (Hsieh and Knuepfer, 2001). Periodic storms increased sediment delivery from hillslopes above the transport capacity, causing fluvial aggradation and strath planation. Then, rivers incised during an intervening cold and dry period in the middle Holocene owing to reduced sediment supply. In the Himalaya, Kothyari et al. (2016) found strath planation corresponded with a strengthened Indian summer monsoon. However, even within neighboring drainages, rivers responded asynchronously, and only one of the two rivers studied planed a strath during early Holocene monsoon intensification (Kothyari et al., 2016).

Early Holocene warming at ~12.7-12.5 and 10 kya initiated an extended period of strath planation in the Tibetan Plateau (Haibing et al., 2005; Mériaux et al., 2005). The warmer and wetter climate during these times increased sediment supply, which led to increased lateral river erosion and planation. After the early Holocene warm period, sediment supply was reduced and river incision initiated. In northeastern Tibet, late Holocene strath terraces were created by punctuated river incision during warm intervals in an arid climate (Van der Woerd et al., 1998). Although the cause of strath planation could not be identified, cosmogenic exposure ages on the terrace surface indicate planation was coincident with early Holocene summer monsoon extension into NE Tibet. The summer monsoons would have transported sediment from the hillslopes into the channel, increasing the sediment cover and lateral mobility and planing a strath.



### 3.4.1.2 Tectonics

Tectonic activity leads to strath terrace formation through changes to base level induced by uplift and subsidence (Fig. 3.2). An increase in rock uplift rate over time will increase the river slope, driving regional incision and strath abandonment (e.g., Van der Woerd et al., 2001; Cheng et al., 2002) (Fig. 3.2). Pazzaglia (2013) noted, based on previous literature, that strath terraces formed from changes in rock uplift rate are more likely to be preserved in slowly deforming regions (e.g., Van Balen et al., 2000; Meyer and Stets, 2002; Gibbard and Lewin, 2009). Fault offset is a spatially discrete tectonic control on base level in which the river crosses the fault scarp and incision or planation may be promoted, depending on the sense of fault slip. For example, Harkins et al. (2005) dated a series of Holocene strath terraces resulting from periodic normal fault slip and slope adjustment along Big Sheep Creek, Montana, wherein the knickpoint originating from the fault scarp propagated upstream and abandoned strath terraces several kilometers upstream of the fault.

Tectonic uplift also contributes to autogenic terrace formation by providing a constant base level drop to sustain long-term incision (Fig. 3.2). Autogenic strath terraces form in meandering bedrock rivers from the combination of meander migration, steady incision, and meander cutoffs as described in Oregon and California (Merritts et al., 1994; Finnegan and Dietrich, 2011). In Oregon, the Smith River, confined within a narrow bedrock valley, formed strath terraces through the pinch-out of meanders, in which case the strath is the former riverbed (Finnegan and Dietrich, 2011). Along the Mattole River, California, where the river was able to meander across a wide valley, steady incision resulted in relative uplift of old meander belts and the formation of strath terraces (Merritts et al., 1994). Numerical simulations by Limaye and Lamb (2016) were able to form strath terraces by imposing a steady base level drop on a continuously meandering river, which formed terraces similar in geometry to those on the Mattole River. In these case studies,

incision was driven by gradual tectonic uplift of the landscape relative to sea level. Sediment and water supply did not need to change for terrace incision and planation to occur.

#### 3.4.1.3 Volcanoes

Changes to river slope induced by volcanic activity have led to strath incision (Baynes et al., 2015) and planation (Ely et al., 2012) (Fig. 3.2). In Iceland, volcanic eruptions near glaciers caused rapid melt and catastrophic flooding that rapidly eroded bedrock and formed knickpoints. Over time, upstream propagation of the knickpoint abandoned straths, creating terraces (Baynes et al., 2015). In this case, terrace planation was not explicitly addressed but was likely owing to preferential erosion along planar lava flow boundaries. The disruption and physical damming of rivers by lava flows can also determine whether rivers incise or plane; In eastern Oregon, Ely et al. (2012) used the age of lava flows and cosmogenic exposure ages of eroded surfaces to determine that lava dams could induce strath terrace planation and incision. Lava dams along the Owyhee River blocked or diverted water flow, lowering the upstream slope. As a result, the river upstream aggraded and widened, and incision rates slowed because of the development of an alluvial cover. Once aggradation reached the lava dam top, the bedload abraded the lava flow and rapidly incised at rates of  $\sim 1.8$  mm/y. Periodic lava dams created cycles of planation and incision, documented by the presence of narrow strath terraces carved into the flows (Ely et al., 2012).

#### 3.4.1.4 Human activity

In the last few thousand years, changes to sediment supply by human activity (e.g., Syvitski and Kettner, 2011) have been documented to drive planation and incision of strath terraces (Fig. 3.2). Two strath terraces in Albania and Greece were planed  $<1$  kya in response to increased sediment from logging and farming, with incision of the strath occurring when the sediment supply lowered post-disturbance (Lewin et al., 1991; Carcaillet et al., 2009). Late Holocene (3.5-1.5 kya)

strath terraces in Italy and Romania likely were incised in response to instream gravel mining, although whether incision was caused by mining-induced changes to slope or sediment supply was not clear (Wegmann and Pazzaglia, 2009; Molin et al., 2012).

In Washington State, USA, century-old strath terraces in the Teanaway and Willapa rivers formed coincident with anthropogenic deforestation, log drives, and the presumed resulting loss of instream wood (Collins et al., 2016; Schanz and Montgomery, 2016) (dashed lines in Fig. 3.2). Logging in these regions at the end of the nineteenth century and beginning of the twentieth century reduced the amount and size of wood in rivers and the supply of wood from riparian forests (Montgomery et al., 2003). Large wood in rivers can cause sediment deposition through the creation of eddies (Abbe and Montgomery, 1996) and jams that physically block sediment transport and increase sediment retention (Montgomery et al., 1996). As a result of the increased sediment retention from large wood, bedrock-floored channels can be converted to alluvial channels. Similarly, the removal of wood can convert a formerly alluvial channel to a bedrock channel (Montgomery et al., 1996; Massong and Montgomery, 2000; Faustini and Jones, 2003). Thus, the loss of large wood through logging, as well as the reduced size of wood from short-rotation forestry, can potentially decrease sediment retention and may convert alluvial channels to bedrock, thereby opening the channel to incision. Collins et al. (2016) and Schanz and Montgomery (2016) noted that artificial dam-burst floods, used to transport timber downstream, and slaking-prone bedrock likely enhanced incision rates in their study regions, leading to discernable strath terrace formation within a century.

### 3.4.2 *Constraining strath terrace age*

To understand what a single strath terrace age represents and to recognize how to compare terrace ages regionally and globally, we examine the different age methods and sample locations

used to date terraces in the database. Strath terraces in our database were dated using 14 different methods (Table 3.1). Samples for dating analyses were collected from the alluvium overlying the strath but below the terrace surface, from loess deposits and exposed cobbles that mantle the terrace surface, or from the top of the bedrock strath. In general, ages derived from samples collected within the buried alluvium that overlies the strath represent when the strath was an active surface and provide maximum age constraints on strath incision and terrace formation. Dating soils and loess deposits from the terrace top gives a minimum age of strath incision, as the soil and loess could not have accumulated until after the surface was abandoned. Similarly, exposed cobbles on the terrace surface, dated using cosmogenic exposure, also provide minimum ages of strath incision because the exposure of the cobble to cosmic rays could not occur until the surface was inactive. Bedrock samples taken directly from the exposed strath, dated for exposure to cosmogenic rays, record the time since the strath was created and thus represent a maximum age constraint on incision.

**Table 3.4. Strath dating methods**

	<b>Material location</b>		
	In terrace alluvium	Terrace surface: loess, cobbles	Top of bedrock strath
Radiocarbon	128	11	
Cosmogenic nuclides	11	32	30
Optically stimulated luminescence	93	11	
Thermal luminescence	5	5	
Paleomagnetism	2	4	
Magnetostratigraphy	4	4	
Electron Spin Resonance	13	2	
IRSL	3		
U/Th	10		
<b>Methods w/o material location:</b>	<b>Material location N/A</b>		
Previous literature reviews		12	
Slip rate		2	
Stratigraphic relationship		6	
Paleosol correlation		1	
MIS correlation		1	
Multiple methods		31	

Conversely, when considering the planation age of the strath rather than the incision age, material that formed or deposited once the terrace surface stabilized, such as soils, loess, and exposed cobbles, provide minimum ages of planation. Ages from bedload deposits on top of the bedrock strath, deposited while the strath was planed, provide the best estimate of planation age. Overbank floodplain sediment on top of the strath could either be deposited when the strath was planed or during incision into the strath, making it hard to interpret a date from such deposits. Cosmogenic exposure ages of the bedrock strath can also date the strath planation, assuming that no additional erosion occurred after the strath was originally planed.

The majority of strath terraces are dated using material from locations that give a maximum age of strath incision. Thirty percent of strath terraces were dated using radiocarbon found within the alluvial sands and cobbles that overly the strath (Table 3.1); this dates the deposition of the material while the strath was an active surface. The second most common method, accounting for 22% of the total, is OSL on fluvial sands in the terrace and also constrains the maximum age of incision. In contrast, the third most common method, representing 8% of our database, is cosmogenic nuclides on terrace surface deposits that dates material that may have become exposed after the terrace was abandoned, thus providing a minimum date of terrace incision. Overall, 71% of the terrace ages in our database are of material from the terrace alluvium or the bedrock strath and are maximum ages of incision. Sixteen percent of terrace ages are from terrace surface material and represent a minimum incision age. The remaining 13% are dated using relative age methods such as slip rate, stratigraphy, or MIS correlation or were dated using multiple methods with different sample locations, and so whether the ages represent a minimum or maximum estimate of terrace incision must be evaluated for each terrace.

Recognizing that the terrace age dates strath planation for most terraces in our database has

important implications for interpreting strath formation. Several studies have found that planation phases are much longer than incisional phases and span 10 ky at least (Wegmann and Pazzaglia, 2002; Collins et al., 2016; Schanz and Montgomery, 2016). Consequently, using a planation age to constrain the environmental forcing responsible for incision can result in substantial uncertainty in how closely the planation age approximates the onset of incision. If strath terrace formation is attributed to a forcing based on similar timing between age constraint and a known climatic, tectonic, volcanic, or anthropogenic event—as is done for 61% of terraces in our database—then the strength of the attribution depends on the original age constraint. The forcing responsible for incision is likely not well constrained if only a planation age is available; a more robust attribution would rely on either an incision age or on an estimated incision age derived from planation ages of two bounding sets of strath terraces.

### 3.4.3 *Timing of strath terrace formation*

Strath terrace ages in our compilation range from 2.9 Mya to 0.03 kya but are concentrated in the Holocene and late Pleistocene (Fig. 3.6). When terrace age is binned by 0.5 kya, the most frequent period of strath formation is 2-2.5 kya, though a generalized peak in terrace formation occurs during the late Holocene from 4 kya to present (Fig. 3.6B). The age distribution of terrace formation also exhibits local maxima during the middle Holocene, from ~5-6.5 kya, and in the early Holocene from 11-11.5 kya.

All four forcings—climate, tectonics, volcanoes, and human action—formed strath terraces in the Holocene, but the relative frequency of each forcing varies. Tectonic terraces are not common but are evenly spread throughout the Holocene, whereas terraces attributed to volcanic activity are infrequent but cluster near the time of volcanism and associated river incision (Baynes et al., 2015). The five terraces identified as caused by anthropogenic forcings all date to after 4.5

kya. Climate is the attributed cause of most terraces in the early Holocene, but the relative frequency of climate-induced strath terraces decreases toward the present day. Instead, although the number of terraces reaches a peak in the late Holocene from 4 kya to present, terraces formed because of climate become less frequent and terraces without an identified forcing make up the majority. In section 4.2, we discuss possible causes of late Holocene terrace formation.

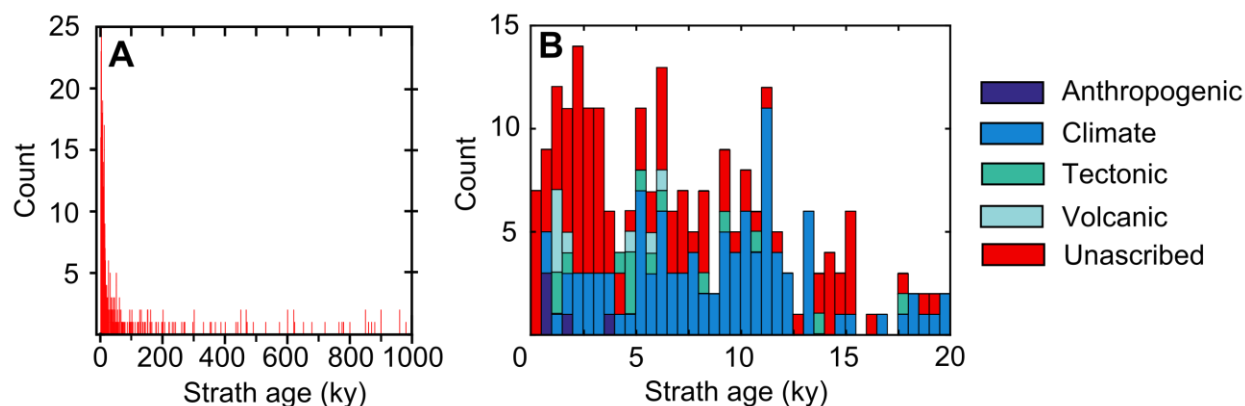


**Figure 3.6.** (A) Age distribution of strath terraces in our database over the last million years. Age is binned by 1 ky. (B) Age distribution for the last 20 ky in 0.5 ky bins and colored by the ascribed forcing.

### 3.5 DISCUSSION

#### 3.5.1 *Global, regional, and watershed controls on terrace formation*

Our results show that a number of general pathways exist between forcing and strath terrace formation (Fig. 3.2) and that these pathways, especially for climate forcings, are modified by global, regional, and watershed-scale characteristics that individualize river response. Bull (1990) recognized that global climate has variable impacts on the landscape when he observed that regional climate zones controlled the timing of aggradation, with rivers in humid and mesic climates aggrading in full glacial periods while arid rivers aggraded in interglacial periods. Moreover, rivers within each climate zone recorded different numbers of aggradation events based

on watershed lithology and vegetation. The strath terraces documented by decades of research since Bull's (1990) findings make it possible to elaborate on how regional and watershed controls interact with global climate forcings on strath terrace formation.

Global-scale MIS climatic variations are often modulated by regional climate patterns, which affect when sediment is produced and transported, thus controlling when straths are planed and incised. In the arid Gobi-Altay range, Mongolia, Vassallo et al. (2007) used cosmogenic exposure ages on terraces and alluvial fans to determine that strath planation occurred during wet interglacial periods when sediment produced in the glacial period was mobilized. In this case, the stream system is transport-limited through most of the glacial cycle. In contrast, rivers in temperate climates appear to be supply-limited during the majority of the glacial cycle, and straths are planed when sediment supply increases in association with MIS variations. In New Zealand, sparse vegetation, indicated by terrace stratigraphy and climate proxy data in the Huangarua River, allowed high hillslope runoff, thereby increasing sediment supply and causing channel braiding and strath planation (Formento-Trigilio et al., 2003). However, strath planation can also occur in interglacial periods in temperate climates. Optically stimulated luminescence (OSL) ages of strath terraces along the South Fork Eel River, California, show strath planation in a temperate climate occurred during interglacial periods, caused by increased sediment supply from precipitation-driven landsliding (Fuller et al., 2009). In the Oregon Coast Range to the north, radiocarbon dates of strath terraces and colluvial hollows also show a temporal correlation between increased landsliding and strath planation in interglacial periods (Personius, 1995). Although these latter two examples support that rivers in temperate climates tend to be supply limited, the timing of increased sediment supply in response to MIS glaciation differs from that found by Formento-Trigilio et al. (2003) and may be indicative of watershed-scale controls on sediment supply.



At the watershed-scale, characteristics such as rock type and glacial proximity further modulate the influence of global climate change on strath terrace formation. In the Musone and Bidente rivers, Italy, radiocarbon ages of strath terraces formed in the two adjoining basins reveal asynchronous strath planation caused by lithologic differences (Wegmann and Pazzaglia, 2009). Carbonate rocks in the Musone basin are subject to rapid periglacial weathering during glacial periods, resulting in high sediment supply. The carbonate sediment helps plane a strath at the onset of glacial periods, but continuous supply causes the river to aggrade and lose contact with the underlying bedrock strath during the full glacial period. In contrast, thinner alluvial deposits overlying the siliciclastic Bidente basin straths indicate less sediment is produced from glacial weathering and so strath planation occurs throughout the glacial period. In the Le Sueur basin, Minnesota, terrace formation was controlled by glacial retreat and the draining of glacial Lake Agassiz, which lowered base level for the Le Sueur River and created a knickpoint (Gran et al., 2013). Watershed-specific characteristics, unspecified by the authors, caused periodic knickpoint stability along the Waihuka River, a tributary of the Waipaoa River in New Zealand, and created unique sets of strath terraces (Berryman et al., 2010). While all tributaries of the Waipaoa River incised in response to increased discharge and decreased sediment supply in the Holocene (Eden et al., 2001), the Waihuka River terraces differ in age from other tributary terraces because of the lithologic control on knickpoint propagation singular to the Waihuka basin.

The extent to which regional and watershed controls affect strath terrace formation in response to global climate is only discussed for 55 of the 232 strath terraces attributed to climate in our database, thus making it hard to ascertain the extent of regional and watershed controls. Of strath terraces attributed to climate, 68% of these were based on temporal correlation between terrace age and MIS stage, and thus those studies did not consider regional or watershed controls

on terrace formation. However, the range in timing of strath formation in response to MIS cycles suggests that regional and watershed controls affect strath formation in many locations. If no intermediary control between MIS climate and strath terrace formation existed, then strath terraces should be planed and incised at similar times. While strath planation predominantly occurs during glacial periods and strath incision is most common in interglacials (Fig. 3.5), this general trend only holds for 55% and 49% of climatic terraces in our database respectively. Contrasting arid and temperate climates shows that generally more terraces are found in temperate regions, but that no recognizable pattern to when straths are incised and planed relative to regional climate is evident. Because several studies, discussed above, demonstrate that regional climate affects the timing of strath incision and planation, the lack of a systematic trend in Fig. 5 implies that watershed-scale controls add further heterogeneity and complexity to the timing of strath formation in response to climate.

Considering that the effect of global forcings on rivers can be influenced by regional and watershed scale variables, channel response is more varied and complex than shown in Fig. 3.2. Rather than the single arrow from climate to channel response, the pathway should go through filters of regional and watershed controls. Figure 3.7 shows an example diagram of pathways using the subset of studies that we discussed above (Personius, 1995; Formento-Trigilio et al., 2003; Vassallo et al., 2007; Fuller et al., 2009; Wegmann and Pazzaglia, 2009) in regard to the process of strath planation only. Incorporating the spatial levels of controls on strath terrace formation, the pathway from global climate change to channel response branches into distinct routes rather than the single line shown in Figs. 3.2 and 3.7A. Each line represents the path through regional and watershed controls on sediment transport capacity and sediment supply that a single location experiences. Despite the same original global forcing through which sediment transport and supply

are ultimately altered, the timing of strath planation varies depending on the pathway (Fig. 3.7B).

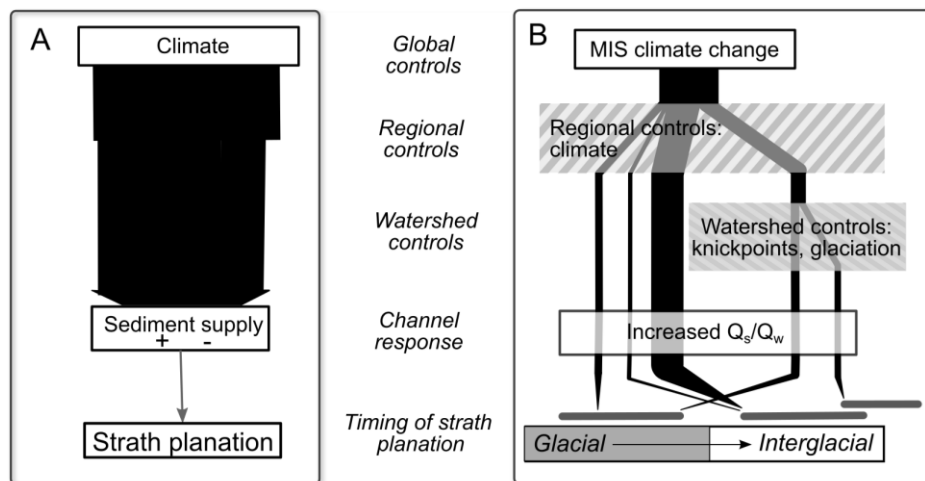


**Figure 3.7.** Pathways from global climate forcings to channel response causing strath planation, contrasting (A) the simplified path from Fig. 2 and (B) the pathways emerging once regional and watershed controls are considered. Black lines in (A) represent the influence of climate on base level, fluvial and glacial erosion, weathering rates, and landsliding rates. In (B), the pathway from MIS climate to planation passes first through regional then watershed controls. The timing of strath planation within the glacial cycle is shown as a grey bar indicating planation in glacial period, interglacials, or transitions between. The thickness of lines represents the number of straths following each path. Each black line represents a different study site and different regional and watershed controls.

### 3.5.2 Resolving potential forcings for late Holocene strath terraces

Terrace frequency in our database peaks from 4 kya to present (Fig. 3.6B), yet terrace formation in the late Holocene does not align with the prevalent idea of glacial cycle forcings. Indeed, most terraces formed during this time are unattributed to any forcing. What caused strath terraces to form in the last 4 ky? Without conducting detailed field investigations of the channel conditions at the time of terrace formation, we cannot definitively assign these terraces to a particular forcing. However, below we use literature reviews of Holocene climate and deforestation and databases of volcanic, tectonic, and glacier activity to further assess the

likelihood of volcanic, tectonic, glacial, and anthropogenic forcings on late Holocene strath terrace formation.

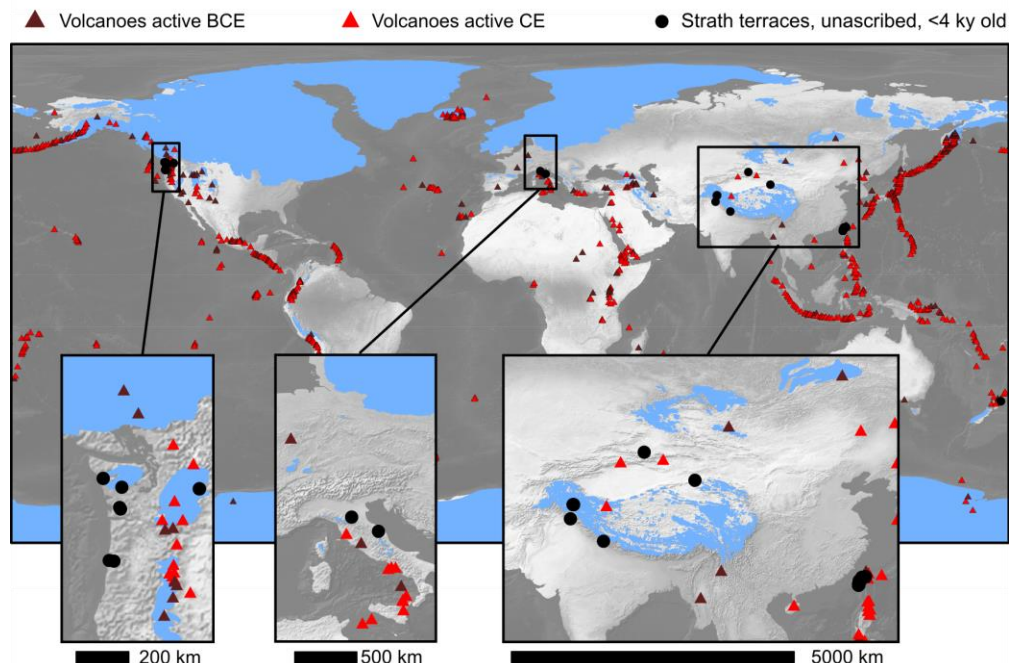


**Figure 3.8.** Locations of late Holocene unscribed strath terraces compared with locations of volcanoes active in the late Holocene and Last Glacial Maximum (LGM) ice extent. Volcanoes are differentiated by whether the last recorded eruption was during current era (CE) or before current era (BCE). The GIS information for the volcanoes and LGM extent are from the Smithsonian Institution (2013) and Ehlers et al. (2011) respectively.

### 3.5.2.1 Volcanic forcings

Comparing volcanic activity in the late Holocene to strath location (Fig. 3.8) shows that 33 of 52 unscribed late Holocene terraces are located more than 100 km away from volcanic centers, making it unlikely that an eruption could trigger strath terrace formation. Of the remaining 19 terraces, 17 are 75 km or farther from active Holocene volcanoes and are also unlikely to be affected by recent eruptions. Lava flows from volcanoes 75 km away are unlikely to dam the river, causing strath planation and incision in the manner documented by Ely et al. (2012). Baynes et al. (2015) found volcanic activity melted ice caps and caused large outburst floods; this is probably

not the cause of the late Holocene terraces lacking an identified forcing because none of the 52 terraces are located in regions with active ice cover and with volcanoes (Fig. 3.8).

### 3.5.2.2 Tectonic forcings

Tectonic forcings produced terraces in our compilation through autogenic processes and increased slope caused by long-term changes in uplift rates or fault offset. Autogenic processes create predictable terrace geometries for given lateral and vertical erosion rates because of characteristic meander bend shapes (Limaye and Lamb, 2016). Terrace geometry is not described for all of the unattributed late Holocene terraces, but 31 of the 52 are found in Taiwan, where they were described as short in length and unpaired (Yanites et al., 2010b). Given the vertical erosion rates of 2-3 mm/y on average and up to 11 mm/y (Dadson et al., 2004; Yanites et al., 2010b), lateral erosion rates would need to be ~18-50 mm/y to create short and unpaired autogenic terraces. However, field observations by Yanites et al. (2010a) and Turowski et al. (2008) suggested lateral erosion rates can be in excess of 180 mm/y and locally up to 1000 mm/y. That the morphology and erosion rates of the majority of late Holocene unattributed terraces does not match predicted autogenic terrace form suggests that autogenic forcings are unlikely to be responsible for terrace formation.

Tectonic activity could cause terrace incision in the late Holocene through fault offset or increasing uplift rates. Without detailed site investigation, we cannot adequately determine the late Holocene fault activity at each study location. However, using peak ground acceleration (PGA), we can classify the localities in the manner of Portenga and Bierman (2011), in which sites expected to experience a magnitude 2.0 earthquake or greater in the next 50 years, or a PGA of 2.0, are considered tectonically active. Of the 52 late Holocene unattributed terraces, 49 are in regions with a PGA of 2.0 or greater and are thus classified as tectonically active (Appendix A).

Of those tectonically active sites, the median PGA is 4.9. The high proportion of late Holocene unattributed terraces in tectonically active regions implies tectonics could have driven the incision of some of these terraces.

### 3.5.2.3 Climatic forcings

The age and location of the late Holocene terraces with no identified forcing make it unlikely that they were formed in response to MIS-scale climatic forcings. The influence of MIS cycles, quantified by the number of terraces ascribed to climate, appears to peak at the Pleistocene-Holocene transition and declines toward the present (Fig. 3.6B). Previous studies in which strath incision occurred in an interglacial period attributed that incision to local base level fall caused by the draining of glacial lakes during ice retreat (e.g., Gran et al., 2013). However, 60% of the late Holocene strath terraces are located in Taiwan, which was sparsely glaciated with mountain glaciers during the LGM (Ono et al., 2005; Fig. 3.8), thus glaciation likely did not cause ice-dammed lakes or affect local base level. Approximately half of the remaining 40% of late Holocene strath terraces are located in regions that were not glaciated at the LGM at all, further removing the possibility that local base level fall caused by glacial retreat is responsible for strath incision (Fig. 3.8). Global base level fall during glaciation can cause strath incision; but if this is the case, then the strath planation ages would predate glaciation. However, 43 of the 52 late Holocene terraces are dated using methods that provide a planation age and so are too young to have formed in response to base level fall from glaciation.

Terrace formation at 4 kya does, however, coincide with fluctuations in Asian monsoon strength and temperature for the 31 terraces in Taiwan. Dates for these terraces, all representing terrace planation, cluster at 2.2 kya, which suggests incision occurred after 2.2 kya. Planation of these terraces may be caused by warm and wet conditions in Taiwan that start between 2.5 and 1.5

kya, as quantified by lake pollen records (Liew and Hsieh, 2000). Increased landsliding associated with this wetter period would increase the sediment supply and cause planation. Additionally, monsoon strength increased periodically over centennial to multidecadal scales during the late Holocene (Dykoski et al., 2005). Increased monsoon strength has previously been tied to increased landsliding and sediment supply, which led to strath planation (Hsieh and Knuepfer, 2001) and may be another mechanism by which Holocene climate fluctuations caused the planation of the unascribed terraces in Taiwan. However, the cause of terrace incision after 2.2 kya is unclear; the warm and wet conditions that started 2.5-1.5 kya, and likely contributed to planation, continue to present day.

The remaining 21 terraces in the late Holocene are found in the Pacific Northwest ( $n = 10$ ), the Himalaya ( $n = 7$ ), New Zealand ( $n = 2$ ), and Italy ( $n = 2$ ). Except for three terraces in the Himalaya, terrace age represents planation. Planation may be in response to increased sediment supply during warm and wet conditions, which occurred globally between 1.1 and 0.7 kya, or from glacial advance and increased sediment supply, which occurred from 2.9 to 2.3 kya in the Pacific Northwest and from 0.9 to 0.8 and 0.55 to 0.1 kya in the Himalaya, New Zealand, and Italy (Mayewski et al., 2004; Wanner et al., 2008). The timing of planation in response to glaciation may vary by regional climate (see section 4.1) but would in general occur in temperate regions during glaciation when sediment is produced, or, for arid regions, after glaciation when wetter conditions promote sediment transport. Comparing planation age against the timing of these glacial advances and warm periods, 12 of the 21 terraces are possibly planed because of climate, while six have planation ages incompatible with interglacial climate variations. The remaining three terraces are inconclusive, based on the age dates and available global climate proxies.

Additionally, interglacial climate fluctuations affect forest composition, which affects the magnitude of sediment retention provided by instream wood. Changing the abundance, size, or durability of wood pieces and wood jams, in turn, can influence how freely sediment can move through the system and thus whether a bedrock channel bed is covered or exposed to erosion (Collins et al., 2016). Wood jam abundance can be altered by variations in fire frequency that are driven by regional climate fluctuations within an interglacial period (Weisberg and Swanson, 2003). The frequency of stand-replacing fires will directly affect the supply of wood for jams, as well as the longevity of existing jams. In Taiwan, wood delivery is often concomitant with monsoon storms (Chen et al., 2013); changing the intensity of monsoons would thus affect instream wood and related sediment retention. Similarly, wood delivery to low-order streams often occurs through debris flows (May and Gresswell, 2003), which would also be sensitive to changes in storminess.

Climate-driven changes to sediment retention could interact with climatic effects on sediment supply and transport (Collins et al., 2016). Weisberg and Swanson (2003) found fire frequency in Oregon and Washington during the last 600 years increased during warmer climatic conditions and decreased during cool conditions. During the warmer periods, stand-replacing fires are potentially more frequent and would periodically decrease wood supply and sediment retention. If so, sediment retention would then be higher during cool periods and lower during warmer periods, potentially resulting in more incision during warm periods and less in cool periods. Since warm conditions tend to be wetter with a higher sediment supply, promoting strath planation, sediment retention changes through stand-replacing fires may lead to punctuated intervals of river incision in a period that is otherwise characterized by planation. The combination of planation from climatically driven changes to sediment supply and incision from fire-caused



retention loss could perhaps help explain the formation of some of the unattributed late Holocene strath terraces in our database.

#### 3.5.2.4 Anthropogenic forcings

Wood supply to river channels and associated changes to sediment retention can also be altered by human activities such as deforestation, logging, and fire suppression. Previous work in Washington State proposed a possible temporal link between splash-dam logging (in which wood jams and associated alluvium were flushed from the system by artificial floods) and the formation of century-old strath terraces (Collins et al., 2016; Schanz and Montgomery, 2016). In Taiwan and the Pacific Northwest, the locations of 41 of the 52 late Holocene unattributed terraces, fire frequency increased with the onset of agricultural activity (Weisberg and Swanson, 2003; Lee et al., 2014) and would have additionally decreased sediment retention over the long term.

To consider if anthropogenically triggered reduction in supply of wood to streams and the associated loss of retention drove the formation of strath terraces in the last 4 ky, we compared terrace age against the earliest record of deforestation and agriculture. Regional deforestation age was found using literature reviews for each strath terrace younger than 8 ky and with no identified forcing (see Appendix A for dates and references). We use the regional deforestation age as a maximum age for when sediment retention could be lowered, as local deforestation and anthropogenic fires (especially in remote upland areas) may have occurred after the onset of regional deforestation.

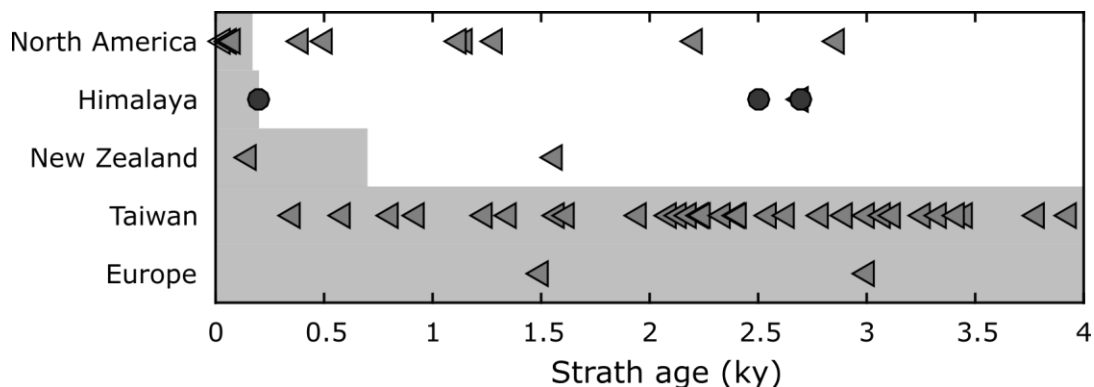


**Figure 3.9.** Ages of late Holocene terraces without an attributed forcing compared with deforestation age for each region. If the terrace age represents terrace planation, the age is marked with a triangle to show that it is a maximum constraint on incision. Terrace ages that date incision are shown as circles. Deforestation age, marked by the gray shading, is for the region in which terraces are found and is a maximum constraint on when local deforestation occurred. All deforestation ages come from literature reviews, as reported in Appendix A.

Strath terrace age is compared against deforestation age in Fig. 3.9. Only three terraces are dated using techniques that provide the strath incision age; of these, one terrace was incised at the same time as the onset of deforestation and the expected decrease in retention. The other two terraces, incised between 2.5 and 2.7 kya, predate the regional onset of deforestation and thus are not formed in response to anthropogenic retention changes. The remaining 49 terraces are dated using techniques that give a planation age. For those outside of the gray boxes in Fig. 9, planation predates the onset of deforestation. These terraces are possibly influenced by deforestation-related retention changes if terrace incision occurred well after planation. For terrace planation ages within the gray boxes, planation occurred after the regional onset of deforestation. However, retention changes may have occurred after the onset of deforestation; rotation forestry would decrease retention each time harvest occurred, and upland areas were likely logged after the onset of regional deforestation. Additionally, anthropogenic fire regimes could reset retention during any point after the onset of deforestation. Thus, for this latter group of terraces, human-caused decreases to retention remain a plausible influence on terrace formation. In summary, 49 of the 52

unascribed late Holocene terraces could have been influenced by human action and decreased retention.

#### 3.5.2.5 Late Holocene terrace forcings

The analyses in this section points to several plausible potential drivers of the unascribed late Holocene terraces. While volcanic activity is not a viable forcing for many of the 52 terraces, interglacial climate fluctuations, human-caused loss of wood recruitment and an associated reduction of sediment retention, and tectonic activity are all possible forcings for many of the terraces. Six terraces are possibly influenced by all three, while 46 of the 52 terraces are likely to be influenced by at least two of the aforementioned forcings.

Our examination of late Holocene strath terraces emphasizes the importance of critically assessing the role of global and regional variations in climate, human, and tectonic action on strath terrace formation. Few previous studies have considered the effects of interglacial climate on terrace formation; however, that monsoon strength shifted significantly and glaciers regionally advanced and retreated in the late Holocene suggests that sediment supply and transport may have varied enough to carve and incise strath terraces. Additionally, the influence of variations in fire frequency and forest structure within an interglacial on sediment retention has received little attention but may be important in the formation of Holocene strath terraces. In the last few thousand years, anthropogenic changes to sediment retention are also an important factor in controlling strath incision and have only been explored in a few studies (Collins et al., 2016; Schanz and Montgomery, 2016). Studies of late Holocene terraces should consider watershed and regional climate and anthropogenic factors when determining or ascribing a cause for strath terrace formation.

### 3.6 CONCLUSION

To examine how and when strath terraces form, especially in response to global climate cycles, we compiled a database of 421 dated strath terraces and used terrace age, age dating method, location, and attributed forcing to examine the multiple pathways, modulated by global, regional, and watershed controls, between strath terrace formation and external forcings (climate, tectonics, volcanoes, and humans). The largest portion of strath terraces are attributed to climate in the form of MIS glacial cycles, but the timing of terrace formation is dependent on regional and watershed factors such as vegetation, rock type, glacial proximity, and precipitation patterns. These exert a first-order control on sediment supply and transport capacity and result in terraces attributed to MIS climate forcings being beveled and incised at different times within a glacial cycle. This finding highlights the need to investigate basin-specific landscape response when attributing strath terrace formation to a landscape forcing. The channel variable responsible for incision or planation should be identified, and the pathway between the forcing — climatic, tectonic, volcanic, or anthropogenic — and channel variable investigated in regard to regional and watershed controls. Additionally, dating methods give different constraints on strath age and are often better estimates of strath planation than incision, complicating the correlation of forcings with strath incision.

Strath terraces ascribed to tectonic activity formed in response to steady rock uplift, changing uplift rates, and fault offset. Volcanic forcings included lava dams, which controlled when rivers incised and planed straths, and eruption-induced floods that altered the river slope. Anthropogenic forcings caused planation from post-settlement alluviation but also drove strath incision from gravel mining and loss of sediment retention from logging. Sediment retention could also potentially be affected by climate variations that alter fire frequency and forest structure. In

the last 4 ky, terrace frequency increased, yet most terraces are unattributed to a forcing. Our results indicate tectonics, interglacial climate changes, and human activity each could potentially have planed and incised strath terraces during this time.

## Chapter 4. ANTHROPOGENIC STRATH TERRACE FORMATION CAUSED BY REDUCED SEDIMENT RETENTION

### 4.1 ABSTRACT

Previous work on anthropogenic river incision has focused on alluvial systems, where rapid erosion and widening has been noted across North America and globally. However, instances of anthropogenic incision into bedrock rivers is limited to local or isolated outcrops. Here, we test whether splash-dam logging, which reduced stream-bed alluvial cover by reducing the amount of alluvium-trapping in-channel wood, caused basin-wide river incision and bedrock terrace formation in a forested mountain catchment in Washington State. We date incision of the youngest of four strath terraces using dendrochronology and radiocarbon dating to between 1893 and 1937 CE in the Middle Fork Teanaway River and 1900 and 1970 CE in the West Fork Teanaway River, coincident with timber harvesting and splash damming in the basins. Other potential drivers of river incision are unlikely to cause the incision, based on the lack of a mechanism or strength of the driver. That and the close temporal correspondence suggests splash damming led to the observed 1.1 to 23 mm yr<sup>-1</sup> of bedrock river incision and reduction of the active floodplain to only 20 to 53% of its pre-incision extent. River incision has had cascading effects on watershed ecology and left an emerging physiographic signature of the Anthropocene. Globally, anthropogenically-reduced wood loads and lowered sediment retention throughout the late Holocene, coincident with late Holocene strath terrace formation, suggests changes to the retention of sediment in bedrock channels mediated by changes to in-channel wood may be a more prevalent driver of river incision than previously recognized.

## 4.2 INTRODUCTION

Anthropogenic river incision has swept westward across North America following the spread of mill-damming, agriculture, large-scale grazing, and deforestation. Severe modification of alluvial systems began by at least the late 1600s with mill dams on the Atlantic Piedmont that impounded sediment and caused subsequent incision when dams were breached or abandoned (Walter and Merritts, 2008). Surface erosion, channelization, and abandonment of diversion structures from agriculture and ranching enhanced channel incision and arroyo formation in alluvial systems in the American Midwest and Southwest (e.g., Knox, 2006; Nichols et al., 2018; Waters and Haynes, 2001), and overgrazing aggravated climatically driven gully incision and erosion in California (Montgomery, 1999; Perroy et al., 2012). Construction around urban waterways, followed by continued urbanization, increased peak flows and caused dramatic widening and excavation (e.g., Trimble, 1997; Wolman, 1967). The effects of human activity in triggering river incision in alluvial channels have been noted all across North America (Montgomery and Wohl, 2003).

In contrast, evidence for recent, human-induced incision into bedrock is limited to a few local exposures of strath terraces in the Pacific Northwest (Fig. 4.1). A saw-cut stump resting in the alluvium overlying an isolated bedrock (strath) terrace 100 m wide in the West Fork Satsop River shows 1.2 m of bedrock incision post 1940s logging (Montgomery, 2004). Locally exposed and century-old strath terraces in the Willapa River (Schanz and Montgomery, 2016) and West Fork Teanaway River (Collins et al., 2016) formed coincident with splash-damming, in which timber is transported downstream to mills in forceful dam-burst floods. Terrace incision was suggested to be in response to the loss of log jams from clearing of the channel before and during splash-damming as well as the loss of recruitable large wood from timber harvest (Collins et al.,

2016; Schanz and Montgomery, 2016). The underlying mechanism of reduced sediment retention is inferred from studies that show log jams retain sediment on the channel bed and force an alluvial cover (Massong and Montgomery, 2000; Montgomery et al., 1996). Hence, loss of such wood has been hypothesized to have exposed the underlying bedrock to incision. These prior observations of bedrock incision are local and rely on a few dates to correlate incision with human action.

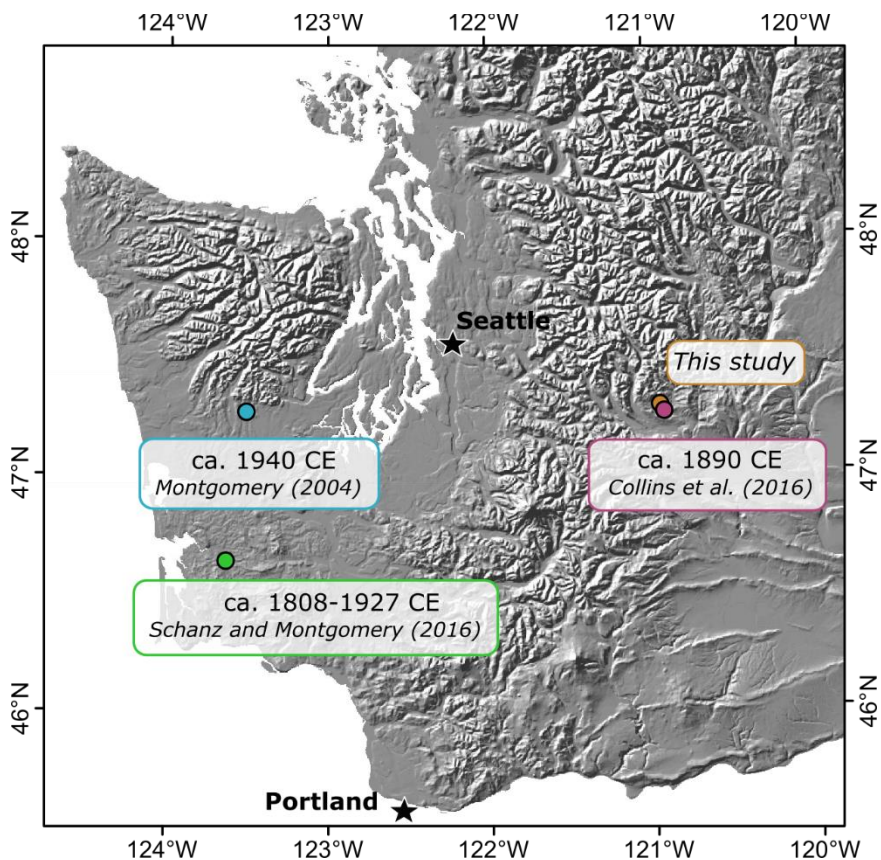


**Figure 4.1.** Locations of previously studied strath terraces in the Pacific Northwest interpreted to have formed in response to anthropogenic timber harvest and splash-damming, including the location of this study.

Here we present new evidence of basin-wide incision and strath terrace formation following splash-damming, which has limited sediment retention to channel sides and gravel bars and removed channel spanning jams that previously retained sediment across the channel. We test the effect of splash-damming on river incision by mapping and dating river terraces in the



West Fork Teanaway River, the lower 3 km of which was studied by Collins et al. (2016), and the Middle Fork Teanaway River. We also examine the possibility that terrace formation is driven by climate, such as changes in runoff and sediment production from the Little Ice Age and from natural fire regimes. We find that bedrock incision of up to 2 meters occurred with or slightly after splash-damming, implying that the conversion of 20-53% of the pre-incision floodplain to a terrace was driven by human action.

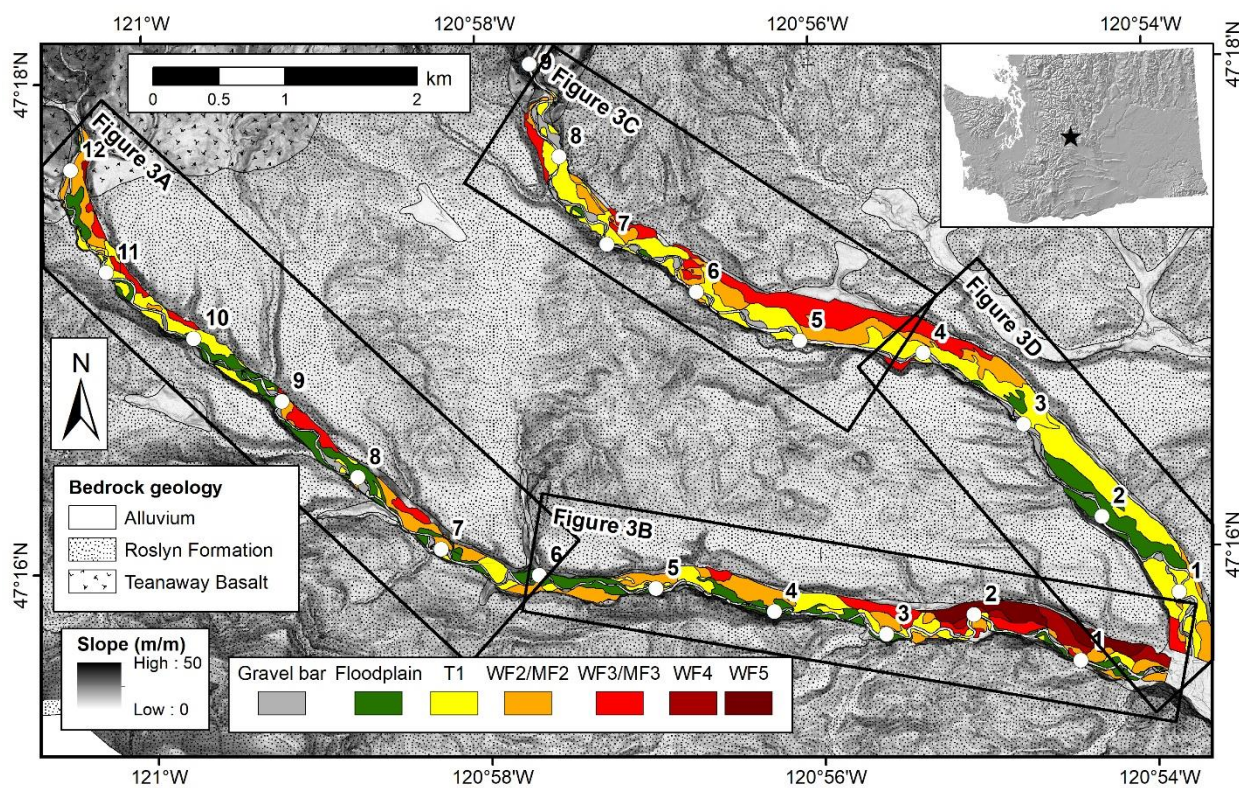


**Figure 4.2.** Location map of the Middle and West fork Teanaway Rivers. Boxes indicate the extent of panels in Figure 4.3. For the valley surfaces, MF = Middle Fork and WF = West Fork. White dots indicate the river kilometer, measured in upstream distance from the confluence of the Middle and West Fork Teanaway rivers.

### 4.3 STUDY SITE

Study sites along the Middle and West Fork Teanaway rivers are located in the central Cascade Range of Washington State (Figs. 4.1, 4.2). These drainage basins are typically snow covered during winter months and receive between 980 and 1230 mm yr<sup>-1</sup> of precipitation (U.S. Geological Survey, 2012). Holocene denudation in nearby basins is on the order of 0.08 mm yr<sup>-1</sup> (Moon et al., 2011), and exhumation rates are 0.05 mm yr<sup>-1</sup> over the last 10<sup>6</sup>-10<sup>7</sup> years (Reiners et al., 2003). Mapped faults in the Teanaway watershed do not cut Quaternary alluvium (Washington Division of Geology and Earth Resources, 2014). Our study focuses on the portion of the watersheds underlain by the easily eroded and friable Eocene Roslyn Formation (Tabor et al., 1982, Fig. 4.2); the lower 3 km of the West Fork Teanaway River was previously described in detail by Collins et al. (2016) who characterized rates and styles of bedrock incision. Channel bedload in the study site is mostly sourced from the erosion-resistant Teanaway Basalt and Swauk Formation immediately upstream, as bedload produced by the Roslyn Formation rapidly weathers to sand-size particles (Collins et al., 2016). The basin remained deglaciated during the Last Glacial Maximum but in previous glaciations was repeatedly overrun by glaciers from the Cle Elum River valley to the west, leaving a high glacial terrace that forms the valley walls and plateaus between the study basins (Porter, 1976). Pollen records at Carp Lake in the eastern Cascade Range of Oregon, a site at similar elevation (714 m) and also in *Pinus ponderosa* forest, suggest the modern forest established by 3.9 kya (Whitlock and Bartlein, 1997).

The study reaches of the Middle and West Fork Teanaway rivers were splash-dammed from 1892 to 1916 (Cle Elum Tribune, 1981; Kittitas County Centennial Committee, 1989). While the exact splash dam locations are unknown, 1910 stream gage reports place the dams at least 13 km upstream of the Middle and West Fork Teanaway rivers' confluence and newspaper accounts

suggest the dams were above river kilometer (rkm) 1.5 of the Middle Fork (Henshaw et al., 1913; McGiffin, 1980). Saw-cut logs buried perpendicular to the flow at rkm 6.8 are similar to the roll dams used to funnel logs downstream of splash dams, as described in Wendler and Deschamps (1955), further suggesting that splash dams were located upstream of the study reach. Previous work in the Oregon Coast Range and southwest Washington State showed that the splash-dam floods simplified channels and reduced wood and sediment loads (Sedell and Luchessa, 1982; Wendler and Deschamps, 1955). Prior to damming, side channels were blocked off and banks reinforced to keep floated timber in the channel (Sedell and Luchessa, 1982). Wood jams were removed both during and before log drives; the removal of these obstructions reduced sediment retention. Although splash-damming ceased in the study site in 1916, the channel has not yet recovered to its prior form. The current channel is mainly single-thread and wood loads are low. Our 2016-17 surveys identified only 15 jams in the 20 km study reach ( $< 1 \text{ jam km}^{-1}$ ). These wood loads are much lower than basin-wide averages in the Yakima, Wenatchee, and Methow rivers, all located east of the Washington Cascade Range, of 3.5 to 12.3 jams  $\text{km}^{-1}$  in watersheds managed by the US Forest Service and 8.1 to 13.8 jams  $\text{km}^{-1}$  in unmanaged watersheds (McIntosh et al., 1994). While we do not know the jam frequency of the Middle and West Fork Teanaway rivers prior to splash-damming, reports by Russell (1898) show at least one large jam complex 6 m deep by 275 m long. That wood loads remain much lower than nearby streams implies sediment retention has decreased and remained low since splash-damming.

## 4.4 METHODS

### 4.4.1 *Geomorphic mapping*

Bedrock strath terraces were mapped in field campaigns from 2015-2017, and floodplain surfaces were identified in the field based on the presence of flood debris, tree size, and forest seral

stage. The lowest (T1) terrace was identified based on the mixed coniferous and deciduous tree cover and greater presence of overbank channels compared with higher terraces, yet a lack of flood debris compared with floodplain surfaces. We also used radiocarbon dates from T1 surfaces to correlate our T1 mapping within and between the Middle and West Fork Teanaway valleys. Higher terraces were identified based on the height and continuation of surfaces. Soil development on the terraces is weak and overbank sedimentation rates are low, so soil development and thickness could not be used to correlate terrace sequences.

**Table 4.5.** Surface height above water

	Middle Fork		West Fork	
	Mean* (m)	Percent of valley bottom	Mean* (m)	Percent of valley bottom
Gravel bar	0.80 ± 0.66	7.5	0.92 ± 0.48	4.2
Floodplain	0.75 ± 0.57	11.1	1.33 ± 0.58	22.7
T1 - alluvial	1.90 ± 0.73	41.2	1.91 ± 0.59	16.7
T1 - strath	2.23 ± 0.66	2.6	1.88 ± 0.59	3.8
T2 - alluvial	3.01 ± 0.62	17.9	2.62 ± 0.66	19.0
T2 - strath	3.53 ± 0.49	0.2	2.97 ± 0.6	6.2
T3 - alluvial	4.90 ± 1.20	19.5	3.33 ± 0.93	9.2
T3 - strath	-	-	4.13 ± 0.78	3.2
T4 - alluvial	-	-	5.2 ± 0.74	5.1
T4 - strath	-	-	5.86 ± 1.06	0.7
T5 - alluvial	-	-	6.68 ± 0.93	9.1

\* ± one standard deviation

We used lidar flown in April-May 2015 (Quantum Spatial, 2015) to quantify bedrock incision and map valley landforms where field access was limited. The lidar dataset is topobathymetric and is thus able to accurately capture the channel bed surface with 0.006 m vertical accuracy in submerged and near-shore areas and 0.082 m average vertical accuracy overall, making it ideal to explore bedrock incision. We constructed height above water surface (HAWS) maps from the lidar bare earth elevation model using the TIN Interpolation Methodology

outlined in Appendix B of Olson (2012). We used the average channel elevation rather than average water surface as the base level because we were interested in channel incision. The HAWS maps were used to extrapolate field mapping to the entire study site (Fig. 4.2). To verify the accuracy of our remote mapping, we compared the strath terrace heights, mapped in the field, with the heights of terraces mapped from the HAWS map (Table 4.5).

#### 4.4.2 *Dating terrace incision*

We used paired dendrochronology and radiocarbon samples to constrain the timing of terrace incision. The charcoal and plant matter sampled for radiocarbon dating was deposited in the basal alluvium overlying the strath when the strath was an active fluvial surface and thus pre-dates incision, while the forest cover established post-incision when the surface became a terrace. Ages and locations are reported in Table 4.6 (radiocarbon) and Table 4.7 (dendrochronology). Tree cores were taken from the largest trees on each surface to estimate when the surface stabilized, thereby providing a minimum age of incision. Where possible, we avoided taking cores of early seral stage trees such as *Alnus rubra* and instead sampled from *Pinus ponderosa*. *Pinus ponderosa* were infrequent on current floodplains, and we inferred that they would establish on a surface only after incision and terrace formation. Tree cores were photographed and counted, and a subset of cores with indistinct rings were mounted and sanded with coarse and fine sandpaper before being photographed. Adjacent to the cored tree, charcoal and plant matter were collected in the basal alluvium overlying the strath and dated using accelerator mass spectrometry. Radiocarbon ages were calibrated using Calib 7.0.2 (Stuiver and Reimer, 1993) using the calibration curves of Reimer et al. (2013) and Stuiver et al. (1998). We also included the radiocarbon ages from Collins et al. (2016) from strath terraces on the West Fork Teanaway River.

**Table 4.6.** Locations and dates of radiocarbon samples

Sample ID	Lab ID*	Latitude (NAD 1983 UTM)	Longitude (NAD 1983 UTM)	Terrace height above avg channel bed (m)	Uncalibrated age (1 sigma)	Calibrated age in cal BP <sup>†</sup> (2 sigma)	Distance upstream of confluence (km)
<u>Middle Fork Teanaway River</u>							
7-2-15-2	D-AMS 011299	5238984	655138	1.2	278 +/- 27	355-434 (0.53); 285-332 (0.45)	6.22
8-25-16-1	D-AMS 018361	5238748	655415	1.9	108 +/- 24	21-144 (0.71); 216-267 (0.29)	5.83
8-25-16-3	UGA-30757	5238691	655521	2.9	620 +/- 20	553-612 (0.61); 620-656 (0.39)	5.68
8-25-16-4	D-AMS 018362	5238704	655623	3.9	1329 +/- 22	1240-1298 (0.89); 1187- 1204 (0.11)	5.57
8-25-16-5	UGA-30758	5238676	655701	3.1	740 +/- 20	663-695	5.52
8-25-16-8	D-AMS 018365	5236695	658935	1.7	22 +/- 25	34-61 (0.58) <sup>‡</sup> ; 117-135 (0.12)	1.12
8-25-16-9	D-AMS 018366	5236251	658996	3.3	53 +/- 23	33-75 (0.55) <sup>‡</sup> ; 114-135 (0.17); 221-242 (0.14)	0.45
<u>West Fork Teanaway River</u>							
6-28-17-5	Beta - 469577	5239123	650840	1.3	240 +/- 30	269-318 (0.57); 147-188 (0.31)	11.14
6-29-15-1	D-AMS 011297	5238853	651060	4.0	1937 +/- 29	1822-1947	10.72
8-22-16-1	D-AMS 018360	5239216	650696	3.0	1994 +/- 23	1893-1993	11.32

\*Samples D-AMS were dated at Direct AMS in Bothell, WA, samples UGA were dated at the Center for Applied Isotope Studies at the University of Georgia, and sample Beta was dated at Beta Analytic in Miami, Florida.

<sup>†</sup>all samples calibrated using the Intcal 2013 calibration from Reimer et al., 2013, except where noted. For samples with multiple age probabilities, each age range with a probability above 0.10 is shown, with the probability in parentheses.

<sup>‡</sup>calibrated using the UW Single Year 1998 calibration from Stuiver et al., 1998.

**Table 4.7.** Locations and dates of dendrochronology samples

Sample ID	Latitude (NAD 1983 UTM)	Longitude (NAD 1983 UTM)	Age*	Associated radiocarbon sample
<u>Middle Fork Teanaway River</u>				
6-8-17-1	5238983	655148	> 124	7-2-15-2
6-8-17-2	5238983	655148	121	no pair
6-8-17-3	5238741	655427	> 80	8-25-16-1,-2
6-8-17-4	5236246	658993	> 88	8-25-16-9
6-27-17-1	5238996	655136	113	7-2-15-2
6-27-17-2	5238691	655502	> 95	8-25-16-3
6-27-17-3	5238710	655622	> 134	8-25-16-4
6-27-17-4	5238710	655700	> 144	8-25-16-5
6-28-17-4	5236686	658935	87	8-25-16-6,-7,-8
<u>West Fork Teanaway River</u>				
6-9-17-1	5239226	650680	> 77	8-22-16-1
6-9-17-2	5238862	651064	> 181	6-29-15-1
6-28-17-2	5236395	657509	29	from Collins et al., 2016
6-28-17-3	5236302	657140	> 47	from Collins et al., 2016
6-28-17-6	5239116	650828	26	8-26-17-5

\*Age is given as years before 2017. Noted as a minimum age where core was incomplete.

#### 4.4.3 *Mid-valley profile*

The active channel and terrace treads were mapped onto a valley longitudinal profile using ArcGIS. We constructed a mid-valley line in the mainstem, West Fork, and Middle Fork Teanaway rivers and drew a perpendicular cross valley line every 100 meters. The average elevation of the channel and each terrace tread was taken along the cross valley line and plotted against the mid-valley distance.

#### 4.5 T1 EXTENT AND TIMING

To test the role of splash-dam logging, wood loss, and sediment retention on river incision, we mapped and dated a low strath terrace, termed T1, in the Middle and West Fork Teanaway valleys. We mapped the extent of T1 throughout the upper West Fork from rkm 3 to 12 and the Middle Fork from rkm 0 to 8.5 to test its regional extent. We also added new dendrochronology and radiocarbon dates to constrain the timing of T1 incision. Since splash-damming operated synchronously in the Middle and West Fork and broadly affected the sediment retention of the basin downstream of the dams, we expect that within our study area river incision should be basin-wide and similarly timed between the Middle and West Fork Teanaway rivers.

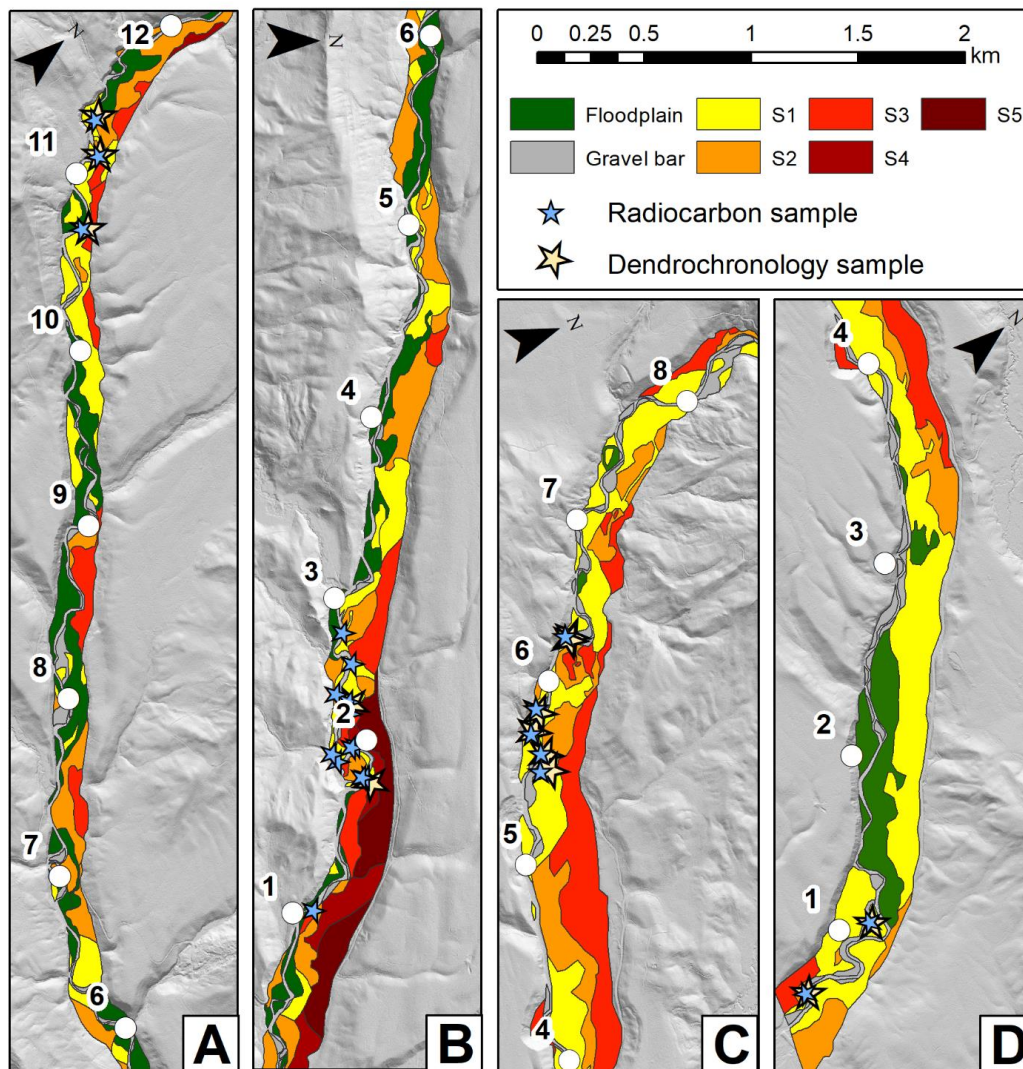


**Figure 4.3.** Geomorphic maps of the West and Middle Fork Teanaway rivers with locations of dendrochronology and radiocarbon samples shown. All panels are at the same scale, and locations of the panels are shown in Figure 4.2. White dots indicate the river kilometer, measured in upstream distance from the confluence of the Middle and West Fork Teanaway rivers.

T1 occupies 44% of the mapped Middle Fork (MF) valley bottom and 21% of the West Fork (WF) valley bottom (Fig. 4.3) and is present as both a bedrock strath and alluvial surface. In many cases, the strath dips below or at the channel bed elevation, transitioning T1 from a strath to an alluvial terrace while keeping a flat terrace tread (Fig. 4.4). The similarity in average height—measured from the average channel bed—between the incisional strath terraces ( $2.2 \pm 0.7$  for the



MF and  $1.9 \pm 0.6$  for the WF) and the alluvial terraces ( $1.9 \pm 0.7$  for the MF and  $1.9 \pm 0.6$  for the WF) suggests the alluvial terrace segments, which likely are underlain by a strath at the current channel bed elevation, record incision rather than floodplain height variability. Additionally, T1 is distinctly higher than the active floodplains ( $0.75 \pm 0.6$  for the MF and  $1.2 \pm 0.6$  for the WF) and gravel bar tops ( $0.8 \pm 0.7$  for the MF and  $0.9 \pm 0.5$  for the WF) (Table 4.5). T1 is continuous through the study reach (Figs. 4.3 and 4.5) and notably extends through knickzones in the lower 1 km of the Middle Fork and lower 3 km of the West Fork (Collins et al., 2016). That the knickzones do not affect T1 incision shows that the driver of incision is basin-wide. Moreover, the presence of T1 on both the inside and outside banks of meanders indicates T1 did not form primarily by meander cutoff (Finnegan and Dietrich, 2011) or migration (Limaye and Lamb, 2016; Merritts et al., 1994).

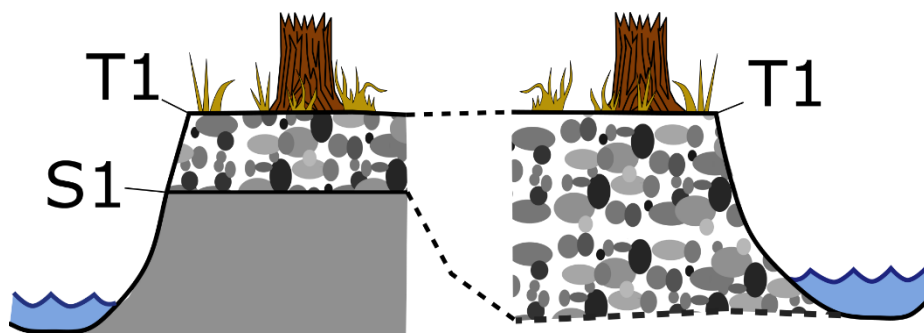


**Figure 4.4.** Schematic representation of terminology for strath (S) and terrace top (T) surfaces. Dashed lines indicate approximate locations and show that T1 surfaces can remain level while the S1 surface varies such that no strath may be present above the water surface.

We constrain incision of the T1 terrace by radiocarbon dating and dendrochronology to between 1900 and 1970 CE (Fig. 4.6). Radiocarbon dates of charcoal and plant debris from the basal alluvium overlying the T1 strath in both rivers range up to 500 calibrated (cal) yr BP but cluster between 50 and 300 cal yr BP, indicating the strath remained an active fluvial surface until around 1900 CE (Table 4.6) and was likely being planed for 300-400 years. The minimum age of

terrace formation is constrained by *Pinus ponderosa* growing on the T1 terrace, which places the abandonment of T1 as a frequently inundated channel or floodplain to before 1970 to 1991 CE for the West Fork and before 1893 to 1937 CE for the Middle Fork Teanaway River. Overall, the age constraints are similar for the Middle and West Forks, and suggest synchronous T1 incision between the two valleys.

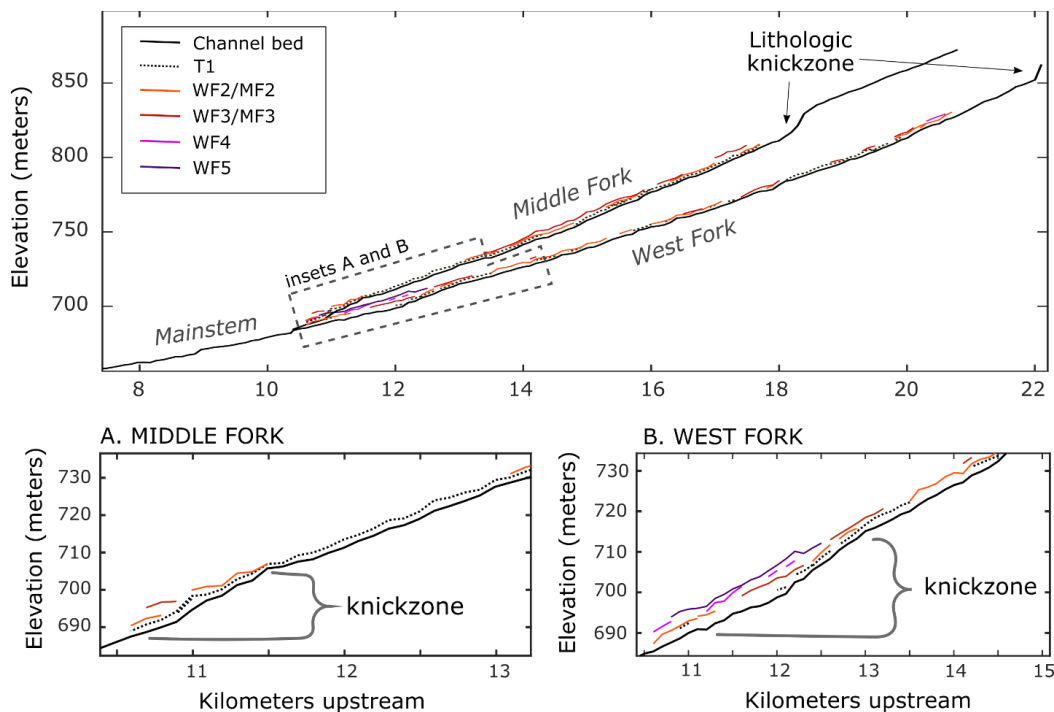


**Figure 4.5.** Mid-valley profile of current channel (black lines) and terrace treads for the Middle and West Fork Teanaway Rivers.

Our age constraints place T1 incision coincident with, or slightly after, splash-dam logging from 1892 to 1916. However, there are older terraces in the valley, dated to c. 830 and 1560 CE (Collins et al., 2016), that could not have formed in response to splash-damming. Did T1 form in response to a similar forcing as these older drivers? Additionally, competent bedload in the study reach is sourced from upstream; did a change in upstream supply drive T1 formation? We evaluate these potential drivers of T1 formation by comparing the geometry of older terraces in the study

site and examining how snowpack and fire frequency may have changed upstream sediment supply to drive incision or planation over the last 200 years.

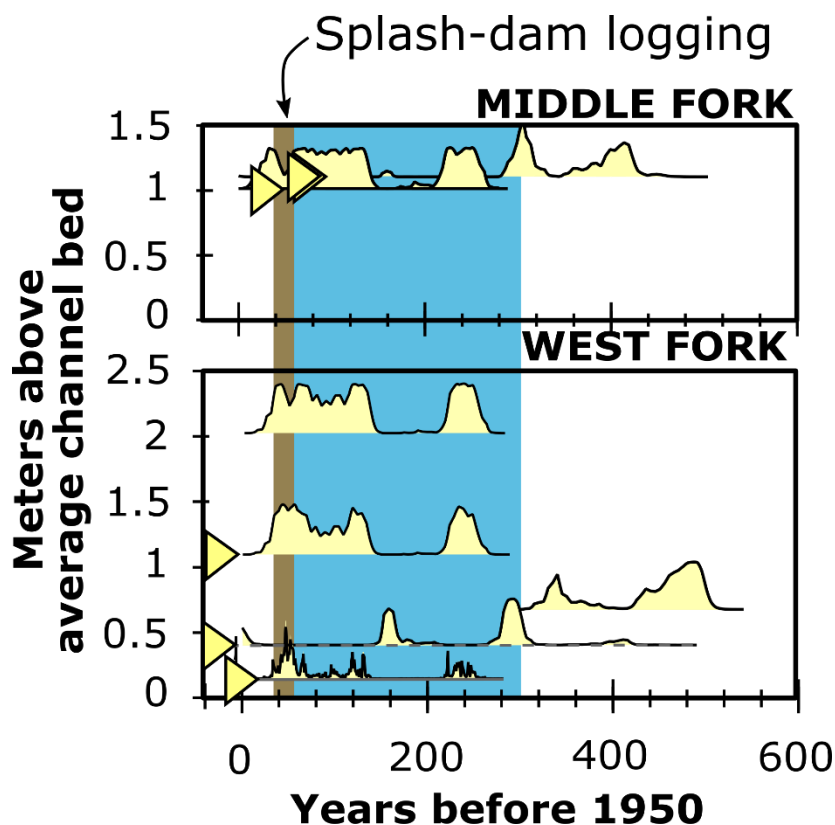


**Figure 4.6.** Timing of S1 terrace incision along the Middle and West Fork Teanaway rivers is constrained by radiocarbon, presented as distribution functions of the calibrated age before present, and dendrochronology, given as arrows wherein the left edge is aligned with tree age. The height of the strath above the average channel bed is noted by the bottom edge of the radiocarbon ages and the midpoint of the tree ages. The timing of Little Ice Age is shown by the blue bar.

#### 4.6 OLDER TERRACES IN THE STUDY SITE

We mapped four terrace surfaces higher than T1 in our analysis of the Middle and West Fork Teanaway valleys (Figs. 4.3 and 4.7). Because soil development is low on top of the terraces and we lack sufficient age constraints, we do not broadly correlate the older terraces across the two valleys, but term them MF2 and MF3 for the Middle Fork and WF2 through WF5 for the West Fork. Lack of exposure in banks and roadcuts does not allow us to determine the geometry of the

underlying strath for MF3, WF4, and WF5. However, MF2, MF3, WF4, and WF5 are not present basin-wide and grade to the top of the knickzones in the lower 1 and 3 km of the Middle and West Fork Teanaway rivers, respectively, suggesting a different formation mechanism than T1, which is basin-wide (Fig. 4.5). WF2 and WF3 are basin-wide and continuous across the knickzone. Prior dates on these strath terraces suggest they formed synchronous with mainstem Teanaway terraces at ca. 830 and 1560 CE (Collins et al., 2016). However, Collins et al. (2016) were unable to ascribe a driver to WF2 and WF3 formation, though they suggest that climatic variations may have changed sediment supply and transport to drive strath planation and incision. Since T1 is similar in extent to WF2 and WF3, climate may have also driven T1 formation; below, we assess how sediment supply would vary in response to known climate fluctuations during T1 formation.

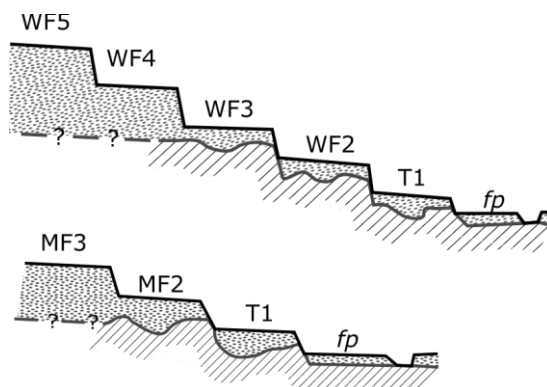


**Figure 4.7.** Full terrace sequence in the West Fork (upper) and Middle Fork (lower) Teanaway valleys, showing naming scheme. Floodplain is noted by “*fp*”.

#### 4.7 POSSIBLE CLIMATIC DRIVERS OF T1 FORMATION

Our radiocarbon ages estimate T1 was planed from ca. 1450 to 1890 CE (Fig. 4.6), which aligns within radiocarbon calibration error to the start of WF2 incision at 1560 CE (Collins et al., 2016), assuming rapid WF2 incision. That T1 was planed for up to 460 years suggests planation was not driven by periodic increases in sediment supply from fires (e.g., Benda et al., 2003; Pierce

et al., 2011). Fires in the bedload-producing upper basin occurred every 7-24 years with 300-350 years between high intensity, stand-replacing events (Agee, 1996; 1994) and would be expected to produce punctuated intervals of high sediment supply and planation rather than the observed extended planation period.

However, the formation of T1 aligns with the extent of the Little Ice Age (LIA) in the Pacific Northwest and may be due to changes in sediment supply driven by snowpack variation. Tree ring records indicate a period of greater snowpack from ca. 1650 to 1890 CE (Pederson et al., 2011), and low temperatures from ca. 1690 to 1900 CE (Graumlich and Brubaker, 1986) during the LIA. Perhaps planation of T1 was caused by enhanced sediment supply during the LIA and incision occurred when sediment supply decreased at the end of the LIA. We do not know how sediment supply in the Teanaway basin was affected by the LIA, but below we assess possible manners in which variations in snowpack could have affected sediment supply.

Sediment in the upper Teanaway basin is sourced directly from the hillslopes; valleys are narrow with little room for storage and hillslope morphology is suggestive of debris flow and avalanche-driven transport. Debris flow frequency has been found to decline during times of greater snowpack; with snow on the ground longer, the period of time over which precipitation events can interact directly with the regolith to create debris flows decreases (Stoffel and Beniston, 2006). In contrast, snow avalanche frequency likely increased during the LIA due to greater snowpack. The amount of sediment supplied from avalanches has not been widely quantified, but in a study in the southern German Alps, Heckmann et al. (2002) found avalanches contributed 1 – 170,000 kg of sediment per event and that the amount was highly variable across the study site and in time. Avalanche deposits dated by Blikra and Selvik (1998) in western Norway formed at a rate of ~1.2 m per 200 years, or ~6 mm yr<sup>-1</sup>. The range in potential avalanche contributions to

sediment load make it hard to assess whether the enhanced snowpack in the upper Teanaway basin drove sediment supply fluctuations and potentially T1 planation and incision. Additionally, that debris flow frequency may increase post-LIA from less snowpack, as observed by Stoffel and Beniston (2006) indicates any decrease in sediment supply from decreased snowpack and avalanche frequency may be offset by debris-flow inputs.

#### 4.8 ANTHROPOGENIC EFFECTS ON THE TEANAWAY LANDSCAPE

Based on the lack of a clear mechanism for a LIA driver of T1 incision, we favor the interpretation that T1 incised as a result of splash-damming and reduced sediment retention. The regional formation of strath terraces at the time of splash-dam logging supports this inference; anthropogenic terraces in the West Fork Satsop River formed 50 years after the LIA in 1940 CE (Montgomery, 2004) and the low elevation headwater hills that source the Willapa River, where terrace formation is coincident with splash-damming (Schanz and Montgomery, 2016), are unlikely to be significantly affected by LIA changes.

As such, Middle and West Fork Teanaway river incision of 1.1 to 23 mm yr<sup>-1</sup>, calculated using the lowest and highest T1 strath heights and the onset and end of splash-damming, is likely driven by splash-damming and decreased sediment retention. While these rates of incision are quite rapid, late Holocene incision rates derived from WF2 and WF3 also range from 1 to 10 mm yr<sup>-1</sup> (Collins et al., 2016), indicating anthropogenic incision rates are within the range of natural incision rates during the late Holocene. If we assume that nearby denudation rates from 7.5 kya to present (Moon et al., 2011) approximate average channel incision, we calculate that the Middle and West Fork Teanaway rivers are incising for 0.3 to 7.3% of the time at rates of 23 mm yr<sup>-1</sup> to 1.1 mm yr<sup>-1</sup>, respectively. These ranges agree with previous estimates that rivers planate for much longer periods than they incise (Hancock and Anderson, 2002; Wegmann and Pazzaglia, 2002).

Additionally, that the rivers spend less than 10% of the time incising, and thus over 90% of the time in planation and lateral migration phases, may explain the lack of Pleistocene and mid-late Holocene terraces in the study area, as the longer planation period would result in erosion of older terrace levels.

The formation of T1 in the Middle and West Fork Teanaway rivers, combined with the evidence of terrace formation in the West Fork Satsop and Willapa rivers in response to human action, shows a regional human impact on river incision. Alluvial river incision in response to human action has been well documented (e.g., Montgomery and Wohl, 2003), but that bedrock river incision can result from human action at timescales of only a century introduces new issues to consider in human-altered landscapes. For example, groundwater response to alluvial river incision has been documented elsewhere to be significant at 1 meter or greater incision (Bravard et al., 1997), but to our knowledge, no one has quantified the impact of bedrock incision on groundwater. Within the Middle and West Fork Teanaway valleys, this most recent cycle of incision has decreased the floodplain to 53 and 20% of the pre-incision area, respectively, and resulted in a loss of floodplain-channel connectivity.

The morphologic changes in the Teanaway valleys demonstrate the importance of anthropogenically-induced changes in sediment retention. Wood clearing and harvesting was ubiquitous worldwide starting as early as 7 kya in some regions (Cremaschi and Nicosia, 2012), and a broad global correspondence between late Holocene strath terrace formation and regional deforestation (Schanz et al., 2018) suggests floodplain abandonment from sediment retention loss may have been more pervasive than previously recognized in deforested watersheds around the world. As such, the topographic response to sediment retention loss may be creating a global

physiographic signature of the Anthropocene recorded in the transformation of floodplain landforms.



## Chapter 5. CONCLUDING THOUGHTS

To summarize the findings from Chapters 2-4 in the same framework as the introduction, I break out results into river response to forcings that is 1) modulated by basin lithology and 2) in response to stimuli in the last 10 ky to 0.1 ky.

I find that rock type exerts a strong control on how signals are propagated and retained in the landscape. Weaker rocks are easier to erode, especially those prone to slaking, and rivers will form wider valleys than their counterparts in resistant bedrock (Schanz and Montgomery, 2016). These wider valleys are able to preserve more coherent sets of terraces, such that past records of climatic and tectonic change will be more apparent in landscapes of easily erodible rock type. Moreover, greater contrast in rock strength between bedload and bedrock, set by the distribution of rock types in the watershed, will lead to more effective abrasion, as was noted by Collins et al. (2016) and Schanz and Montgomery (2016). Finally, differences in rock type between basins will create heterogeneity in timing and pace of landscape response to forcings (Schanz et al., 2018). For example, neighboring basins of carbonate and siliciclastic rocks weather at different rates, producing disparity in sediment supply between basins and resulting in basin-specific timing of strath planation, despite the same regional climate forcing (Wegmann and Pazzaglia, 2009).

Landscapes can respond to forcings exerted only 10 ky to 0.1 ky ago, though the sensitivity of the landscape to short timescale response may be modulated by basin characteristics like rock type and glacial history. Despite the prominence of marine isotope stage glacial cycles in strath terrace formation, a peak in strath terrace ages at 2.5 kya is indicative of a strong late Holocene forcing (Schanz et al., 2018). Although terrace forcings cannot be accurately established for the terraces at 2.5 kya, comparison with regional and global climate records suggests interglacial variations in climate could cause terrace planation and incision. Mechanisms for terrace formation

include the advance and retreat of glaciers during the Little Ice Age, centennial monsoon strengthening, and forest fire frequency. Forest fires affect the abundance of large wood, which in turn affects the sediment retention, the storage of sediment on the riverbed. Removal of wood by humans only a century ago resulted in up to 2.0 meters of bedrock incision in the central Cascades of Washington State (Schanz et al., in prep). These basins, un-glaciated for 100 ky and composed of slaking-prone bedrock with a more resistant bedload, had 20-40% of their valley bottoms altered by wood loss in just over one century, indicating fluvial response to forcings can be extremely rapid.

These findings broaden the geomorphic understanding of how rivers and landscapes respond to forcings such as climate, tectonics, and rock type. That the geomorphic response is strongly dependent on rock type, of both bedload and bedrock, suggests basins in different lithologies will not display the same response to a shared external forcing. The presence of a terrace in one basin and not another does not indicate that only one basin experienced change. Similarly, understanding that river incision and terrace formation can be driven by forcings at short timescales indicates fluvial systems are much more sensitive than previously thought and that relatively rapid (0.1 to 2.5 ky) transformation of the landscape is possible. Finally, the anthropogenic strath terraces created by wood and retention loss have reduced riparian habitat in those valleys, suggesting changing sediment retention is another mechanism by which human effects are propagated across a landscape.

## BIBLIOGRAPHY

- Abbe, T.B., Montgomery, D.R., 1996. Large woody debris jams, channel hydraulics and habitat formation in large rivers. *Regulated Rivers: Research & Management* 12, 201–221.
- Agee, J.K., 1996. *Fire Ecology of Pacific Northwest Forests*. Island Press.
- Agee, J.K., 1994. Fire and weather disturbances in terrestrial ecosystems of the eastern Cascades (General Technical Report No. PNW-GTR-320). US. Department of Agriculture, Pacific Northwest Research Station.
- Amos, C.B., Burbank, D.W., Nobes, D.C., Read, S.A.L., 2007. Geomorphic constraints on listric thrust faulting: Implications for active deformation in the Mackenzie Basin, South Island, New Zealand. *Journal of Geophysical Research: Solid Earth* 112. B03S11. doi:10.1029/2006JB004291
- Antoine, P., Lautridou, J.P., Laurent, M., 2000. Long-term fluvial archives in NW France: response of the Seine and Somme rivers to tectonic movements, climatic variations and sea-level changes. *Geomorphology* 33, 183–207. doi:10.1016/S0169-555X(99)00122-1
- Ashworth, P.J., Best, J.L., Jones, M., 2004. Relationship between sediment supply and avulsion frequency in braided rivers. *Geology* 32, 21–24. <https://doi.org/10.1130/G19919.1>
- Barnard, P.L., Owen, L.A., Finkel, R.C., 2004. Style and timing of glacial and paraglacial sedimentation in a monsoon-influenced high Himalayan environment, the upper Bhagirathi Valley, Garhwal Himalaya. *Sedimentary Geology* 165, 199–221. doi:10.1016/j.sedgeo.2003.11.009
- Baynes, E.R.C., Attal, M., Niedermann, S., Kirstein, L.A., Dugmore, A.J., Naylor, M., 2015. Erosion during extreme flood events dominates Holocene canyon evolution in northeast Iceland. *Proceedings of the National Academy of Sciences* 112, 2355–2360. doi:10.1073/pnas.1415443112
- Benda, L., Miller, D., Bigelow, P., Andras, K., 2003. Effects of post-wildfire erosion on channel environments, Boise River, Idaho. *Forest Ecology and Management, The Effect of Wildland Fire on Aquatic Ecosystems in the Western USA*. 178, 105–119. [https://doi.org/10.1016/S0378-1127\(03\)00056-2](https://doi.org/10.1016/S0378-1127(03)00056-2)
- Berryman, K., Marden, M., Palmer, A., Wilson, K., Mazengarb, C., Litchfield, N., 2010. The post-glacial downcutting history in the Waihuka tributary of Waipaoa River, Gisborne district: Implications for tectonics and landscape evolution in the Hikurangi subduction margin, New Zealand. *Marine Geology* 270, 55–71. <https://doi.org/10.1016/j.margeo.2009.10.001>
- Blikra, L.H., Selvik, S.F., 1998. Climatic signals recorded in snow avalanche-dominated colluvium in western Norway: depositional facies successions and pollen records. *The Holocene*; London 8, 631–658.

- Brandon, M.T., Roden-Tice, M.K., Garver, J.I., 1998. Late Cenozoic exhumation of the Cascadia accretionary wedge in the Olympic Mountains, northwest Washington State. *Geological Society of America Bulletin* 110, 985–1009. doi:10.1130/0016-7606(1998)110<0985:LCEOTC>2.3.CO;2
- Bravard, J.-P., Amoros, C., Pautou, G., Bornette, G., Bournaud, M., Creuze des Chatelliers, M., Gibert, J., Peiry, J.-L., Perrin, J.-F., Tachet, H., 1997. River incision in south-east France: morphological phenomena and ecological effects. *Regulated Rivers: Research & Management* 13, 75–90. [https://doi.org/10.1002/\(SICI\)1099-1646\(199701\)13:1<75::AID-RRR444>3.0.CO;2-6](https://doi.org/10.1002/(SICI)1099-1646(199701)13:1<75::AID-RRR444>3.0.CO;2-6)
- Bull, W.B., 1990. Stream-terrace genesis: implications for soil development. *Geomorphology* 3, 351–367. doi:10.1016/0169-555X(90)90011-E
- Carcaillet, J., Mugnier, J.L., Koçi, R., Jouanne, F., 2009. Uplift and active tectonics of southern Albania inferred from incision of alluvial terraces. *Quaternary Research* 71, 465–476. doi:10.1016/j.yqres.2009.01.002
- Chen, S.-C., Chao, Y.-C., Chan, H.-C., 2013. Typhoon-dominated influence on wood debris distribution and transportation in a high gradient headwater catchment. *Journal of Mountain Science* 10, 509–521. <https://doi.org/10.1007/s11629-013-2741-2>
- Cheng, S., Deng, Q., Zhou, S., Yang, G., 2002. Strath terraces of Jinshaan Canyon, Yellow River, and Quaternary tectonic movements of the Ordos Plateau, North China. *Terra Nova* 14, 215–224. doi:10.1046/j.1365-3121.2002.00350.x
- Cle Elum Tribune, 1981. Cle Elum Tribune page 4.
- Collins, B.D., Montgomery, D.R., Schanz, S.A., Larsen, I.J., 2016. Rates and mechanisms of bedrock incision and strath terrace formation in a forested catchment, Cascade Range, Washington. *Geological Society of America Bulletin* B31340.1. doi:10.1130/B31340.1
- Constantine, J.A., Dunne, T., Ahmed, J., Legleiter, C., Lazarus, E.D., 2014. Sediment supply as a driver of river meandering and floodplain evolution in the Amazon Basin. *Nature Geoscience* 7, 899–903. <https://doi.org/10.1038/ngeo2282>
- Cook, K.L., Whipple, K.X., Heimsath, A.M., Hanks, T.C., 2009. Rapid incision of the Colorado River in Glen Canyon – insights from channel profiles, local incision rates, and modeling of lithologic controls. *Earth Surface Processes and Landforms* 34, 994–1010. doi:10.1002/esp.1790
- Cremaschi, M., Nicosia, C., 2012. Sub-Boreal aggradation along the Apennine margin of the Central Po Plain: geomorphological and geoarchaeological aspects. *Géomorphologie : relief, processus, environnement* 18, 155–174. <https://doi.org/10.4000/geomorphologie.9810>
- Cunha, P.P., Martins, A.A., Huot, S., Murray, A., Raposo, L., 2008. Dating the Tejo river lower terraces in the Ródão area (Portugal) to assess the role of tectonics and uplift. *Geomorphology* 102, 43–54. <https://doi.org/10.1016/j.geomorph.2007.05.019>
- Dadson, S.J., Hovius, N., Chen, H., Dade, W.B., Hsieh, M.-L., Willett, S.D., Hu, J.-C., Horng, M.-J., Chen, M.-C., Stark, C.P., Lague, D., Lin, J.-C., 2003. Links between erosion, runoff variability and seismicity in the Taiwan orogen. *Nature* 426, 648–651. <https://doi.org/10.1038/nature02150>

- Duvall, A., Kirby, E., Burbank, D., 2004. Tectonic and lithologic controls on bedrock channel profiles and processes in coastal California. *Journal of Geophysical Research: Earth Surface* 109. doi:10.1029/2003JF000086
- Dykoski, C.A., Edwards, R.L., Cheng, H., Yuan, D., Cai, Y., Zhang, M., Lin, Y., Qing, J., An, Z., Revenaugh, J., 2005. A high-resolution, absolute-dated Holocene and deglacial Asian monsoon record from Dongge Cave, China. *Earth and Planetary Science Letters* 233, 71–86. <https://doi.org/10.1016/j.epsl.2005.01.036>
- Eden, D.N., Palmer, A.S., Cronin, S.J., Marden, M., Berryman, K.R., 2001. Dating the culmination of river aggradation at the end of the last glaciation using distal tephra compositions, eastern North Island, New Zealand. *Geomorphology* 38, 133–151. doi:10.1016/S0169-555X(00)00077-5
- Ehlers, J., Gibbard, P.L., Hughes, P.D. (Eds.), 2011. *Quaternary Glaciations - Extent and Chronology: a closer look*. Elsevier, Amsterdam.
- Ely, L.L., Brossy, C.C., House, P.K., Safran, E.B., O'Connor, J.E., Champion, D.E., Fenton, C.R., Bondre, N.R., Orem, C.A., Grant, G.E., Henry, C.D., Turrin, B.D., 2012. Owyhee River intracanyon lava flows: Does the river give a dam? *Geological Society of America Bulletin* 124, 1667–1687. doi:10.1130/B30574.1
- Faustini, J.M., Jones, J.A., 2003. Influence of large woody debris on channel morphology and dynamics in steep, boulder-rich mountain streams, western Cascades, Oregon. *Geomorphology* 51, 187–205. [https://doi.org/10.1016/S0169-555X\(02\)00336-7](https://doi.org/10.1016/S0169-555X(02)00336-7)
- Finnegan, N.J., Balco, G., 2013. Sediment supply, base level, braiding, and bedrock river terrace formation: Arroyo Seco, California, USA. *Geological Society of America Bulletin* 125, 1114–1124. doi:10.1130/B30727.1
- Finnegan, N.J., Dietrich, W.E., 2011. Episodic bedrock strath terrace formation due to meander migration and cutoff. *Geology* 39, 143–146. doi:10.1130/G31716.1
- Finnegan, N.J., Schumer, R., Finnegan, S., 2014. A signature of transience in bedrock river incision rates over timescales of  $10^4$ - $10^7$  years. *Nature* 505, 391–394. doi:10.1038/nature12913
- Formento-Trigilio, M.L., Burbank, D.W., Nicol, A., Shulmeister, J., Rieser, U., 2003. River response to an active fold-and-thrust belt in a convergent margin setting, North Island, New Zealand. *Geomorphology* 49, 125–152. doi:10.1016/S0169-555X(02)00167-8
- Fuller, T.K., Perg, L.A., Willenbring, J.K., Lepper, K., 2009. Field evidence for climate-driven changes in sediment supply leading to strath terrace formation. *Geology* 37, 467–470. doi:10.1130/G25487A.1
- Gallen, S.F., Pazzaglia, F.J., Wegmann, K.W., Pederson, J.L., Gardner, T.W., 2015. The dynamic reference frame of rivers and apparent transience in incision rates. *Geology* 43, 623–626. doi:10.1130/G36692.1
- García, A.F., 2006. Thresholds of strath genesis deduced from landscape response to stream piracy by Pancho Rico Creek in the Coast Ranges of central California. *American Journal of Science* 306, 655–681. doi:10.2475/08.2006.03

- García, A.F., Mahan, S.A., 2014. The notion of climate-driven strath-terrace production assessed via dissimilar stream-process response to late Quaternary climate. *Geomorphology* 214, 223–244. doi:10.1016/j.geomorph.2014.02.008
- García, A.F., Zhu, Z., Ku, T.L., Chadwick, O.A., Chacón Montero, J., 2004. An incision wave in the geologic record, Alpujarran Corridor, southern Spain (Almería). *Geomorphology* 60, 37–72. doi:10.1016/j.geomorph.2003.07.012
- Gardner, T.W., 1983. Experimental study of knickpoint and longitudinal profile evolution in cohesive, homogeneous material. *Geological Society of America Bulletin* 94, 664–672. doi:10.1130/0016-7606(1983)94<664:ESOKAL>2.0.CO;2
- Giardini, D., Grunthal, G., Shedlock, K.M., Zhang, P., 1999. The GSHAP Global Seismic Hazard Map. *Annali Di Geofisica* 42, 1225–1230.
- Gilbert, G.K., 1877. Report on the Geology of the Henry Mountains. US Government Printing Office.
- Gibbard, P.L., Lewin, J., 2009. River incision and terrace formation in the Late Cenozoic of Europe. *Tectonophysics*, 474, 41–55. doi:10.1016/j.tecto.2008.11.017
- Glade, T., 2003. Landslide occurrence as a response to land use change: a review of evidence from New Zealand. *Catena* 51, 297–314. doi:10.1016/S0341-8162(02)00170-4
- Gran, K.B., Finnegan, N., Johnson, A.L., Belmont, P., Wittkop, C., Rittenour, T., 2013. Landscape evolution, valley excavation, and terrace development following abrupt postglacial base-level fall. *Geological Society of America Bulletin* 125, 1851–1864. doi:10.1130/B30772.1
- Graumlich, L.J., Brubaker, L.B., 1986. Reconstruction of annual temperature (1590–1979) for Longmire, Washington, derived from tree rings. *Quaternary Research* 25, 223–234.
- Haibing, L., Van der Woerd, J., Tapponnier, P., Klinger, Y., Xuexiang, Q., Jingsui, Y., Yintang, Z., 2005. Slip rate on the Kunlun fault at Hongshui Gou, and recurrence time of great events comparable to the 14/11/2001, Mw~7.9 Kokoxili earthquake. *Earth and Planetary Science Letters* 237, 285–299. doi:10.1016/j.epsl.2005.05.041
- Hancock, G.S., Anderson, R.S., 2002. Numerical modeling of fluvial strath-terrace formation in response to oscillating climate. *Geological Society of America Bulletin* 114, 1131–1142. doi:10.1130/0016-7606(2002)114<1131:NMOFST>2.0.CO;2
- Hancock, G.S., Small, E.E., Wobus, C., 2011. Modeling the effects of weathering on bedrock-floored channel geometry. *Journal of Geophysical Research: Earth Surface* 116, F03018. doi:10.1029/2010JF001908
- Harkins, N.W., Anastasio, D.J., Pazzaglia, F.J., 2005. Tectonic geomorphology of the Red Rock fault, insights into segmentation and landscape evolution of a developing range front normal fault. *Journal of Structural Geology* 27, 1925–1939. doi:10.1016/j.jsg.2005.07.005
- Harkins, N., Kirby, E., Heimsath, A., Robinson, R., Reiser, U., 2007. Transient fluvial incision in the headwaters of the Yellow River, northeastern Tibet, China. *J. Geophys. Res.* 112, F03S04. <https://doi.org/10.1029/2006JF000570>

Heckmann, T., Wichmann, V., Becht, M., 2002. Quantifying sediment transport by avalanches in the Bavarian Alps—first results. *Zeitschrift für Geomorphologie NF, Suppl* 127, 137–152.

Henshaw, F.F., La Rue, E.C., Stevens, G.C., 1913. Surface water supply of the United States, 1910: Part 12. North Pacific Coast (USGS Numbered Series No. 292), Water Supply Paper. U.S. Government Print Office.

Hsieh, M.-L., Knuepfer, P.L.K., 2001. Middle–late Holocene river terraces in the Erhjen River Basin, southwestern Taiwan—implications of river response to climate change and active tectonic uplift. *Geomorphology* 38, 337–372. doi:10.1016/S0169-555X(00)00105-7

Kittitas County Centennial Committee, 1989. A history of Kittitas County, Washington. Taylor Publishing Company, Dallas, TX.

Knox, J.C., 2006. Floodplain sedimentation in the Upper Mississippi Valley: Natural versus human accelerated. *Geomorphology, 37th Binghamton Geomorphology Symposium* 79, 286–310. <https://doi.org/10.1016/j.geomorph.2006.06.031>

Kothyari, G.C., Shukla, A.D., Juyal, N., 2016. Reconstruction of Late Quaternary climate and seismicity using fluvial landforms in Pindar River valley, Central Himalaya, Uttarakhand, India. *Quaternary International*. doi:10.1016/j.quaint.2016.06.001

Lamb, M.P., Finnegan, N.J., Scheingross, J.S., Sklar, L.S., 2015. New insights into the mechanics of fluvial bedrock erosion through flume experiments and theory. *Geomorphology* 244, 33–55. <https://doi.org/10.1016/j.geomorph.2015.03.003>

Larson, P.H., Dorn, R.I., 2014. Strath development in small arid watersheds: Case study of South Mountain, Sonoran Desert, Arizona. *Am J Sci* 314, 1202–1223. doi:10.2475/08.2014.02

Lavé, J., Avouac, J.P., 2000. Active folding of fluvial terraces across the Siwaliks Hills, Himalayas of central Nepal. *Journal of Geophysical Research: Solid Earth* 105, 5735–5770. doi:10.1029/1999JB900292

Lavé, J., Avouac, J.P., 2001. Fluvial incision and tectonic uplift across the Himalayas of central Nepal. *Journal of Geophysical Research: Solid Earth* 106, 26561–26591. <https://doi.org/10.1029/2001JB000359>

Lee, C.-Y., Chang, C.-L., Liew, P.-M., Lee, T.-Q., Song, S.-R., 2014. Climate change, vegetation history, and agricultural activity of Lake Li-yu Tan, central Taiwan, during the last 2.6 ka BP. *Quaternary International, Holocene Palynology and Tropical Paleoecology* 325, 105–110. <https://doi.org/10.1016/j.quaint.2013.05.029>

Leopold, L.B., Wolman, M.G., Miller, J.P., 1964. *Fluvial Processes in Geomorphology*. W.H. Freeman, San Francisco.

Lewin, J., Macklin, M.G., Woodward, J.C., 1991. Late Quaternary fluvial sedimentation in the Voidomatis basin, Epirus, Northwest Greece. *Quaternary Research* 35, 103–115. doi:10.1016/0033-5894(91)90098-P

Lewis, C.J., McDonald, E.V., Sancho, C., Peña, J.L., Rhodes, E.J., 2009. Climatic implications of correlated Upper Pleistocene glacial and fluvial deposits on the Cinca and Gállego Rivers (NE

Spain) based on OSL dating and soil stratigraphy. *Global and Planetary Change* 67, 141–152. doi:10.1016/j.gloplacha.2009.01.001

Liew, P.-M., Hsieh, M.-L., 2000. Late Holocene (2 ka) sea level, river discharge and climate interrelationship in the Taiwan region. *Journal of Asian Earth Sciences* 18, 499–505. [https://doi.org/10.1016/S1367-9120\(99\)00081-4](https://doi.org/10.1016/S1367-9120(99)00081-4)

Limaye, A.B.S., Lamb, M.P., 2016. Numerical model predictions of autogenic fluvial terraces and comparison to climate change expectations. *Journal of Geophysical Research: Earth Surface* 121. doi:10.1002/2014JF003392

Maser, J. 1999, Nehalem River Watershed Assessment: <http://web.pdx.edu/~maserj/project/project1/> (Nov 2014).

Massong, T.M., Montgomery, D.R., 2000. Influence of sediment supply, lithology, and wood debris on the distribution of bedrock and alluvial channels. *Geological Society of America Bulletin* 112, 591–599. doi:10.1130/0016-7606(2000)112<591:IOSSLA>2.0.CO;2

May, C.L., Gresswell, R.E., 2003. Large wood recruitment and redistribution in headwater streams in the southern Oregon Coast Range, U.S.A. *Canadian Journal of Forest Research*. 33, 1352–1362. <https://doi.org/10.1139/x03-023>

Mayewski, P.A., Rohling, E.E., Curt Stager, J., Karlén, W., Maasch, K.A., David Meeker, L., Meyerson, E.A., Gasse, F., van Kereveld, S., Holmgren, K., Lee-Thorp, J., Rosqvist, G., Rack, F., Staubwasser, M., Schneider, R.R., Steig, E.J., 2004. Holocene climate variability. *Quaternary Research* 62, 243–255. <https://doi.org/10.1016/j.yqres.2004.07.001>

McGiffin, J., 1980. Hometown heritage: A remembered history of 1910 in Kittitas County, Washington. *The Daily Record*, Ellensburg, WA.

McIntosh, B.A., Sedell, J.R., Smith, J.E., Wissmar, R.C., Clarke, S.E., Reeves, G.H., Brown, L.A., 1994. Management history of eastside ecosystems: changes in fish habitat over 50 years, 1935-1992. U.S. Department of Agriculture, Forest Service, Pacific Northwest Research Station General Technical Report PNW-GTR-321 55. <https://doi.org/10.2737/PNW-GTR-321>

Mériaux, A.-S., Tapponnier, P., Ryerson, F.J., Xiwei, X., King, G., Van der Woerd, J., Finkel, R.C., Haibing, L., Caffee, M.W., Zhiqin, X., Wenbin, C., 2005. The Aksay segment of the northern Altyn Tagh fault: Tectonic geomorphology, landscape evolution, and Holocene slip rate. *Journal of Geophysical Research: Solid Earth* 110, B04404. doi:10.1029/2004JB003210

Merritts, D.J., Vincent, K.R., Wohl, E.E., 1994. Long river profiles, tectonism, and eustasy: A guide to interpreting fluvial terraces. *Journal of Geophysical Research: Solid Earth* 99, 14031–14050. doi:10.1029/94JB00857

Meyer, G.A., Wells, S.G., Jull, A.J.T., 1995. Fire and alluvial chronology in Yellowstone National Park: Climatic and intrinsic controls on Holocene geomorphic processes. *Geological Society of America Bulletin* 107, 1211–1230. [https://doi.org/10.1130/0016-7606\(1995\)107<1211:FAACIY>2.3.CO;2](https://doi.org/10.1130/0016-7606(1995)107<1211:FAACIY>2.3.CO;2)

Meyer, W.T., Stets, J., 2002. Pleistocene to recent tectonics in the Rhenish Massif (Germany). *Netherlands Journal of Geosciences* 81, 217–222.



- Molin, P., Fubelli, G., Nocentini, M., Sperini, S., Ignat, P., Grecu, F., Dramis, F., 2012. Interaction of mantle dynamics, crustal tectonics, and surface processes in the topography of the Romanian Carpathians: A geomorphological approach. *Global and Planetary Change* 90–91, 58–72. doi:10.1016/j.gloplacha.2011.05.005
- Montgomery, D.R., 2004. Observations on the role of lithology in strath terrace formation and bedrock channel width. *American Journal of Science* 304, 454–476. doi:10.2475/ajs.304.5.454
- Montgomery, D.R., 1999. Erosional processes at an abrupt channel head: Implications for channel entrenchment and discontinuous gully formation, in: *Incised River Channels*, Edited by S. Darby and A. Simon. John Wiley & Sons, Ltd, pp. 247–276.
- Montgomery, D.R., Abbe, T.B., Buffington, J.M., Peterson, N.P., Schmidt, K.M., Stock, J.D., 1996. Distribution of bedrock and alluvial channels in forested mountain drainage basins. *Nature* 381, 587–589. doi:10.1038/381587a0
- Montgomery, D.R., Gran, K.B., 2001. Downstream variations in the width of bedrock channels. *Water Resources Research* 37, 1841–1846. doi:10.1029/2000WR900393
- Montgomery, D.R., Collins, B.D., Buffington, J.M., Abbe, T.B., 2003. Geomorphic effects of wood in rivers, in: Gregory, S., Boyer, K.L., Gurnell, A.M. (Eds.), *The Ecology and Management of Wood in World Rivers*. American Fisheries Society Symposium, pp. 21–47.
- Montgomery, D.R., Wohl, E.E., 2003. Rivers and riverine landscapes, in: *Developments in Quaternary Sciences, The Quaternary Period in the United States*. Elsevier, pp. 221–246.
- Moon, S., Page Chamberlain, C., Blisniuk, K., Levine, N., Rood, D.H., Hilley, G.E., 2011. Climatic control of denudation in the deglaciated landscape of the Washington Cascades. *Nature Geosci* 4, 469–473. <https://doi.org/10.1038/ngeo1159>
- Nichols, M.H., Magirl, C., Sayre, N.F., Shaw, J.R., 2018. The geomorphic legacy of water and erosion control structures in a semiarid rangeland watershed. *Earth Surface Processes and Landforms* 43, 909–918. <https://doi.org/10.1002/esp.4287>
- O'Connor, J.E., Mangano, J.F., Anderson, S.W., Wallick, J.R., Jones, K.L., Keith, M.K., 2014. Geologic and physiographic controls on bed-material yield, transport, and channel morphology for alluvial and bedrock rivers, western Oregon. *Geological Society of America Bulletin* B30831.1. doi:10.1130/B30831.1
- Olson, P., 2012. Quality assurance project plan for: Channel migration assessments of Puget Sound SMA streams (No. 12-06-006). Washington Department of Ecology, Olympia, Washington.
- Ono, Y., Aoki, T., Hasegawa, H., Dali, L., 2005. Mountain glaciation in Japan and Taiwan at the global Last Glacial Maximum. *Quaternary International* 138–139, 79–92. doi:10.1016/j.quaint.2005.02.007
- Owenby, J.R. and Ezell, D.S., 1992. *Monthly Station Normals of Temperature, Precipitation, and Heating and Cooling Degree Days, 1961-1990: Washington*. U.S. Department of Commerce, National Oceanic and Atmospheric Administration, National Climatic Data Center.

- Pan, B., Burbank, D., Wang, Y., Wu, G., Li, J., Guan, Q., 2003. A 900 k.y. record of strath terrace formation during glacial-interglacial transitions in northwest China. *Geology* 31, 957–960. doi:10.1130/G19685.1
- Pazzaglia, F.J., 2013. Fluvial Terraces, in: *Treatise on Geomorphology*. Elsevier, pp. 379–412.
- Pazzaglia, F.J., Brandon, M.T., 2001. A Fluvial Record of Long-term Steady-state Uplift and Erosion Across the Cascadia Forearc High, Western Washington State. *American Journal of Science* 301, 385–431. doi:10.2475/ajs.301.4-5.385
- Pederson, G.T., Gray, S.T., Woodhouse, C.A., Betancourt, J.L., Fagre, D.B., Littell, J.S., Watson, E., Luckman, B.H., Graumlich, L.J., 2011. The Unusual Nature of Recent Snowpack Declines in the North American Cordillera. *Science* 333, 332–335. <https://doi.org/10.1126/science.1201570>
- Personius, S.F., 1995. Late Quaternary stream incision and uplift in the forearc of the Cascadia subduction zone, western Oregon. *Journal of Geophysical Research: Solid Earth* 100, 20193–20210. doi:10.1029/95JB01684
- Personius, S.F., Kelsey, H.M., Grabau, P.C., 1993. Evidence for regional stream aggradation in the Central Oregon Coast Range during the Pleistocene-Holocene transition. *Quaternary Research* 40, 297–308. doi:10.1006/qres.1993.1083
- Perroy, R.L., Bookhagen, B., Chadwick, O.A., Howarth, J.T., 2012. Holocene and Anthropocene Landscape Change: Arroyo Formation on Santa Cruz Island, California. *Annals of the Association of American Geographers* 102, 1229–1250.
- Pierce, J.L., Meyer, G.A., Rittenour, T., 2011. The relation of Holocene fluvial terraces to changes in climate and sediment supply, South Fork Payette River, Idaho. *Quaternary Science Reviews* 30, 628–645. <https://doi.org/10.1016/j.quascirev.2010.11.013>
- Porter, S.C., 1976. Pleistocene glaciation in the southern part of the North Cascade Range, Washington. *Geological Society of America Bulletin* 87, 61–75. [https://doi.org/10.1130/0016-7606\(1976\)87<61:PGITSP>2.0.CO;2](https://doi.org/10.1130/0016-7606(1976)87<61:PGITSP>2.0.CO;2)
- Picotti, V., Pazzaglia, F.J., 2008. A new active tectonic model for the construction of the Northern Apennines mountain front near Bologna (Italy). *Journal of Geophysical Research: Solid Earth* 113, B08412. doi:10.1029/2007JB005307
- Portenga, E.W., Bierman, P.R., 2011. Understanding Earth's eroding surface with <sup>10</sup>Be. *Geological Society of America Today* 21, 4–10. <https://doi.org/10.1130/G111A.1>
- Quantum Spatial, 2015. Teanaway streams topobathymetric LiDAR.
- Rau, W.W., 1951. Tertiary Foraminifera from the Willapa River Valley of Southwest Washington. *Journal of Paleontology* 25, 417–453. doi:10.2307/1299745
- Reimer, P.J., Bard, E., Bayliss, A., Beck, J.W., Blackwell, P.G., Ramsey, C.B., Buck, C.E., Cheng, H., Edwards, R.L., Friedrich, M., Grootes, P.M., Guilderson, T.P., Haflidason, H., Hajdas, I., Hatté, C., Heaton, T.J., Hoffmann, D.L., Hogg, A.G., Hughen, K.A., Kaiser, K.F., Kromer, B., Manning, S.W., Niu, M., Reimer, R.W., Richards, D.A., Scott, E.M., Southon, J.R., Staff, R.A., Turney, C.S.M., Plicht, J. van der, 2013. IntCal13 and Marine13 Radiocarbon Age

Calibration Curves 0–50,000 Years cal BP. *Radiocarbon* 55, 1869–1887.  
[https://doi.org/10.2458/azu\\_js\\_rc.55.16947](https://doi.org/10.2458/azu_js_rc.55.16947)

Reiners, P.W., Ehlers, T.A., Mitchell, S.G., Montgomery, D.R., 2003. Coupled spatial variations in precipitation and long-term erosion rates across the Washington Cascades. *Nature* 426, 645–647. <https://doi.org/10.1038/nature02111>

Reneau, S.L., Dietrich, W.E., Donahue, D.J., Jull, A.J.T., and Rubin, M., 1990. Late Quaternary history of colluvial deposition and erosion in hollows, central California Coast Ranges: *Bulletin of the Geological Society of America*, v. 102, p. 969–982, doi: 10.1130/0016-7606(1990)102<0969:LQHOC>2.3.CO;2.

Retallack, G.J., Roering, J.J., 2012. Wave-cut or water-table platforms of rocky coasts and rivers? *GSA Today* 4–10. doi:10.1130/GSATG144A.1

Rockwell, T.K., Keller, E.A., Clark, M.N., Johnson, D.L., 1984. Chronology and rates of faulting of Ventura River terraces, California. *Geological Society of America Bulletin* 95, 1466–1474. [https://doi.org/10.1130/0016-7606\(1984\)95<1466:CAROFO>2.0.CO;2](https://doi.org/10.1130/0016-7606(1984)95<1466:CAROFO>2.0.CO;2)

Schanz, S.A., Montgomery, D.R., 2016. Lithologic controls on valley width and strath terrace formation. *Geomorphology* 258, 58–8. doi:10.1016/j.geomorph.2016.01.015

Schanz, S.A., Montgomery, D.R., Collins, B.D., Duvall, A.R., 2018. Multiple paths to straths: A review and reassessment of terrace genesis. *Geomorphology* 312, 12–23. <https://doi.org/10.1016/j.geomorph.2018.03.028>

Scheingross, J.S., Brun, F., Lo, D.Y., Omerdin, K., Lamb, M.P., 2014. Experimental evidence for fluvial bedrock incision by suspended and bedload sediment. *Geology* 42, 523–526. <https://doi.org/10.1130/G35432.1>

Schoenbohm, L.M., Whipple, K.X., Burchfiel, B.C., Chen, L., 2004. Geomorphic constraints on surface uplift, exhumation, and plateau growth in the Red River region, Yunnan Province, China. *Geological Society of America Bulletin* 116, 895–909. doi:10.1130/B25364.1

Sedell, J.R., Luchessa, K.J., 1982. Using the historical record as an aid to salmonid habitat enhancement. Forest Service.

Seidl, M.A., Dietrich, W.E., 1992. The problem of channel erosion into bedrock, in: Schmidt, K.-H., de Ploey, J. (Eds.), *Functional Geomorphology: Landform Analysis and Models*, Catena Supplement. pp. 101–124.

Sklar, L.S., Dietrich, W.E., 2001. Sediment and rock strength controls on river incision into bedrock. *Geology* 29, 1087–1090. doi:10.1130/0091-7613(2001)029<1087:SARSCO>2.0.CO;2

Smithsonian Institution., 2013. *Global Volcanism Program*. Retrieved from [http://volcano.si.edu/list\\_volcano\\_holocene.cfm](http://volcano.si.edu/list_volcano_holocene.cfm) (accessed 8.30.17).

Snyder, N.P., Kammer, L.L., 2008. Dynamic adjustments in channel width in response to a forced diversion: Gower Gulch, Death Valley National Park, California. *Geology* 36, 187–190. doi:10.1130/G24217A.1

- Stock, J.D., Montgomery, D.R., 1999. Geologic constraints on bedrock river incision using the stream power law. *Journal of Geophysical Research: Solid Earth* 104, 4983–4993. doi:10.1029/98JB02139
- Stock, J.D., Montgomery, D.R., Collins, B.D., Dietrich, W.E., Sklar, L., 2005. Field measurements of incision rates following bedrock exposure: Implications for process controls on the long profiles of valleys cut by rivers and debris flows. *Geological Society of America Bulletin* 117, 174–194. doi:10.1130/B25560.1
- Stoffel, M., Beniston, M., 2006. On the incidence of debris flows from the early Little Ice Age to a future greenhouse climate: A case study from the Swiss Alps. *Geophysical Research Letters* 33. <https://doi.org/10.1029/2006GL026805>
- Stuiver, M., Reimer, P.J., 1993. Extended 14C data base and revised CALIB 3.014 C age calibration program. *Radiocarbon* 35, 215–230.
- Stuiver, M., Reimer, P.J., Bard, E., Beck, J.W., Burr, G.S., Hughen, K.A., Kromer, B., McCormac, G., Plicht, J.V.D., Spurk, M., 1998. INTCAL98 Radiocarbon Age Calibration, 24,000–0 cal BP. *Radiocarbon* 40, 1041–1083. <https://doi.org/10.1017/S0033822200019123>
- Syvitski, J.P.M., Kettner, A., 2011. Sediment flux and the Anthropocene. *Philosophical Transactions of the Royal Society of London A: Mathematical, Physical and Engineering Sciences* 369, 957–975. doi:10.1098/rsta.2010.0329
- Tabor, R.W., Waitt, Jr., R.B., Frizzell, Jr., V.A., Swanson, D.A., Byerly, G.R., Bentley, R.D., 1982. Geologic map of the Wenatchee 1:100,000 quadrangle, central Washington.
- Trimble, S.W., 1997. Contribution of Stream Channel Erosion to Sediment Yield from an Urbanizing Watershed. *Science* 278, 1442–1444. <https://doi.org/10.1126/science.278.5342.1442>
- Tucker, G.E., Whipple, K.X., 2002. Topographic outcomes predicted by stream erosion models: Sensitivity analysis and intermodel comparison. *Journal of Geophysical Research: Solid Earth* 107, 2179. doi:10.1029/2001JB000162
- Turowski, J.M., Lague, D., Hovius, N., 2007. Cover effect in bedrock abrasion: A new derivation and its implications for the modeling of bedrock channel morphology. *Journal of Geophysical Research: Earth Surface* 112, F04006. doi:10.1029/2006JF000697
- Turowski, J.M., Hovius, N., Meng-Long, H., Lague, D., Men-Chiang, C., 2008. Distribution of erosion across bedrock channels. *Earth Surface Processes and Landforms* 33, 353–363. <https://doi.org/10.1002/esp.1559>
- U.S. Geological Survey, 2012. The StreamStats program for Washington [WWW Document]. URL <http://water.usgs.gov/osw/streamstats/Washington.html> (accessed 1.5.18).
- Van Balen, R.T., Houtgast, R.F., Van der Wateren, F.M., Vandenberghe, J., Bogaart, P.W., 2000. Sediment budget and tectonic evolution of the Meuse catchment in the Ardennes and the Roer Valley Rift System. *Global and Planetary Change* 27, 113–129. doi:10.1016/S0921-8181(01)00062-5
- Van der Woerd, J., Ryerson, F.J., Tapponnier, P., Gaudemer, Y., Finkel, R., Meriaux, A.S., Caffee, M., Guoguang, Z., Qunlu, H., 1998. Holocene left-slip rate determined by cosmogenic

- surface dating on the Xidatan segment of the Kunlun fault (Qinghai, China). *Geology* 26, 695–698. doi:10.1130/0091-7613(1998)026<0695:HLSRDB>2.3.CO;2
- Van der Woerd, J., Xu, X., Li, H., Tapponnier, P., Meyer, B., Ryerson, F.J., Meriaux, A.-S., Xu, Z., 2001. Rapid active thrusting along the northwestern range front of the Tanghe Nan Shan (western Gansu, China). *Journal of Geophysical Research: Solid Earth* 106, 30475–30504. doi:10.1029/2001JB000583
- Vassallo, R., Ritz, J.-F., Braucher, R., Jolivet, M., Carretier, S., Larroque, C., Chauvet, A., Sue, C., Todbileg, M., Bourlès, D., Arzhannikova, A., Arzhannikov, S., 2007. Transpressional tectonics and stream terraces of the Gobi-Altay, Mongolia. *Tectonics* 26, TC5013, doi:10.1029/2006TC002081
- Walsh, T.J., Korosec, M.A., Phillips, W.M., Logan, R.L., Schasse, H.W., 1987, *Geologic Map of Washington, Southwest Quadrant [Map]: Washington Division of Geology and Earth Resources, scale 1:100,000, 1 sheet.*
- Walter, R.C., Merritts, D.J., 2008. Natural Streams and the Legacy of Water-Powered Mills. *Science* 319, 299–304. <https://doi.org/10.1126/science.1151716>
- Wang, X., Vandenberghe, J., Yi, S., Van Balen, R., Lu, H., 2015. Climate-dependent fluvial architecture and processes on a suborbital timescale in areas of rapid tectonic uplift: An example from the NE Tibetan Plateau. *Global and Planetary Change* 133, 318–329. doi:10.1016/j.gloplacha.2015.09.009
- Wanner, H., Beer, J., Bütikofer, J., Crowley, T.J., Cubasch, U., Flückiger, J., Goosse, H., Grosjean, M., Joos, F., Kaplan, J.O., Küttel, M., Müller, S.A., Prentice, I.C., Solomina, O., Stocker, T.F., Tarasov, P., Wagner, M., Widmann, M., 2008. Mid- to Late Holocene climate change: an overview. *Quaternary Science Reviews* 27, 1791–1828. <https://doi.org/10.1016/j.quascirev.2008.06.013>
- Washington Division of Geology and Earth Resources, 2014. Surface geology, 1:24,000--GIS data, June 2014, Washington Division of Geology and Earth Resources Digital Data Series DS-10, version 1.0.
- Waters, M.R., Haynes, C.V., 2001. Late Quaternary arroyo formation and climate change in the American Southwest. *Geology* 29, 399–402. [https://doi.org/10.1130/0091-7613\(2001\)029<0399:LQAFAC>2.0.CO;2](https://doi.org/10.1130/0091-7613(2001)029<0399:LQAFAC>2.0.CO;2)
- Wegmann, K.W., Pazzaglia, F.J., 2002. Holocene strath terraces, climate change, and active tectonics: The Clearwater River basin, Olympic Peninsula, Washington State. *Geological Society of America Bulletin* 114, 731–744. doi:10.1130/0016-7606(2002)114<0731:HSTCCA>2.0.CO;2
- Wegmann, K.W., Pazzaglia, F.J., 2009. Late Quaternary fluvial terraces of the Romagna and Marche Apennines, Italy: Climatic, lithologic, and tectonic controls on terrace genesis in an active orogen. *Quaternary Science Reviews* 28, 137–165. doi:10.1016/j.quascirev.2008.10.006
- Weisberg, P.J., Swanson, F.J., 2003. Regional synchronicity in fire regimes of western Oregon and Washington, USA. *Forest Ecology and Management* 172, 17–28. [https://doi.org/10.1016/S0378-1127\(01\)00805-2](https://doi.org/10.1016/S0378-1127(01)00805-2)

- Wendler, H.O., Deschamps, G., 1955. Logging dams on coastal Washington streams. Washington Department of Fisheries, Fisheries Research Papers 1, 27–38.
- Whitlock, C., Bartlein, P.J., 1997. Vegetation and climate change in northwest America during the past 125 kyr. *Nature* 388, 57–61. <https://doi.org/10.1038/40380>
- Wohl, E., 2008. The effect of bedrock jointing on the formation of straths in the Cache la Poudre River drainage, Colorado Front Range. *Journal of Geophysical Research: Earth Surface* 113, F01007. doi:10.1029/2007JF000817
- Wolman, M.G., 1967. A Cycle of Sedimentation and Erosion in Urban River Channels. *Geografiska Annaler. Series A, Physical Geography* 49, 385–395. <https://doi.org/10.2307/520904>
- Wright, C.S., 1996. Fire history of the Teanaway River drainage, Washington. (MS Thesis). University of Washington, Seattle, Washington.
- Yanites, B.J., Tucker, G.E., 2010. Controls and limits on bedrock channel geometry. *Journal of Geophysical Research: Earth Surface* 115, F04019. doi:10.1029/2009JF001601
- Yanites, B.J., Tucker, G.E., Mueller, K.J., Chen, Y.-G., 2010a. How rivers react to large earthquakes: Evidence from central Taiwan. *Geology* 38, 639–642. <https://doi.org/10.1130/G30883.1>
- Yanites, B.J., Tucker, G.E., Mueller, K.J., Chen, Y.-G., Wilcox, T., Huang, S.-Y., Shi, K.-W., 2010b. Incision and channel morphology across active structures along the Peikang River, central Taiwan: Implications for the importance of channel width. *Geological Society of America Bulletin* 122, 1192–1208. <https://doi.org/10.1130/B30035.1>

## APPENDIX A

Author	Year	Age (kya)	Latitude	Longitude	Location
Amos et al	2007	15	-44.75	170.00	Ohau River, New Zealand
Amos et al	2007	21	-44.75	170.00	Ohau River, New Zealand
Amos et al	2007	66.5	-44.75	170.00	Ohau River, New Zealand
Amos et al	2007	85	-44.75	170.00	Ohau River, New Zealand
Amos et al	2007	160	-44.75	170.00	Ohau River, New Zealand
Amos et al	2007	270.5	-44.75	170.00	Ohau River, New Zealand
Antoine et al	2000	95	50.00	2.00	Somme River, NW France
Antoine et al	2000	200	50.00	2.00	Somme River, NW France
Antoine et al	2000	296	50.00	2.00	Somme River, NW France
Antoine et al	2000	400	50.00	2.00	Somme River, NW France
Antoine et al	2000	600	50.00	2.00	Somme River, NW France
Antoine et al	2000	997	50.00	2.00	Somme River, NW France
Antoine et al	2000	1105	50.00	2.00	Somme River, NW France
Barnard et al.	2001	12.6	30.30	79.05	Alaknanda River, N India - monsoonal
Barnard et al.	2001	14.3	30.30	79.06	Alaknanda River, N India - monsoonal
Barnard et al.	2001	15	30.30	79.06	Alaknanda River, N India - monsoonal
Barnard et al.	2001	16.3	30.30	79.06	Alaknanda River, N India - monsoonal
Barnard et al.	2004a Late	5.2	30.20	80.23	Western Himalaya - monsoonal
Barnard et al.	2004b Style	4.05	31.00	78.90	Western Himalaya - monsoonal
Baynes	2015	1.2	65.80	-16.40	Iceland
Baynes	2015	1.2	65.80	-16.40	Iceland
Baynes	2015	1.3	65.80	-16.40	Iceland
Baynes	2015	1.4	65.80	-16.40	Iceland
Baynes	2015	1.7	65.80	-16.40	Iceland
Baynes	2015	4.7	65.80	-16.40	Iceland
Baynes	2015	5.9	65.80	-16.40	Iceland
Baynes	2015	6.3	65.80	-16.40	Iceland
Bender et al	2016	200	46.90	-120.49	Yakima River, Washington
Bender et al	2016	900	46.81	-120.44	Yakima River, Washington
Bender et al	2016	1000	46.91	-120.50	Yakima River, Washington
Bender et al	2016	1600	46.83	-120.46	Yakima River, Washington
Bender et al	2016	1600	46.85	-120.46	Yakima River, Washington
Bender et al	2016	2900	46.91	-120.50	Yakima River, Washington
Berryman et al	2010	0.15	-38.45	177.33	Waihuka River, New Zealand
Berryman et al	2010	1.56	-38.45	177.33	Waihuka River, New Zealand
Berryman et al	2010	4.07	-38.45	177.33	Waihuka River, New Zealand
Berryman et al	2010	8.12	-38.45	177.33	Waihuka River, New Zealand
Berryman et al	2010	8.81	-38.45	177.33	Waihuka River, New Zealand
Berryman et al	2010	9.05	-38.45	177.33	Waihuka River, New Zealand
Berryman et al	2010	9.3	-38.45	177.33	Waihuka River, New Zealand
Berryman et al	2010	17.6	-38.45	177.33	Waihuka River, New Zealand
Berryman et al	2010	18.5	-38.45	177.33	Waihuka River, New Zealand
Bhattacharjee et al	2016	14	21.37	77.77	Purna River, central India
Bhattacharjee et al	2016	19	21.40	77.63	Arna River, central India
Bhattacharjee et al	2016	34	21.43	78.00	Maru River, central India
Bhattacharjee et al	2016	37	21.43	78.00	Maru River, central India
Bhattacharjee et al	2016	50	21.40	77.63	Arna River, central India
Burbank et al	1996	6	35.50	75.00	Indus River
Burbank et al	1996	7	35.50	75.00	Indus River

Author	Forcing	Strength of ascribed forcing?	If climate, when did incision occur in glacial cycle?	If climate, when did planation occur in glacial cycle?
Amos et al	Climate	good		full glacial
Amos et al	Climate	good		full glacial
Amos et al	Climate	good		full glacial
Amos et al	Climate	good		full glacial
Amos et al	Climate	good		full glacial
Amos et al	Climate	good		full glacial
Antoine et al	Climate	good	interglacial to glacial	
Antoine et al	Climate	good	interglacial to glacial	
Antoine et al	Climate	good	interglacial to glacial	
Antoine et al	Climate	good	interglacial to glacial	
Antoine et al	Climate	good	interglacial to glacial	
Antoine et al	Climate	good	interglacial to glacial	
Antoine et al	Climate	good	interglacial to glacial	
Barnard et al.	Indeterminate			
Barnard et al.	Indeterminate			
Barnard et al.	Indeterminate			
Barnard et al.	Indeterminate			
Barnard et al.	Climate	poor		glacial to interglacial
Barnard et al.	Climate	good		glacial to interglacial
Baynes	Base level	good		
Baynes	Base level	good		
Baynes	Base level	good		
Baynes	Base level	good		
Baynes	Base level	good		
Baynes	Base level	good		
Baynes	Base level	good		
Baynes	Base level	good		
Bender et al	Indeterminate			
Bender et al	Indeterminate			
Bender et al	Indeterminate			
Bender et al	Indeterminate			
Bender et al	Indeterminate			
Bender et al	Indeterminate			
Berryman et al	Indeterminate			
Berryman et al	Indeterminate			
Berryman et al	Indeterminate			
Berryman et al	Climate	poor	glacial to interglacial	
Berryman et al	Climate	poor	glacial to interglacial	
Berryman et al	Climate	poor	glacial to interglacial	
Berryman et al	Climate	poor	glacial to interglacial	
Berryman et al	Indeterminate			
Berryman et al	Indeterminate			
Bhattacharjee et al	Indeterminate			
Bhattacharjee et al	Indeterminate			
Bhattacharjee et al	Indeterminate			
Bhattacharjee et al	Indeterminate			
Bhattacharjee et al	Indeterminate			
Burbank et al	Indeterminate			
Burbank et al	Indeterminate			



Author	Dating method & sample location	If Holocene & forested, deforestation age	Deforestation reference	Peak ground acceleration
Amos et al	Multiple methods	13th century	Dawson, 2007	2.0
Amos et al	Multiple methods	13th century	Dawson, 2007	2.0
Amos et al	Multiple methods	13th century	Dawson, 2007	2.0
Amos et al	Multiple methods	13th century	Dawson, 2007	2.0
Amos et al	Multiple methods	13th century	Dawson, 2007	2.0
Amos et al	Multiple methods	13th century	Dawson, 2007	2.0
Antoine et al	U/Th, in terrace			0.4
Antoine et al	ESR, in terrace			0.4
Antoine et al	ESR, in terrace			0.4
Antoine et al	ESR, in terrace			0.4
Antoine et al	ESR, in terrace			0.4
Antoine et al	ESR, in terrace			0.4
Antoine et al	ESR, in terrace			0.4
Barnard et al.	CRN, terrace surface			3.8
Barnard et al.	CRN, terrace surface			3.8
Barnard et al.	CRN, terrace surface			3.8
Barnard et al.	CRN, terrace surface			3.8
Barnard et al.	CRN, terrace surface	200 yr BP	Wasson et al., 2008	4.6
Barnard et al.	CRN, terrace surface	200 yr BP	Wasson et al., 2008	3.8
Baynes	CRN, strath	1140 yr BP to 150 yr BP	Eysteinsson, 2009	2.1
Baynes	CRN, strath	1140 yr BP to 150 yr BP	Eysteinsson, 2010	2.1
Baynes	CRN, strath	1140 yr BP to 150 yr BP	Eysteinsson, 2011	2.1
Baynes	CRN, strath	1140 yr BP to 150 yr BP	Eysteinsson, 2012	2.1
Baynes	CRN, strath	1140 yr BP to 150 yr BP	Eysteinsson, 2013	2.1
Baynes	CRN, strath	1140 yr BP to 150 yr BP	Eysteinsson, 2014	2.1
Baynes	CRN, strath	1140 yr BP to 150 yr BP	Eysteinsson, 2015	2.1
Baynes	CRN, strath	1140 yr BP to 150 yr BP	Eysteinsson, 2016	2.1
Bender et al	CRN, in terrace			1.0
Bender et al	CRN, in terrace			1.0
Bender et al	CRN, in terrace			1.0
Bender et al	CRN, in terrace			1.0
Bender et al	CRN, in terrace			1.0
Bender et al	CRN, in terrace			1.0
Berryman et al	Radiocarbon, in terrace	700 yr BP	Jones 1988	4.5
Berryman et al	Radiocarbon, in terrace	700 yr BP	Jones 1988	4.5
Berryman et al	Radiocarbon, in terrace	700 yr BP	Jones 1988	4.5
Berryman et al	Radiocarbon, in terrace	700 yr BP	Jones 1988	4.5
Berryman et al	Radiocarbon, in terrace	700 yr BP	Jones 1988	4.5
Berryman et al	Radiocarbon, in terrace	700 yr BP	Jones 1988	4.5
Berryman et al	Radiocarbon, in terrace	700 yr BP	Jones 1988	4.5
Berryman et al	Radiocarbon, in terrace	700 yr BP	Jones 1988	4.5
Berryman et al	Radiocarbon, in terrace	700 yr BP	Jones 1988	4.5
Berryman et al	Radiocarbon, in terrace	700 yr BP	Jones 1988	4.5
Bhattacharjee et al	OSL, in terrace			0.3
Bhattacharjee et al	OSL, in terrace			0.3
Bhattacharjee et al	OSL, in terrace			0.3
Bhattacharjee et al	OSL, in terrace			0.3
Bhattacharjee et al	OSL, in terrace			0.3
Burbank et al	CRN, strath	200 yr BP	Wasson et al., 2008	2.5
Burbank et al	CRN, strath	200 yr BP	Wasson et al., 2008	2.5

Author	Year	Age (kya)	Latitude	Longitude	Location
Burbank et al	1996	7	35.50	75.00	Indus River
Burbank et al	1996	14	35.50	75.00	Indus River
Burbank et al	1996	32	35.50	75.00	Indus River
Burbank et al	1996	61	35.50	75.00	Indus River
Burbank et al	1996	67	35.50	75.00	Indus River
Calle et al	2013	10	42.03	-0.13	Alcanadre River, Ebro Basin, Spain
Calle et al	2013	19	42.06	-0.12	Alcanadre River, Ebro Basin, Spain
Calle et al	2013	44	41.92	-0.13	Alcanadre River, Ebro Basin, Spain
Calle et al	2013	780	42.00	-0.13	Alcanadre River, Ebro Basin, Spain
Calle et al	2013	1000	42.00	-0.13	Alcanadre River, Ebro Basin, Spain
Carcaillet et al	2009	0.67	40.60	20.20	Southern Albania
Carcaillet et al	2009	11.45	40.60	20.20	Southern Albania
Carcaillet et al	2009	18.75	40.60	20.20	Southern Albania
Carcaillet et al	2009	19.8	40.60	20.20	Southern Albania
Carcaillet et al	2009	34.47	40.60	20.20	Southern Albania
Carcaillet et al	2009	42.15	40.60	20.20	Southern Albania
Carcaillet et al	2009	50.7	40.60	20.20	Southern Albania
Carcaillet et al	2009	52.59	40.60	20.20	Southern Albania
Carcaillet et al	2009	54.5	40.60	20.20	Southern Albania
Cheng et al	2002	5.4	36.00	111.00	Yumenkou, China
Cheng et al	2002	17.6	38.00	111.00	Yumenkou, China
Cheng et al	2002	44	38.00	111.00	Yumenkou, China
Cheng et al	2002	76.4	38.00	111.00	Yumenkou, China
Cheng et al	2002	196.7	39.00	111.00	Yumenkou, China
Cheng et al	2002	1409.8	38.00	111.00	Yumenkou, China
Collins et al.	2016	0.06	47.25	-120.92	Teanaway River, Washington
Collins et al.	2016	0.39	47.25	-120.92	Teanaway River, Washington
Collins et al.	2016	1.12	47.25	-120.92	Teanaway River, Washington
Cook et al	2009	3	38.00	-110.50	Trachyte Creek, Arizona
Cook et al	2009	13.27	38.00	-110.50	Trachyte Creek, Arizona
Cook et al	2009	158.6	37.96	-110.50	Trachyte Creek, Arizona
Cook et al	2009	164.1	37.96	-110.50	Trachyte Creek, Arizona
Cook et al	2009	177.9	37.96	-110.50	Trachyte Creek, Arizona
Cook et al	2009	205	37.95	-110.50	Trachyte Creek, Arizona
Cook et al	2009	219.1	37.95	-110.50	Trachyte Creek, Arizona
Cook et al	2009	267.1	37.95	-110.50	Trachyte Creek, Arizona
Crow et al	2014	351	36.25	-111.82	Colorado River
Crow et al	2014	368	36.25	-111.82	Colorado River
Crow et al	2014	386	36.25	-111.82	Colorado River
Crow et al	2014	467	36.20	-112.44	Colorado River
Crow et al	2014	467	36.10	-111.83	Colorado River
Crow et al	2014	574	35.82	-113.65	Colorado River
Crow et al	2014	623	36.14	-111.81	Colorado River
Crow et al	2014	651	36.20	-112.45	Colorado River
Crow et al	2014	678	36.20	-112.45	Colorado River
Crow et al	2014	880	38.38	-112.49	Colorado River
Crow et al	2014	980	36.39	-112.52	Colorado River
Cunha et al	2008	31	39.50	-8.00	Tejo River, Portugal
Cunha et al	2008	100	39.50	-8.00	Tejo River, Portugal
Cyr et al	2015	24.3	34.95	-116.56	Mojave River
Dadson et al.	2003	0.356	23.14	120.39	Tsengwen River, Taiwan
Dadson et al.	2003	0.5895	23.06	120.39	Tsengwen River, Taiwan
Dadson et al.	2003	0.808	23.57	120.48	Potzu River, Taiwan

<b>Author</b>	<b>Forcing</b>	<b>Strength of ascribed forcing?</b>	<b>If climate, when did incision occur in glacial cycle?</b>	<b>If climate, when did planation occur in glacial cycle?</b>
Burbank et al	Indeterminate			
Burbank et al	Indeterminate			
Burbank et al	Indeterminate			
Burbank et al	Indeterminate			
Burbank et al	Indeterminate			
Calle et al	climate	poor	Unclear	
Calle et al	Climate	poor	Unclear	
Calle et al	Climate	poor	Unclear	
Calle et al	Climate	poor	Unclear	
Calle et al	Climate	poor	Unclear	
Carcaillet et al	Anthropogenic	poor		
Carcaillet et al	Climate	poor	full interglacial	full glacial
Carcaillet et al	Climate	poor	full interglacial	full glacial
Carcaillet et al	Climate	poor	full interglacial	full glacial
Carcaillet et al	Climate	poor	full interglacial	full glacial
Carcaillet et al	Climate	poor	full interglacial	full glacial
Carcaillet et al	Climate	poor	full interglacial	full glacial
Carcaillet et al	Climate	poor	full interglacial	full glacial
Carcaillet et al	Climate	poor	full interglacial	full glacial
Cheng et al	Tectonics	good		
Cheng et al	Tectonics	good		
Cheng et al	Tectonics	good		
Cheng et al	Tectonics	good		
Cheng et al	Tectonics	good		
Cheng et al	Tectonics	good		
Collins et al.	Indeterminate			
Collins et al.	Indeterminate			
Collins et al.	Indeterminate			
Cook et al	Climate	poor	Unclear	
Cook et al	Climate	poor	Unclear	
Cook et al	Climate	poor	Unclear	
Cook et al	Climate	poor	Unclear	
Cook et al	Climate	poor	Unclear	
Cook et al	Climate	poor	Unclear	
Cook et al	Climate	poor	Unclear	
Cook et al	Climate	poor	Unclear	
Crow et al	Indeterminate			
Crow et al	Indeterminate			
Crow et al	Indeterminate			
Crow et al	Indeterminate			
Crow et al	Indeterminate			
Crow et al	Indeterminate			
Crow et al	Indeterminate			
Crow et al	Indeterminate			
Crow et al	Indeterminate			
Crow et al	Indeterminate			
Crow et al	Indeterminate			
Cunha et al	Base level	poor	full glacial	
Cunha et al	Tectonics	poor		
Cyr et al	Indeterminate			
Dadson et al.	Indeterminate			
Dadson et al.	Indeterminate			
Dadson et al.	Indeterminate			

Author	Dating method & sample location	If Holocene & forested, deforestation age	Deforestation reference	Peak ground acceleration
Burbank et al	CRN, strath	200 yr BP	Wasson et al., 2008	2.5
Burbank et al	CRN, strath			2.5
Burbank et al	CRN, strath			2.5
Burbank et al	CRN, strath			2.5
Burbank et al	CRN, strath			2.5
Calle et al	OSL, in terrace	6500 yr BP	Gonzalez-Samperiz et al., 2002	0.3
Calle et al	OSL, in terrace	pre-3000 yr BP	Gonzalez-Samperiz et al., 2002	0.3
Calle et al	OSL, in terrace	pre-3000 yr BP	Gonzalez-Samperiz et al., 2002	0.3
Calle et al	Paleomagnetism, in terrace	pre-3000 yr BP	Gonzalez-Samperiz et al., 2002	0.3
Calle et al	Paleomagnetism, in terrace	pre-3000 yr BP	Gonzalez-Samperiz et al., 2002	0.3
Carcaillet et al	Radiocarbon, terrace top	6400 yr BP	Karkanas et al	2.3
Carcaillet et al	Radiocarbon, terrace top	6400 yr BP	Karkanas et al	2.3
Carcaillet et al	CRN, terrace surface			2.3
Carcaillet et al	CRN, terrace surface			2.3
Carcaillet et al	Radiocarbon, terrace top			2.3
Carcaillet et al	Radiocarbon, terrace top			2.3
Carcaillet et al	Radiocarbon, terrace top			2.3
Carcaillet et al	Radiocarbon, terrace top			2.3
Carcaillet et al	CRN, terrace surface			2.3
Carcaillet et al	Radiocarbon, terrace top			2.3
Cheng et al	TL, in terrace			1.2
Cheng et al	TL, in terrace			0.4
Cheng et al	TL, in terrace			0.4
Cheng et al	TL, in terrace			0.4
Cheng et al	ESR, in terrace			0.4
Cheng et al	ESR, in terrace			0.4
Collins et al.	Radiocarbon, in terrace	150 yr BP	Kittitas County, 1989	1.4
Collins et al.	Radiocarbon, in terrace	150 yr BP	Kittitas County, 1989	1.4
Collins et al.	Radiocarbon, in terrace	150 yr BP	Kittitas County, 1989	1.4
Cook et al	CRN, terrace surface			0.6
Cook et al	CRN, terrace surface			0.6
Cook et al	CRN, terrace surface			0.6
Cook et al	CRN, terrace surface			0.6
Cook et al	CRN, terrace surface			0.6
Cook et al	CRN, terrace surface			0.6
Cook et al	CRN, terrace surface			0.6
Cook et al	CRN, terrace surface			0.6
Crow et al	U/Th, in terrace			1.1
Crow et al	U/Th, in terrace			1.1
Crow et al	U/Th, in terrace			1.1
Crow et al	U/Th, in terrace			1.2
Crow et al	U/Th, in terrace			1.3
Crow et al	CRN, in terrace			0.7
Crow et al	U/Th, in terrace			1.2
Crow et al	U/Th, in terrace			1.2
Crow et al	U/Th, in terrace			1.2
Crow et al	CRN, in terrace			1.4
Crow et al	CRN, in terrace			1.0
Cunha et al	OSL, in terrace			1.4
Cunha et al	OSL, in terrace			1.4
Cyr et al	OSL, in terrace			2.3
Dadson et al.	Radiocarbon, in terrace	4000 yr BP	Winkler and Wang, 1993	4.9
Dadson et al.	Radiocarbon, in terrace	4000 yr BP	Winkler and Wang, 1993	4.9
Dadson et al.	Radiocarbon, in terrace	4000 yr BP	Winkler and Wang, 1993	5.5

Author	Year	Age (kya)	Latitude	Longitude	Location
Dadson et al.	2003	0.9265	22.88	120.38	Erjen River, Taiwan
Dadson et al.	2003	1.244	22.89	120.39	Erjen River, Taiwan
Dadson et al.	2003	1.5705	22.87	120.36	Erjen River, Taiwan
Dadson et al.	2003	1.617	22.89	120.38	Erjen River, Taiwan
Dadson et al.	2003	1.9455	22.89	120.39	Erjen River, Taiwan
Dadson et al.	2003	2.1795	22.87	120.36	Erjen River, Taiwan
Dadson et al.	2003	2.231	22.88	120.35	Erjen River, Taiwan
Dadson et al.	2003	2.238	22.88	120.38	Erjen River, Taiwan
Dadson et al.	2003	2.248	22.87	120.36	Erjen River, Taiwan
Dadson et al.	2003	2.3365	23.06	120.41	Tsengwen River, Taiwan
Dadson et al.	2003	2.4045	24.19	121.48	Erjen River, Taiwan
Dadson et al.	2003	2.409	22.88	120.38	Liwu River, Taiwan
Dadson et al.	2003	2.5455	24.23	121.47	Liwu River, Taiwan
Dadson et al.	2003	2.632	23.39	120.54	Pachang River, Taiwan
Dadson et al.	2003	3.3345	23.06	120.40	Tsengwen River, Taiwan
Dadson et al.	2003	3.4185	23.06	120.40	Tsengwen River, Taiwan
Dadson et al.	2003	4.213	23.47	121.49	Hsiukuluan River, Taiwan
Dadson et al.	2003	5.7915	22.89	120.38	Erjen River, Taiwan
Dadson et al.	2003	6.2605	23.06	120.40	Tsengwen River, Taiwan
Dadson et al.	2003	6.2605	22.84	120.40	Erjen River, Taiwan
Dadson et al.	2003	8.343	23.07	120.40	Tsengwen River, Taiwan
Dadson et al.	2003	10.759	23.08	120.50	Tsengwen River, Taiwan
Dadson et al.	2003	13.5355	24.92	121.30	Tahan River, Taiwan
Delano	2016	7.4	47.30	123.65	Wynoochee River, Washington
Delano	2016	11.9	47.30	123.65	Wynoochee River, Washington
Delano	2016	14.7	47.30	123.65	Wynoochee River, Washington
Delano	2016	37.2	47.30	123.65	Wynoochee River, Washington
Delano	2016	41.8	47.30	123.65	Wynoochee River, Washington
Formento-Trigilio et al	2003	10	-41.60	175.00	Huangerua River, New Zealand
Formento-Trigilio et al	2003	12	-41.60	175.00	Huangerua River, New Zealand
Formento-Trigilio et al	2003	18	-41.60	175.00	Huangerua River, New Zealand
Formento-Trigilio et al	2003	20.5	-41.60	175.00	Huangerua River, New Zealand
Formento-Trigilio et al	2003	30.5	-41.60	175.00	Huangerua River, New Zealand
Formento-Trigilio et al	2003	73	-41.60	175.00	Huangerua River, New Zealand
Formento-Trigilio et al	2003	78	-41.60	175.00	Huangerua River, New Zealand
Fuller et al	2009	6.4	39.75	-123.63	SF Eel River, California
Fuller et al	2009	7.5	39.73	-123.65	SF Eel River, California
Fuller et al	2009	8.3	39.73	-123.65	SF Eel River, California
Fuller et al	2009	9.2	39.73	-123.65	SF Eel River, California
Fuller et al	2009	11.8	39.73	-123.65	SF Eel River, California
Fuller et al	2009	20.5	39.73	-123.65	SF Eel River, California
Fuller et al	2009	33.3	39.73	-123.65	SF Eel River, California
Gao et al	2016	1031	35.00	104.60	Weihe River, central China
Gao et al	2016	1081	35.00	104.50	Weihe River, central China
Gao et al	2016	1114	35.00	104.50	Weihe River, central China
Garcia and Mahan	2014	19.9	36.15	-120.75	Gabilan Mesa, California
Garcia and Mahan	2014	20.4	36.10	-120.70	Pancho Rico, Gabilan Mesa, California
Garcia and Mahan	2014	25.1	36.10	-120.70	Pancho Rico, Gabilan Mesa, California
Garcia and Mahan	2014	30.5	36.15	-120.75	Gabilan Mesa, California
Garcia and Mahan	2014	43.5	36.15	-120.75	Gabilan Mesa, California
Garcia and Mahan	2014	44.2	36.15	-120.75	Gabilan Mesa, California
Garcia and Mahan	2014	48.3	36.15	-120.75	Gabilan Mesa, California
Garcia and Mahan	2014	49	36.15	-120.75	Gabilan Mesa, California





Author	Year	Age (kya)	Latitude	Longitude	Location
Gran et al	2011	1.54	44.10	-93.75	Le Sueur River, Minnesota
Gran et al	2011	2.17	44.10	-93.75	Le Sueur River, Minnesota
Gran et al	2011	2.75	44.10	-93.75	Le Sueur River, Minnesota
Gran et al	2011	3.18	44.10	-93.75	Le Sueur River, Minnesota
Gran et al	2011	3.3	44.10	-93.75	Le Sueur River, Minnesota
Gran et al	2011	3.94	44.10	-93.75	Le Sueur River, Minnesota
Gran et al	2011	4.91	44.10	-93.75	Le Sueur River, Minnesota
Gran et al	2011	5.01	44.10	-93.75	Le Sueur River, Minnesota
Gran et al	2011	5.25	44.10	-93.75	Le Sueur River, Minnesota
Gran et al	2011	5.26	44.10	-93.75	Le Sueur River, Minnesota
Gran et al	2011	5.46	44.10	-93.75	Le Sueur River, Minnesota
Gran et al	2011	5.78	44.10	-93.75	Le Sueur River, Minnesota
Gran et al	2011	6.08	44.10	-93.75	Le Sueur River, Minnesota
Gran et al	2011	6.35	44.10	-93.75	Le Sueur River, Minnesota
Gran et al	2011	6.85	44.10	-93.75	Le Sueur River, Minnesota
Gran et al	2011	7.41	44.10	-93.75	Le Sueur River, Minnesota
Gran et al	2011	7.95	44.10	-93.75	Le Sueur River, Minnesota
Gran et al	2011	11.46	44.10	-93.75	Le Sueur River, Minnesota
Gran et al	2011	13.04	44.10	-93.75	Le Sueur River, Minnesota
Haibing et al	2005	2.9	36.00	92.25	Kunlun Shan, Tibetan Plateau, China
Haibing et al	2005	5.96	36.00	92.25	Kunlun Shan, Tibetan Plateau, China
Hancock et al	1999	121.5	44.25	-109.00	Wind River, Wyoming
Hancock et al	1999	220	44.25	-109.00	Wind River, Wyoming
Hancock et al	1999	470	44.25	-109.00	Wind River, Wyoming
Harkins et al	2005	1.3	44.67	-112.75	Big Sheep Creek, Montana
Harkins et al	2005	4	44.67	-112.75	Big Sheep Creek, Montana
Harkins et al	2005	10.5	44.67	-112.75	Big Sheep Creek, Montana
He et al	2015	25	27.50	101.80	Yalong River, SE Tibetan Plateau
He et al	2015	50	27.50	101.80	Yalong River, SE Tibetan Plateau
He et al	2015	720	27.50	101.80	Yalong River, SE Tibetan Plateau
He et al	2015	900	27.50	101.80	Yalong River, SE Tibetan Plateau
He et al	2015	1100	27.50	101.80	Yalong River, SE Tibetan Plateau
Hsieh and Knuepfer	2001	0.76	22.85	120.40	Erhjen River, Taiwan
Hsieh and Knuepfer	2001	0.93	22.85	120.40	Erhjen River, Taiwan
Hsieh and Knuepfer	2001	1.2	22.85	120.40	Erhjen River, Taiwan
Hsieh and Knuepfer	2001	2	22.85	120.40	Erhjen River, Taiwan
Hsieh and Knuepfer	2001	5.8	22.85	120.40	Erhjen River, Taiwan
Hsieh and Knuepfer	2001	6.3	22.85	120.40	Erhjen River, Taiwan
Hsieh and Knuepfer	2001	9.5	22.85	120.40	Erhjen River, Taiwan
Hu et al	2015	34	37.80	102.50	Jinta River, Qilian Shan
Hu et al	2015	57	37.80	102.50	Jinta River, Qilian Shan
Hu et al	2015	69	37.80	102.50	Jinta River, Qilian Shan
Jayangondaperumal et al	2016	25	31.75	76.00	Janauri hill, sub-Himalaya
Jia et al	2016	71.84	41.29	107.83	Yellow River, Hetao basin
Jia et al	2016	118.6	41.31	107.84	Yellow River, Hetao basin
Jiang et al	2016	93	30.00	103.05	Qingyi River, Longmen Shan, China
Jiang et al	2016	185	29.98	102.98	Qingyi River, Longmen Shan, China
Jiang et al	2016	300	29.98	102.98	Qingyi River, Longmen Shan, China
Jochems and Pederson	2015	25	38.75	-109.35	Colorado River near Moab
Jochems and Pederson	2015	35	38.75	-109.35	Colorado River near Moab
Jochems and Pederson	2015	45	38.75	-109.35	Colorado River near Moab
Jochems and Pederson	2015	65	38.75	-109.35	Colorado River near Moab



Author	Forcing	Strength of ascribed forcing?	If climate, when did incision occur in glacial cycle?	If climate, when did planation occur in glacial cycle?
Gran et al	Base level	good	glacial to interglacial	
Gran et al	Base level	good	glacial to interglacial	
Gran et al	Base level	good	glacial to interglacial	
Gran et al	Base level	good	glacial to interglacial	
Gran et al	Base level	good	glacial to interglacial	
Gran et al	Base level	good	glacial to interglacial	
Gran et al	Base level	good	glacial to interglacial	
Gran et al	Base level	good	glacial to interglacial	
Gran et al	Base level	good	glacial to interglacial	
Gran et al	Base level	good	glacial to interglacial	
Gran et al	Base level	good	glacial to interglacial	
Gran et al	Base level	good	glacial to interglacial	
Gran et al	Base level	good	glacial to interglacial	
Gran et al	Base level	good	glacial to interglacial	
Gran et al	Base level	good	glacial to interglacial	
Gran et al	Base level	good	glacial to interglacial	
Gran et al	Base level	good	glacial to interglacial	
Haibing et al	Climate	poor	Unclear	
Haibing et al	Climate	poor	full interglacial	glacial to interglacial
Hancock et al	Climate	good		full glacial
Hancock et al	Climate	poor		full glacial
Hancock et al	Climate	poor		full glacial
Harkins et al	Tectonics	good		
Harkins et al	Tectonics	good		
Harkins et al	Tectonics	good		
He et al	Climate	poor	glacial to interglacial	full glacial
He et al	Climate	poor	glacial to interglacial	full glacial
He et al	Climate	poor	glacial to interglacial	full glacial
He et al	Climate	poor	glacial to interglacial	full glacial
He et al	Climate	poor	glacial to interglacial	full glacial
Hsieh and Knuepfer	Climate	poor	full interglacial	full interglacial
Hsieh and Knuepfer	Climate	poor	full interglacial	full interglacial
Hsieh and Knuepfer	Climate	poor	full interglacial	full interglacial
Hsieh and Knuepfer	Climate	poor	full interglacial	full interglacial
Hsieh and Knuepfer	Climate	poor	full interglacial	full interglacial
Hsieh and Knuepfer	Climate	poor	full interglacial	full interglacial
Hsieh and Knuepfer	Climate	poor	full interglacial	full interglacial
Hu et al	Indeterminate			
Hu et al	Indeterminate			
Hu et al	Indeterminate			
Jayangondaperumal et al	Indeterminate			
Jia et al	Climate	poor	Unclear	
Jia et al	Climate	poor	Unclear	
Jiang et al	Indeterminate			
Jiang et al	Indeterminate			
Jiang et al	Indeterminate			
Jochems and Pederson	climate	poor	Unclear	
Jochems and Pederson	climate	poor	Unclear	
Jochems and Pederson	climate	poor	Unclear	
Jochems and Pederson	Climate	poor	Unclear	

Author	Dating method & sample location	If Holocene & forested, deforestation age	Deforestation reference	Peak ground acceleration
Gran et al	OSL, in terrace	170 yr BP	Gran et al, 2011	0.1
Gran et al	OSL, in terrace	170 yr BP	Gran et al, 2011	0.1
Gran et al	Radiocarbon, in terrace	170 yr BP	Gran et al, 2011	0.1
Gran et al	Radiocarbon, in terrace	170 yr BP	Gran et al, 2011	0.1
Gran et al	OSL, in terrace	170 yr BP	Gran et al, 2011	0.1
Gran et al	Radiocarbon, in terrace	170 yr BP	Gran et al, 2011	0.1
Gran et al	Radiocarbon, in terrace	170 yr BP	Gran et al, 2011	0.1
Gran et al	OSL, in terrace	170 yr BP	Gran et al, 2011	0.1
Gran et al	Radiocarbon, in terrace	170 yr BP	Gran et al, 2011	0.1
Gran et al	Radiocarbon, in terrace	170 yr BP	Gran et al, 2011	0.1
Gran et al	Radiocarbon, in terrace	170 yr BP	Gran et al, 2011	0.1
Gran et al	Radiocarbon, in terrace	170 yr BP	Gran et al, 2011	0.1
Gran et al	OSL, in terrace	170 yr BP	Gran et al, 2011	0.1
Gran et al	Radiocarbon, in terrace	170 yr BP	Gran et al, 2011	0.1
Gran et al	Radiocarbon, in terrace	170 yr BP	Gran et al, 2011	0.1
Gran et al	Radiocarbon, in terrace	170 yr BP	Gran et al, 2011	0.1
Gran et al	Radiocarbon, in terrace	170 yr BP	Gran et al, 2011	0.1
Gran et al	OSL, in terrace			0.1
Haibing et al	TL, terrace top			0.8
Haibing et al	TL, terrace top			0.8
Hancock et al	CRN, terrace surface			0.7
Hancock et al	CRN, terrace surface			0.7
Hancock et al	CRN, terrace surface			0.7
Harkins et al	Radiocarbon, in terrace	120 yr BP	The Nature Conservancy, 2012	1.9
Harkins et al	Radiocarbon, in terrace	120 yr BP	The Nature Conservancy, 2012	1.9
Harkins et al	Radiocarbon, in terrace	120 yr BP	The Nature Conservancy, 2012	1.9
He et al	OSL, in terrace			3.2
He et al	OSL, in terrace			3.2
He et al	ESR, in terrace			3.2
He et al	ESR, in terrace			3.2
He et al	ESR, in terrace			3.2
Hsieh and Knuepfer	Radiocarbon, in terrace	4000 yr BP	Winkler and Wang, 1993	5.0
Hsieh and Knuepfer	Radiocarbon, in terrace	4000 yr BP	Winkler and Wang, 1993	5.0
Hsieh and Knuepfer	Radiocarbon, in terrace	4000 yr BP	Winkler and Wang, 1993	5.0
Hsieh and Knuepfer	Radiocarbon, in terrace	4000 yr BP	Winkler and Wang, 1993	5.0
Hsieh and Knuepfer	Radiocarbon, in terrace	4000 yr BP	Winkler and Wang, 1993	5.0
Hsieh and Knuepfer	Radiocarbon, in terrace	4000 yr BP	Winkler and Wang, 1993	5.0
Hsieh and Knuepfer	Radiocarbon, in terrace	4000 yr BP	Winkler and Wang, 1993	5.0
Hu et al	OSL, terrace top			5.2
Hu et al	OSL, terrace top			5.2
Hu et al	OSL, terrace top			5.2
Jayangondaperumal et al	OSL, in terrace			2.7
Jia et al	OSL, in terrace			1.8
Jia et al	OSL, in terrace			1.7
Jiang et al	OSL, in terrace			2.7
Jiang et al	ESR, in terrace			3.0
Jiang et al	ESR, in terrace			3.0
Jochems and Pederson	OSL, in terrace			0.5
Jochems and Pederson	OSL, in terrace			0.5
Jochems and Pederson	OSL, in terrace			0.5
Jochems and Pederson	OSL, in terrace			0.5

Author	Year	Age (kya)	Latitude	Longitude	Location
Kothyari and Luirei	2016	2.7	29.84	79.78	Saryu River, Himalaya
Kothyari and Luirei	2016	7.8	29.70	79.89	Saryu River, Himalaya
Kothyari and Luirei	2016	8	30.00	79.92	Saryu River, Himalaya
Kothyari and Luirei	2016	9.1	29.50	80.10	Saryu River, Himalaya
Kothyari and Luirei	2016	14.9	29.87	79.78	Saryu River, Himalaya
Kothyari and Luirei	2016	15.3	29.88	79.80	Saryu River, Himalaya
Kothyari and Luirei	2016	35.7	30.00	79.92	Saryu River, Himalaya
Kothyari et al	2016	6.6	30.05	79.55	Pindar River, Himalaya
Kothyari et al	2016	13	30.10	79.90	Pindar River, Himalaya
Kothyari et al	2016	13.4	30.20	79.30	Pindar River, Himalaya
Kothyari et al	2016	16.7	30.10	79.90	Pindar River, Himalaya
Kothyari et al	2016	17.5	30.05	79.60	Pindar River, Himalaya
Kothyari et al	2016	25.3	30.05	79.60	Pindar River, Himalaya
Lasserre et al	1999	7.6	37.00	103.50	Gansu, China, NE edge Tibetan Plateau
Lave and Avouac	2000	2.2	27.30	85.50	Bakeya and Bagmati Rivers
Lave and Avouac	2000	3.7	27.30	85.50	Bakeya and Bagmati Rivers
Lave and Avouac	2000	6.15	27.30	85.50	Bakeya and Bagmati Rivers
Lave and Avouac	2000	9.2	27.30	85.50	Bakeya and Bagmati Rivers
Leland et al.	1998	0.2	35.67	74.92	Middle gorge Indus River
Leland et al.	1998	2.5	35.63	75.02	Middle gorge Indus River
Leland et al.	1998	2.7	35.63	75.02	Middle gorge Indus River
Leland et al.	1998	5.9	35.63	75.02	Middle gorge Indus River
Leland et al.	1998	6.7	35.71	74.75	Middle gorge Indus River
Leland et al.	1998	6.8	35.51	75.35	Middle gorge Indus River
Leland et al.	1998	7.2	35.72	74.63	Middle gorge Indus River
Leland et al.	1998	9.5	35.72	74.65	Middle gorge Indus River
Leland et al.	1998	11	35.78	74.63	Middle gorge Indus River
Leland et al.	1998	27.1	35.67	74.92	Middle gorge Indus River
Leland et al.	1998	41.3	35.63	75.06	Middle gorge Indus River
Leland et al.	1998	56.1	35.48	75.40	Middle gorge Indus River
Leland et al.	1998	65	35.48	75.39	Middle gorge Indus River
Lewin et al	1991	0.67	40.00	20.75	Voidomatis basin, Greece
Lewin et al	1991	0.89	40.00	20.75	Voidomatis basin, Greece
Lewis et al	2009	11	42.00	0.00	Cinca River, NE Spain
Lewis et al	2009	45	42.00	-1.00	Gallego River, NE Spain
Lewis et al	2009	47	42.00	0.00	Cinca River, NE Spain
Lewis et al	2009	61	42.00	0.00	Cinca River, NE Spain
Lewis et al	2009	68	42.00	-1.00	Gallego River, NE Spain
Lewis et al	2009	97	42.00	0.00	Cinca River, NE Spain
Lewis et al	2009	151	42.00	-1.00	Gallego River, NE Spain
Lewis et al	2009	178	42.00	0.00	Cinca River, NE Spain
Li et al	1997	10	35.50	103.00	Yellow River, Eastern Tibetan Plateau, China
Li et al	1997	55	35.50	103.00	Yellow River, Eastern Tibetan Plateau, China
Li et al	1997	120	35.50	103.00	Yellow River, Eastern Tibetan Plateau, China
Li et al	1997	600	35.50	103.00	Yellow River, Eastern Tibetan Plateau, China
Li et al	1997	1100	35.50	103.00	Yellow River, Eastern Tibetan Plateau, China
Li et al	1997	1400	35.50	103.00	Yellow River, Eastern Tibetan Plateau, China
Li et al	1997	1660	35.50	103.00	Yellow River, Eastern Tibetan Plateau, China
Li et al	2015	130	31.20	104.50	Kai River, Longmenshan
Liu et al	2015	5	30.25	102.80	Qingyijiang River, Longmen Shan
Liu et al	2015	31	30.25	102.80	Qingyijiang River, Longmen Shan
Liu et al	2015	93	30.25	102.80	Qingyijiang River, Longmen Shan
Liu et al	2015	129	30.25	102.80	Qingyijiang River, Longmen Shan



Author	Dating method & sample location	If Holocene & forested, deforestation age	Deforestation reference	Peak ground acceleration
Kothyari and Luirei	OSL, in terrace	200 yr BP	Wasson et al., 2008	4.0
Kothyari and Luirei	OSL, in terrace	200 yr BP	Wasson et al., 2008	3.8
Kothyari and Luirei	OSL, in terrace	200 yr BP	Wasson et al., 2008	4.2
Kothyari and Luirei	OSL, in terrace	200 yr BP	Wasson et al., 2008	3.7
Kothyari and Luirei	OSL, in terrace			4.0
Kothyari and Luirei	OSL, in terrace			4.0
Kothyari and Luirei	OSL, in terrace			4.2
Kothyari et al	OSL, in terrace	200 yr BP	Wasson et al., 2008	4.0
Kothyari et al	OSL, in terrace			4.3
Kothyari et al	OSL, in terrace			3.9
Kothyari et al	OSL, in terrace			4.3
Kothyari et al	OSL, in terrace			4.0
Kothyari et al	OSL, in terrace			4.0
Lasserre et al	Radiocarbon, in terrace			3.1
Lave and Avouac	Radiocarbon, in terrace	200 yr BP	Wasson et al., 2008	3.7
Lave and Avouac	Radiocarbon, in terrace	200 yr BP	Wasson et al., 2008	3.7
Lave and Avouac	Radiocarbon, in terrace	200 yr BP	Wasson et al., 2008	3.7
Lave and Avouac	Radiocarbon, in terrace	200 yr BP	Wasson et al., 2008	3.7
Leland et al.	CRN, strath	200 yr BP	Wasson et al., 2008	2.7
Leland et al.	CRN, strath	200 yr BP	Wasson et al., 2008	2.4
Leland et al.	CRN, strath	200 yr BP	Wasson et al., 2008	2.4
Leland et al.	CRN, strath	200 yr BP	Wasson et al., 2008	2.4
Leland et al.	CRN, strath	200 yr BP	Wasson et al., 2008	3.0
Leland et al.	CRN, strath	200 yr BP	Wasson et al., 2008	1.9
Leland et al.	CRN, strath	200 yr BP	Wasson et al., 2008	3.3
Leland et al.	CRN, strath	200 yr BP	Wasson et al., 2008	3.2
Leland et al.	CRN, strath	200 yr BP	Wasson et al., 2008	3.2
Leland et al.	CRN, strath			2.7
Leland et al.	CRN, strath			2.4
Leland et al.	CRN, strath			1.9
Leland et al.	CRN, strath			1.9
Lewin et al	Radiocarbon, in terrace	4000 yr BP	Amanatidou, 2005	2.1
Lewin et al	Radiocarbon, in terrace	4000 yr BP	Amanatidou, 2005	2.1
Lewis et al	OSL, in terrace	6500 yr BP	Gonzalez-Samperiz et al., 2002	0.3
Lewis et al	OSL, in terrace			0.3
Lewis et al	OSL, in terrace			0.3
Lewis et al	OSL, in terrace			0.3
Lewis et al	OSL, in terrace			0.3
Lewis et al	OSL, in terrace			0.3
Lewis et al	OSL, in terrace			0.3
Lewis et al	OSL, in terrace			0.3
Lewis et al	OSL, in terrace			0.3
Li et al	Radiocarbon, terrace top	1080 yr BP	Fang and Xie, 1994	1.3
Li et al	Multiple methods			1.3
Li et al	TL, terrace top			1.3
Li et al	Magnetostratigraphy, in terrace			1.3
Li et al	Magnetostratigraphy, in terrace			1.3
Li et al	Magnetostratigraphy, in terrace			1.3
Li et al	Magnetostratigraphy, in terrace			1.3
Li et al	OSL, in terrace			0.6
Liu et al	Previous literature			2.8
Liu et al	Previous literature			2.8
Liu et al	Previous literature			2.8
Liu et al	Previous literature			2.8

Author	Year	Age (kya)	Latitude	Longitude	Location
Lu et al	2010	1.8	44.00	86.25	Northern Tian Shan
Lu et al	2010	10	44.00	86.25	Northern Tian Shan
Lu et al	2010	300	44.00	86.25	Northern Tian Shan
Lu et al	2010	530	44.00	86.25	Northern Tian Shan
Maddy	1997	18	51.80	-1.30	Thames River, Southern England
Maddy	1997	125	51.80	-1.30	Thames River, Southern England
Maddy	1997	260	51.80	-1.30	Thames River, Southern England
Maddy	1997	450	51.80	-1.30	Thames River, Southern England
Maddy	1997	850	51.80	-1.30	Thames River, Southern England
Maddy	1997	1800	51.80	-1.30	Thames River, Southern England
Meriaux et al	2005	2.2	39.50	94.30	Aksay, northern Altyn Tagh, Tibet
Meriaux et al	2005	6.5	39.50	94.30	Aksay, northern Altyn Tagh, Tibet
Merritts et al	1994	1.228	40.30	-124.20	Mattole River, California
Merritts et al	1994	4.764	40.30	-124.20	Mattole River, California
Merritts et al	1994	4.85	40.30	-124.20	Mattole River, California
Merritts et al	1994	5.9	40.30	-124.20	Mattole River, California
Merritts et al	1994	6.24	40.30	-124.20	Mattole River, California
Molin et al.	2012	3.61	45.23	26.75	Romanian Carpathians, Slanic River
Molnar et al	1994	25	44.50	84.70	North flank Tien Shan
Molnar et al	1994	35	44.50	84.70	North flank Tien Shan
Pan et al	2003	135	37.50	102.80	Shagau River, N China
Pan et al	2003	235	37.50	102.80	Shagau River, N China
Pan et al	2003	434	37.50	102.80	Shagau River, N China
Pan et al	2003	870	37.50	102.80	Shagau River, N China
Pan et al	2009	10	36.08	103.80	Yellow River, Eastern Tibetan Plateau, China
Pan et al	2009	50	36.08	103.80	Yellow River, Eastern Tibetan Plateau, China
Pan et al	2009	130	36.08	103.80	Yellow River, Eastern Tibetan Plateau, China
Pan et al	2009	860	36.08	103.80	Yellow River, Eastern Tibetan Plateau, China
Pan et al	2009	960	36.08	103.80	Yellow River, Eastern Tibetan Plateau, China
Pan et al	2009	1050	36.08	103.80	Yellow River, Eastern Tibetan Plateau, China
Pan et al	2009	1240	36.08	103.80	Yellow River, Eastern Tibetan Plateau, China
Pazzaglia and Brandon	2001	60	47.70	-124.20	Clearwater River
Pazzaglia and Brandon	2001	150	47.70	-124.20	Clearwater River
Personius	1995	0.5	44.80	-124.00	Siletz River
Personius	1995	2.21	44.78	-123.83	Siletz River
Personius	1995	6.19	46.09	-123.72	NF Klaskanine
Personius	1995	7.3	43.50	-123.52	Umpqua River
Personius	1995	7.81	44.51	-123.88	Siuslaw River
Personius	1995	8.57	45.81	-123.77	NF Nehalem
Personius	1995	9.53	43.63	-123.57	Umpqua River
Personius	1995	9.92	44.78	-123.80	Siletz River
Personius	1995	9.97	43.52	-123.54	Umpqua River
Personius	1995	10.32	45.76	-123.30	Nehalem
Personius	1995	10.5	43.89	-123.48	Siuslaw River
Personius	1995	10.5	43.78	-123.55	Smith River
Personius	1995	10.86	44.73	-123.92	Siletz River
Personius	1995	10.92	43.52	-123.54	Umpqua River
Personius	1995	11	44.38	-123.67	Alsea River
Personius	1995	11	45.01	-123.90	Salmon River
Personius	1995	11	44.54	-123.72	Big Elk Creek
Personius	1995	11	46.09	-123.72	NF Klaskanine
Personius	1995	11	45.28	-123.74	Nestucca River



Author	Dating method & sample location	If Holocene & forested, deforestation age	Deforestation reference	Peak ground acceleration
Lu et al	OSL, in terrace			3.5
Lu et al	OSL, in terrace			3.5
Lu et al	ESR, terrace top			3.5
Lu et al	ESR, terrace top			3.5
Maddy	Previous literature			0.3
Maddy	Previous literature			0.3
Maddy	Previous literature			0.3
Maddy	Previous literature			0.3
Maddy	Previous literature			0.3
Maddy	Previous literature			0.3
Meriaux et al	Multiple methods			2.6
Meriaux et al	Multiple methods			2.6
Merritts et al	Radiocarbon, in terrace	170 yr BP	Coastal Watershed assessment	6.2
Merritts et al	Radiocarbon, in terrace	170 yr BP	Coastal Watershed assessment	6.2
Merritts et al	Radiocarbon, in terrace	170 yr BP	Coastal Watershed assessment	6.2
Merritts et al	Radiocarbon, in terrace	170 yr BP	Coastal Watershed assessment	6.2
Merritts et al	Radiocarbon, in terrace	170 yr BP	Coastal Watershed assessment	6.2
Molin et al.	Radiocarbon, in terrace	3800 yr BP	Tantau et al, 2009	3.4
Molnar et al	Multiple methods			1.7
Molnar et al	Multiple methods			1.7
Pan et al	TL, terrace top			5.4
Pan et al	TL, terrace top			5.4
Pan et al	Paleosol correlation			5.4
Pan et al	Paleomagnetism, terrace top			5.4
Pan et al	Radiocarbon, terrace top	1080 yr BP	Fang and Xie, 1994	1.7
Pan et al	IRSL, in terrace			1.7
Pan et al	OSL, terrace top			1.7
Pan et al	Magnestratigraphy, terrace top			1.7
Pan et al	Magnestratigraphy, terrace top			1.7
Pan et al	Magnestratigraphy, terrace top			1.7
Pan et al	Magnestratigraphy, terrace top			1.7
Pazzaglia and Brandon	stratigraphic relationship			2.7
Pazzaglia and Brandon	stratigraphic relationship			2.7
Personius	Radiocarbon, in terrace	135-60 yr BP	Miller, 2010	2.6
Personius	Radiocarbon, in terrace	135-60 yr BP	Miller, 2010	2.6
Personius	Radiocarbon, in terrace	135-60 yr BP	Miller, 2010	2.5
Personius	Radiocarbon, in terrace	135-60 yr BP	Miller, 2010	2.1
Personius	Radiocarbon, in terrace	135-60 yr BP	Miller, 2010	2.8
Personius	Radiocarbon, in terrace	135-60 yr BP	Miller, 2010	2.6
Personius	Radiocarbon, in terrace	135-60 yr BP	Miller, 2010	2.2
Personius	Radiocarbon, in terrace	135-60 yr BP	Miller, 2010	2.6
Personius	Radiocarbon, in terrace	135-60 yr BP	Miller, 2010	2.1
Personius	Radiocarbon, in terrace	135-60 yr BP	Miller, 2010	2.2
Personius	Radiocarbon, in terrace	135-60 yr BP	Miller, 2010	2.0
Personius	Radiocarbon, in terrace	135-60 yr BP	Miller, 2010	2.2
Personius	Radiocarbon, in terrace	135-60 yr BP	Miller, 2010	2.7
Personius	Radiocarbon, in terrace	135-60 yr BP	Miller, 2010	2.1
Personius	Radiocarbon, in terrace	135-60 yr BP	Miller, 2010	2.4
Personius	Radiocarbon, in terrace	135-60 yr BP	Miller, 2010	2.5
Personius	Radiocarbon, in terrace	135-60 yr BP	Miller, 2010	2.6
Personius	Radiocarbon, in terrace	135-60 yr BP	Miller, 2010	2.6
Personius	Radiocarbon, in terrace	135-60 yr BP	Miller, 2010	2.5



Author	Year	Age (kya)	Latitude	Longitude	Location
Personius	1995	11	44.65	-123.75	Yaquina River
Personius	1995	11	45.70	-123.76	Nehalem
Personius	1995	11.8	45.98	-123.37	Nehalem
Personius	1995	11.92	44.47	-123.96	Drift Creek
Personius	1995	12.01	44.51	-123.83	Drift Creek
Personius	1995	12.03	45.80	-123.82	NF Nehalem
Personius	1995	14.3	44.72	-123.93	Siletz River
Personius	1995	15	45.29	-123.74	Nestucca River
Personius	1995	15.4	45.28	-123.78	Nestucca River
Personius	1995	41.6	44.79	-123.80	Siletz River
Personius	1995	125	43.64	-123.61	Umpqua River
Picotti and Pazzaglia	2008	1.5	44.43	11.25	Italy, Reno Valley
Picotti and Pazzaglia	2008	6	44.43	11.25	Italy, Reno Valley
Picotti and Pazzaglia	2008	9	44.43	11.25	Italy, Reno Valley
Picotti and Pazzaglia	2008	13	44.43	11.25	Italy, Reno Valley
Picotti and Pazzaglia	2008	22	44.43	11.25	Italy, Reno Valley
Prizomwala et al	2016	14.7	23.33	70.00	Lotia River, Western India
Repka et al	1997	60	38.36	-110.91	Fremont River, Utah
Repka et al	1997	102	38.36	-110.91	Fremont River, Utah
Repka et al	1997	151	38.36	-110.91	Fremont River, Utah
Robinson et al	2015	198	37.33	75.34	Karakoram Fault
Rockwell et al	1984	30	34.40	-119.30	Ventura River, California
Rockwell et al	1984	38	34.40	-119.30	Ventura River, California
Rockwell et al	1984	54	34.40	-119.30	Ventura River, California
Rockwell et al	1984	92	34.40	-119.30	Ventura River, California
Ruszkiczay-Rudiger et al	2016	91	47.70	18.00	Danube River, Hungary
Ruszkiczay-Rudiger et al	2016	143	47.70	18.00	Danube River, Hungary
Schanz and Montgomery	2016	0.08	46.61	-123.64	Willapa River, Washington
Schanz and Montgomery	2016	2.86	46.56	-123.61	Willapa River, Washington
Schildgen et al	2012	30	36.67	33.50	Mut Basin, southern Turkey
Schildgen et al	2012	100	36.67	33.50	Mut Basin, southern Turkey
Seong et al	2016	15	33.35	-112.00	Pima Wash, Sonoran Desert
Seong et al	2016	60	33.35	-112.00	Pima Wash, Sonoran Desert
Simoës et al	2007	13.6	23.75	120.73	Taiwan
Stock et al	2005	1.29	47.30	-123.56	WF Satsop River, Washington
Stock et al	2005	7.4	47.30	-123.56	WF Satsop River, Washington
Tyracek et al	2004	50	50.00	14.40	Elbe, Czech Republic
Tyracek et al	2004	150	50.00	14.40	Elbe, Czech Republic
Tyracek et al	2004	240	50.00	14.40	Elbe, Czech Republic
Tyracek et al	2004	355	50.00	14.40	Elbe, Czech Republic
Tyracek et al	2004	490	50.00	14.40	Elbe, Czech Republic
Tyracek et al	2004	620	50.00	14.40	Elbe, Czech Republic
Tyracek et al	2004	765	50.00	14.40	Elbe, Czech Republic
Tyracek et al	2004	850	50.00	14.40	Elbe, Czech Republic
Tyracek et al	2004	960	50.00	14.40	Elbe, Czech Republic
Tyracek et al	2004	2075	50.00	14.40	Elbe, Czech Republic
Van der Woerd et al.	1998	1.778	35.74	94.30	unnamed stream, Xidatan, Kunlun fault
Van der Woerd et al.	1998	2.914	35.74	94.30	unnamed stream, Xidatan, Kunlun fault
Van der Woerd et al.	1998	5.106	35.74	94.30	unnamed stream, Xidatan, Kunlun fault
Van der Woerd et al.	2001	4.6	39.50	94.70	western Gansu, China near Altyn Tagh
Van der Woerd et al.	2001	8.4	39.50	94.70	western Gansu, China near Altyn Tagh
Van der Woerd et al.	2001	9.2	39.50	94.70	western Gansu, China near Altyn Tagh

Author	Forcing	Strength of ascribed forcing?	If climate, when did incision occur in glacial cycle?	If climate, when did planation occur in glacial cycle?
Personius	Climate	good	full interglacial	glacial to interglacial
Personius	Climate	good	full interglacial	glacial to interglacial
Personius	Climate	good	full interglacial	glacial to interglacial
Personius	Climate	good	full interglacial	glacial to interglacial
Personius	Climate	good	full interglacial	glacial to interglacial
Personius	Climate	good	full interglacial	glacial to interglacial
Personius	Indeterminate			
Personius	Indeterminate			
Personius	Indeterminate			
Personius	Indeterminate			
Personius	Indeterminate			
Picotti and Pazzaglia	Indeterminate			
Picotti and Pazzaglia	Indeterminate			
Picotti and Pazzaglia	Indeterminate			
Picotti and Pazzaglia	Climate	good		full glacial
Picotti and Pazzaglia	Climate	good		full glacial
Prizomwala et al	Indeterminate			
Repka et al	Climate	poor		full glacial
Repka et al	Climate	poor		full glacial
Repka et al	Climate	poor		full glacial
Robinson et al	Indeterminate			
Rockwell et al	Climate	poor	full glacial	full interglacial
Rockwell et al	Climate	poor	full glacial	full interglacial
Rockwell et al	Climate	poor	full glacial	full interglacial
Rockwell et al	Climate	poor	full glacial	full interglacial
Ruszkiczay-Rudiger et al	climate	poor	glacial to interglacial	full glacial
Ruszkiczay-Rudiger et al	climate	poor	glacial to interglacial	full glacial
Schanz and Montgomery	Indeterminate			
Schanz and Montgomery	Indeterminate			
Schildgen et al	Climate	poor	full interglacial	
Schildgen et al	Climate	poor	full interglacial	
Seong et al	Indeterminate			
Seong et al	Indeterminate			
Simoës et al	Tectonics	good		
Stock et al	Indeterminate			
Stock et al	Indeterminate			
Tyracek et al	Climate	poor		full glacial
Tyracek et al	Climate	poor		full glacial
Tyracek et al	Climate	poor		full glacial
Tyracek et al	Climate	poor		full glacial
Tyracek et al	Climate	poor		full glacial
Tyracek et al	Climate	poor		full glacial
Tyracek et al	Climate	poor		full glacial
Tyracek et al	Climate	poor		full glacial
Tyracek et al	Climate	poor		full glacial
Tyracek et al	Climate	poor		full glacial
Van der Woerd et al.	Climate	poor	full interglacial	full interglacial
Van der Woerd et al.	Climate	poor	full interglacial	full interglacial
Van der Woerd et al.	Climate	poor	full interglacial	full interglacial
Van der Woerd et al.	Tectonics	good		
Van der Woerd et al.	Tectonics	good		
Van der Woerd et al.	Tectonics	good		

Author	Dating method & sample location	If Holocene & forested, deforestation age	Deforestation reference	Peak ground acceleration
Personius	Radiocarbon, in terrace	135-60 yr BP	Miller, 2010	2.5
Personius	Radiocarbon, in terrace	135-60 yr BP	Miller, 2010	2.6
Personius	Radiocarbon, in terrace	135-60 yr BP	Miller, 2010	2.2
Personius	Radiocarbon, in terrace	135-60 yr BP	Miller, 2010	2.8
Personius	Radiocarbon, in terrace			2.7
Personius	Radiocarbon, in terrace			2.6
Personius	Radiocarbon, in terrace			2.8
Personius	Radiocarbon, in terrace			2.6
Personius	Radiocarbon, in terrace			2.6
Personius	Radiocarbon, in terrace			2.6
Personius	TL, in terrace			2.2
Picotti and Pazzaglia	Radiocarbon, in terrace	7000 yr BP	Cremachia and Nicosia, 2012	2.1
Picotti and Pazzaglia	Radiocarbon, in terrace	7000 yr BP	Cremachia and Nicosia, 2012	2.1
Picotti and Pazzaglia	Radiocarbon, in terrace	7000 yr BP	Cremachia and Nicosia, 2012	2.1
Picotti and Pazzaglia	Radiocarbon, in terrace			2.1
Picotti and Pazzaglia	Radiocarbon, in terrace			2.1
Prizomwala et al	OSL, in terrace			2.0
Repka et al	CRN, terrace surface			0.8
Repka et al	CRN, terrace surface			0.8
Repka et al	CRN, terrace surface			0.8
Robinson et al	U/Th, in terrace			3.6
Rockwell et al	Radiocarbon, in terrace			6.5
Rockwell et al	Radiocarbon, in terrace			6.5
Rockwell et al	Slip rate			6.5
Rockwell et al	Slip rate			6.5
Ruszkiczay-Rudiger et al	IRSL, in terrace			1.2
Ruszkiczay-Rudiger et al	IRSL, in terrace			1.2
Schanz and Montgomery	Radiocarbon, in terrace	170 yr BP	Williams, 1930	2.6
Schanz and Montgomery	Radiocarbon, in terrace	170 yr BP	Williams, 1930	2.5
Schildgen et al	CRN, terrace surface			0.9
Schildgen et al	CRN, terrace surface			0.9
Seong et al	CRN, strath			0.5
Seong et al	CRN, strath			0.5
Simoes et al	Previous literature			5.8
Stock et al	Radiocarbon, in terrace	80-70 yr BP	Stock et al., 2005	3.0
Stock et al	Radiocarbon, in terrace	80-70 yr BP	Stock et al., 2005	3.0
Tyracek et al	Multiple methods			0.3
Tyracek et al	Multiple methods			0.3
Tyracek et al	Multiple methods			0.3
Tyracek et al	Multiple methods			0.3
Tyracek et al	Multiple methods			0.3
Tyracek et al	Multiple methods			0.3
Tyracek et al	Multiple methods			0.3
Tyracek et al	Multiple methods			0.3
Tyracek et al	Multiple methods			0.3
Tyracek et al	Multiple methods			0.3
Van der Woerd et al.	CRN, terrace surface			0.7
Van der Woerd et al.	CRN, terrace surface			0.7
Van der Woerd et al.	CRN, terrace surface			0.7
Van der Woerd et al.	Radiocarbon, terrace top			2.4
Van der Woerd et al.	Radiocarbon, terrace top			2.4
Van der Woerd et al.	Radiocarbon, terrace top			2.4

Author	Year	Age (kya)	Latitude	Longitude	Location
Vassallo et al	2007	5	44.99	100.38	Gobi-Altay, Mongolia
Vassallo et al	2007	110	45.04	100.38	Gobi-Altay, Mongolia
Vassallo et al	2007	230	45.04	100.38	Gobi-Altay, Mongolia
Vassallo et al	2007	330	45.05	100.37	Gobi-Altay, Mongolia
Vassallo et al	2015	3.8	33.39	74.51	Chenab River, western Himalaya syntaxis
Vassallo et al	2015	24	33.01	74.79	Chenab River, western Himalaya syntaxis
Vignon et al	2016	36	33.70	74.50	Nodda River, Himalaya
Vignon et al	2016	38	33.70	74.50	Nodda River, Himalaya
von Suchodoletz et al	2015	11	41.40	45.00	Algeti River, SE Georgia
Wang et al	2015	13.7	36.65	101.72	Huang Shui, Huang He rivers, NE Tibetan Plateau
Wang et al	2015	32	36.10	103.02	Huang Shui, Huang He rivers, NE Tibetan Plateau
Wang et al	2015	51	36.14	103.50	Huang Shui, Huang He rivers, NE Tibetan Plateau
Wang et al	2015	70	36.00	103.50	Huang Shui, Huang He rivers, NE Tibetan Plateau
Wang et al	2015	103	36.00	103.50	Huang Shui, Huang He rivers, NE Tibetan Plateau
Wegmann and Pazzaglia	2002	0.03	47.60	124.20	Clearwater River
Wegmann and Pazzaglia	2002	1.15	47.60	124.20	Clearwater River
Wegmann and Pazzaglia	2002	5	47.60	124.20	Clearwater River
Wegmann and Pazzaglia	2002	8	47.60	124.20	Clearwater River
Wegmann and Pazzaglia	2009	1.5	44.00	12.00	Bidente River, North Apennines, Italy
Wegmann and Pazzaglia	2009	3	43.40	13.20	Musone River, North Apennines, Italy
Wegmann and Pazzaglia	2009	6	44.00	12.00	Bidente River, North Apennines, Italy
Wegmann and Pazzaglia	2009	9	43.98	11.91	Bidente River, North Apennines, Italy
Wegmann and Pazzaglia	2009	10	43.40	13.20	Musone River, North Apennines, Italy
Wegmann and Pazzaglia	2009	13	44.00	12.00	Bidente River, North Apennines, Italy
Wegmann and Pazzaglia	2009	22	44.13	12.00	Bidente River, North Apennines, Italy
Wegmann and Pazzaglia	2009	27	43.40	13.20	Musone River, North Apennines, Italy
Wegmann and Pazzaglia	2009	30	44.00	12.00	Bidente River, North Apennines, Italy
Wegmann and Pazzaglia	2009	40	43.40	13.20	Musone River, North Apennines, Italy
Wegmann and Pazzaglia	2009	140	44.00	12.00	Bidente River, North Apennines, Italy
Wegmann and Pazzaglia	2009	160	43.40	13.20	Musone River, North Apennines, Italy
Wegmann and Pazzaglia	2009	440	44.00	12.00	Bidente River, North Apennines, Italy
Wegmann and Pazzaglia	2009	450	43.40	13.20	Musone River, North Apennines, Italy
Wegmann and Pazzaglia	2009	620	44.00	12.00	Bidente River, North Apennines, Italy
Wegmann and Pazzaglia	2009	775	43.40	13.20	Musone River, North Apennines, Italy
Wegmann and Pazzaglia	2009	800	44.00	12.00	Bidente River, North Apennines, Italy
Wesnousky et al	1999	1.665	30.20	77.70	Himalaya frontal thrust
Yanites et al	2010	1.35	24.04	120.90	Peikang River, Taiwan
Yanites et al	2010	2.09	24.04	120.90	Peikang River, Taiwan
Yanites et al	2010	2.13	24.04	120.90	Peikang River, Taiwan
Yanites et al	2010	2.79	24.04	120.90	Peikang River, Taiwan
Yanites et al	2010	2.9	24.04	120.90	Peikang River, Taiwan
Yanites et al	2010	3	24.04	120.90	Peikang River, Taiwan
Yanites et al	2010	3.07	24.04	120.90	Peikang River, Taiwan
Yanites et al	2010	3.12	24.04	120.90	Peikang River, Taiwan
Yanites et al	2010	3.26	24.04	120.90	Peikang River, Taiwan
Yanites et al	2010	3.45	24.04	120.90	Peikang River, Taiwan







## Appendix A bibliography

- Amos, C.B., Burbank, D.W., Nobes, D.C., Read, S.A.L., 2007. Geomorphic constraints on listric thrust faulting: Implications for active deformation in the Mackenzie Basin, South Island, New Zealand. *Journal of Geophysical Research: Solid Earth* 112. <https://doi.org/10.1029/2006JB004291>
- Antoine, P., Lautridou, J.P., Laurent, M., 2000. Long-term fluvial archives in NW France: response of the Seine and Somme rivers to tectonic movements, climatic variations and sea-level changes. *Geomorphology* 33, 183–207. [https://doi.org/10.1016/S0169-555X\(99\)00122-1](https://doi.org/10.1016/S0169-555X(99)00122-1)
- Barnard, P.L., Owen, L.A., Finkel, R.C., 2004a. Style and timing of glacial and paraglacial sedimentation in a monsoon-influenced high Himalayan environment, the upper Bhagirathi Valley, Garhwal Himalaya. *Sedimentary Geology* 165, 199–221. <https://doi.org/10.1016/j.sedgeo.2003.11.009>
- Barnard, P.L., Owen, L.A., Sharma, M.C., Finkel, R.C., 2004b. Late Quaternary (Holocene) landscape evolution of a monsoon-influenced high Himalayan valley, Gori Ganga, Nanda Devi, NE Garhwal. *Geomorphology* 61, 91–110. <https://doi.org/10.1016/j.geomorph.2003.12.002>
- Barnard, P.L., Owen, L.A., Sharma, M.C., Finkel, R.C., 2001. Natural and human-induced landsliding in the Garhwal Himalaya of northern India. *Geomorphology* 40, 21–35. [https://doi.org/10.1016/S0169-555X\(01\)00035-6](https://doi.org/10.1016/S0169-555X(01)00035-6)
- Baynes, E.R.C., Attal, M., Niedermann, S., Kirstein, L.A., Dugmore, A.J., Naylor, M., 2015. Erosion during extreme flood events dominates Holocene canyon evolution in northeast Iceland. *Proceedings of the National Academy of Sciences* 112, 2355–2360. <https://doi.org/10.1073/pnas.1415443112>
- Bender, A.M., Amos, C.B., Bierman, P., Rood, D.H., Staisch, L., Kelsey, H., Sherrod, B., 2016. Differential uplift and incision of the Yakima River terraces, central Washington State. *Journal of Geophysical Research: Solid Earth* 121, 2015JB012303. <https://doi.org/10.1002/2015JB012303>
- Berryman, K., Marden, M., Palmer, A., Wilson, K., Mazengarb, C., Litchfield, N., 2010. The post-glacial downcutting history in the Waihuka tributary of Waipaoa River, Gisborne district: Implications for tectonics and landscape evolution in the Hikurangi subduction margin, New Zealand. *Marine Geology* 270, 55–71. <https://doi.org/10.1016/j.margeo.2009.10.001>
- Bhattacharjee, D., Jain, V., Chattopadhyay, A., Biswas, R.H., Singhvi, A.K., 2016. Geomorphic evidences and chronology of multiple neotectonic events in a cratonic area: Results from the Gavilgarh Fault Zone, central India. *Tectonophysics* 677–678, 199–217. <https://doi.org/10.1016/j.tecto.2016.04.022>
- Burbank, D.W., Leland, J., Fielding, E., Anderson, R.S., Brozovic, N., Reid, M.R., Duncan, C., 1996. Bedrock incision, rock uplift and threshold hillslopes in the northwestern Himalayas. *Nature* 379, 505–510. <https://doi.org/10.1038/379505a0>
- Calle, M., Sancho, C., Peña, J.L., Cunha, P., Oliva-Urcia, B., Pueyo, E.L., 2013. The sequence of quaternary fluvial terraces of the Alcanadre river (Huesca): characterization and paleoenvironmental aspects. *Cuadernos de Investigación Geográfica* 39, 159–178. <https://doi.org/10.18172/cig.2004>



- Carcaillet, J., Mugnier, J.L., Koçi, R., Jouanne, F., 2009. Uplift and active tectonics of southern Albania inferred from incision of alluvial terraces. *Quaternary Research* 71, 465–476. <https://doi.org/10.1016/j.yqres.2009.01.002>
- Cheng, S., Deng, Q., Zhou, S., Yang, G., 2002. Strath terraces of Jinshaan Canyon, Yellow River, and Quaternary tectonic movements of the Ordos Plateau, North China. *Terra Nova* 14, 215–224. <https://doi.org/10.1046/j.1365-3121.2002.00350.x>
- Collins, B.D., Montgomery, D.R., Schanz, S.A., Larsen, I.J., 2016. Rates and mechanisms of bedrock incision and strath terrace formation in a forested catchment, Cascade Range, Washington. *Geological Society of America Bulletin* B31340.1. <https://doi.org/10.1130/B31340.1>
- Cook, K.L., Whipple, K.X., Heimsath, A.M., Hanks, T.C., 2009. Rapid incision of the Colorado River in Glen Canyon – insights from channel profiles, local incision rates, and modeling of lithologic controls. *Earth Surface Processes and Landforms* 34, 994–1010. <https://doi.org/10.1002/esp.1790>
- Crow, R., Karlstrom, K., Darling, A., Crossey, L., Polyak, V., Granger, D., Asmerom, Y., Schmandt, B., 2014. Steady incision of Grand Canyon at the million year timeframe: A case for mantle-driven differential uplift. *Earth and Planetary Science Letters* 397, 159–173. <https://doi.org/10.1016/j.epsl.2014.04.020>
- Cunha, P.P., Martins, A.A., Huot, S., Murray, A., Raposo, L., 2008. Dating the Tejo river lower terraces in the Ródão area (Portugal) to assess the role of tectonics and uplift. *Geomorphology* 102, 43–54. <https://doi.org/10.1016/j.geomorph.2007.05.019>
- Cyr, A.J., Miller, D.M., Mahan, S.A., 2015. Paleodischarge of the Mojave River, southwestern United States, investigated with single-pebble measurements of  $^{10}\text{Be}$ . *Geosphere* 11, 1158–1171. <https://doi.org/10.1130/GES01134.1>
- Dadson, S.J., Hovius, N., Chen, H., Dade, W.B., Hsieh, M.-L., Willett, S.D., Hu, J.-C., Horng, M.-J., Chen, M.-C., Stark, C.P., Lague, D., Lin, J.-C., 2003. Links between erosion, runoff variability and seismicity in the Taiwan orogen. *Nature* 426, 648–651. <https://doi.org/10.1038/nature02150>
- Delano, J., 2016. Fluvial Incision, Upper Plate Faulting, and Short-Term Deformation in the Southern Olympic Mountains of Washington State (MS Thesis). Western Washington University.
- Formento-Trigilio, M.L., Burbank, D.W., Nicol, A., Shulmeister, J., Rieser, U., 2003. River response to an active fold-and-thrust belt in a convergent margin setting, North Island, New Zealand. *Geomorphology* 49, 125–152. [https://doi.org/10.1016/S0169-555X\(02\)00167-8](https://doi.org/10.1016/S0169-555X(02)00167-8)
- Fuller, T.K., Perg, L.A., Willenbring, J.K., Lepper, K., 2009. Field evidence for climate-driven changes in sediment supply leading to strath terrace formation. *Geology* 37, 467–470. <https://doi.org/10.1130/G25487A.1>
- Gao, H., Li, Z., Ji, Y., Pan, B., Liu, X., 2016. Climatic and tectonic controls on strath terraces along the upper Weihe River in central China. *Quaternary Research* 86, 326–334. <https://doi.org/10.1016/j.yqres.2016.08.004>
- García, A.F., Mahan, S.A., 2014. The notion of climate-driven strath-terrace production assessed via dissimilar stream-process response to late Quaternary climate. *Geomorphology* 214, 223–244. <https://doi.org/10.1016/j.geomorph.2014.02.008>
- Gran, K., Belmont, P., Day, S., Jennings, C., Lauer, J.W., Viparelli, E., Wilcock, P., Parker, G., 2011. An integrated sediment budget for the Le Sueur River Basin. Minnesota Pollution Control Agency Report wq-iw7-29o.

- Haibing, L., Van der Woerd, J., Tapponnier, P., Klinger, Y., Xuexiang, Q., Jingsui, Y., Yintang, Z., 2005. Slip rate on the Kunlun fault at Hongshui Gou, and recurrence time of great events comparable to the 14/11/2001, Mw~7.9 Kokoxili earthquake. *Earth and Planetary Science Letters* 237, 285–299. <https://doi.org/10.1016/j.epsl.2005.05.041>
- Hancock, G.S., Anderson, R.S., Chadwick, O.A., Finkel, R.C., 1999. Dating fluvial terraces with <sup>10</sup>Be and <sup>26</sup>Al profiles: application to the Wind River, Wyoming. *Geomorphology* 27, 41–60. [https://doi.org/10.1016/S0169-555X\(98\)00089-0](https://doi.org/10.1016/S0169-555X(98)00089-0)
- Harkins, N.W., Anastasio, D.J., Pazzaglia, F.J., 2005. Tectonic geomorphology of the Red Rock fault, insights into segmentation and landscape evolution of a developing range front normal fault. *Journal of Structural Geology* 27, 1925–1939. <https://doi.org/10.1016/j.jsg.2005.07.005>
- He, Z., Zhang, X., Bao, S., Qiao, Y., Sheng, Y., Liu, X., He, X., Yang, X., Zhao, J., Liu, R., Lu, C., 2015. Multiple climatic cycles imprinted on regional uplift-controlled fluvial terraces in the lower Yalong River and Anning River, SE Tibetan Plateau. *Geomorphology* 250, 95–112. <https://doi.org/10.1016/j.geomorph.2015.08.010>
- Hsieh, M.-L., Knuepfer, P.L.K., 2001. Middle–late Holocene river terraces in the Erhjen River Basin, southwestern Taiwan—implications of river response to climate change and active tectonic uplift. *Geomorphology* 38, 337–372. [https://doi.org/10.1016/S0169-555X\(00\)00105-7](https://doi.org/10.1016/S0169-555X(00)00105-7)
- Hu, X., Pan, B., Kirby, E., Gao, H., Hu, Z., Cao, B., Geng, H., Li, Q., Zhang, G., 2015. Rates and kinematics of active shortening along the eastern Qilian Shan, China, inferred from deformed fluvial terraces. *Tectonics* 34, 2015TC003978. <https://doi.org/10.1002/2015TC003978>
- Jayangondaperumal, R., Kumahara, Y., Thakur, V.C., Kumar, A., Srivastava, P., Dubey, S., Joevivek, V., Dubey, A.K., 2017. Great earthquake surface ruptures along backthrust of the Janauri anticline, NW Himalaya. *Journal of Asian Earth Sciences* 133, 89–101. <https://doi.org/10.1016/j.jseaes.2016.05.006>
- Jia, L., Zhang, X., Ye, P., Zhao, X., He, Z., He, X., Zhou, Q., Li, J., Ye, M., Wang, Z., Meng, J., 2016. Development of the alluvial and lacustrine terraces on the northern margin of the Hetao Basin, Inner Mongolia, China: Implications for the evolution of the Yellow River in the Hetao area since the late Pleistocene. *Geomorphology* 263, 87–98. <https://doi.org/10.1016/j.geomorph.2016.03.034>
- Jiang, D., Zhang, S., Li, W., 2016. Research on the Quaternary fluvial geomorphological surface sequence of the foreland region in southern Longmen Shan, eastern Tibet. *Geomorphology* 269, 133–148. <https://doi.org/10.1016/j.geomorph.2016.06.036>
- Jochems, A.P., Pederson, J.L., 2015. Active salt deformation and rapid, transient incision along the Colorado River near Moab, Utah. *Journal of Geophysical Research: Earth Surface* 120, 2014JF003169. <https://doi.org/10.1002/2014JF003169>
- Kothyari, G.C., Luirei, K., 2016. Late Quaternary tectonic landforms and fluvial aggradation in the Saryu River valley: Central Kumaun Himalaya. *Geomorphology* 268, 159–176. <https://doi.org/10.1016/j.geomorph.2016.06.010>
- Kothyari, G.C., Shukla, A.D., Juyal, N., 2016. Reconstruction of Late Quaternary climate and seismicity using fluvial landforms in Pindar River valley, Central Himalaya, Uttarakhand, India. *Quaternary International*. <https://doi.org/10.1016/j.quaint.2016.06.001>
- Lasserre, C., Morel, P.-H., Gaudemer, Y., Tapponnier, P., Ryerson, F.J., King, G.C.P., Métivier, F., Kasser, M., Kashgarian, M., Liu, B., Lu, T., Yuan, D., 1999. Postglacial left slip rate and

- past occurrence of  $M \geq 8$  earthquakes on the Western Haiyuan Fault, Gansu, China. *Journal of Geophysical Research: Solid Earth* 104, 17633–17651. <https://doi.org/10.1029/1998JB900082>
- Lavé, J., Avouac, J.P., 2000. Active folding of fluvial terraces across the Siwaliks Hills, Himalayas of central Nepal. *Journal of Geophysical Research: Solid Earth* 105, 5735–5770. <https://doi.org/10.1029/1999JB900292>
- Leland, J., Reid, M.R., Burbank, D.W., Finkel, R., Caffee, M., 1998. Incision and differential bedrock uplift along the Indus River near Nanga Parbat, Pakistan Himalaya, from  $^{10}\text{Be}$  and  $^{26}\text{Al}$  exposure age dating of bedrock straths. *Earth and Planetary Science Letters* 154, 93–107. [https://doi.org/10.1016/S0012-821X\(97\)00171-4](https://doi.org/10.1016/S0012-821X(97)00171-4)
- Lewin, J., Macklin, M.G., Woodward, J.C., 1991. Late Quaternary fluvial sedimentation in the Voidomatis basin, Epirus, Northwest Greece. *Quaternary Research* 35, 103–115. [https://doi.org/10.1016/0033-5894\(91\)90098-P](https://doi.org/10.1016/0033-5894(91)90098-P)
- Lewis, C.J., McDonald, E.V., Sancho, C., Peña, J.L., Rhodes, E.J., 2009. Climatic implications of correlated Upper Pleistocene glacial and fluvial deposits on the Cinca and Gállego Rivers (NE Spain) based on OSL dating and soil stratigraphy. *Global and Planetary Change* 67, 141–152. <https://doi.org/10.1016/j.gloplacha.2009.01.001>
- Li, J.-J., Fang, X.-M., Van der Voo, R., Zhu, J.-J., Niocail, C.M., Ono, Y., Pan, B.-T., Zhong, W., Wang, J.-L., Sasaki, T., Zhang, Y.-T., Cao, J.-X., Kang, S.-C., Wang, J.-M., 1997. Magnetostratigraphic dating of river terraces: Rapid and intermittent incision by the Yellow River of the northeastern margin of the Tibetan Plateau during the Quaternary. *Journal of Geophysical Research: Solid Earth* 102, 10121–10132. <https://doi.org/10.1029/97JB00275>
- Li, K., Xu, X.-W., Tan, X.-B., Chen, G.-H., Xu, C., Kang, W.-J., 2015. Late Quaternary deformation of the Longquan anticline in the Longmenshan thrust belt, eastern Tibet, and its tectonic implication. *Journal of Asian Earth Sciences* 112, 1–10. <https://doi.org/10.1016/j.jseaes.2015.08.022>
- Liu, S., Zhang, S., Ding, R., Ren, J., Liu, H., Jiang, D., Xie, F., 2015. Upper crustal folding of the 2013 Lushan earthquake area in southern Longmen Shan, China, insights from Late Quaternary fluvial terraces. *Tectonophysics* 639, 99–108. <https://doi.org/10.1016/j.tecto.2014.11.016>
- Lu, H., Burbank, D.W., Li, Y., 2010. Alluvial sequence in the north piedmont of the Chinese Tian Shan over the past 550 kyr and its relationship to climate change. *Palaeogeography, Palaeoclimatology, Palaeoecology* 285, 343–353. <https://doi.org/10.1016/j.palaeo.2009.11.031>
- Maddy, D., 1997. Uplift-driven valley incision and river terrace formation in southern England. *Journal of Quaternary Science* 12, 539–545. [https://doi.org/10.1002/\(SICI\)1099-1417\(199711/12\)12:6<539::AID-JQS350>3.0.CO;2-T](https://doi.org/10.1002/(SICI)1099-1417(199711/12)12:6<539::AID-JQS350>3.0.CO;2-T)
- Mériaux, A.-S., Tapponnier, P., Ryerson, F.J., Xiwei, X., King, G., Van der Woerd, J., Finkel, R.C., Haibing, L., Caffee, M.W., Zhiqin, X., Wenbin, C., 2005. The Aksay segment of the northern Altyn Tagh fault: Tectonic geomorphology, landscape evolution, and Holocene slip rate. *Journal of Geophysical Research: Solid Earth* 110, B04404. <https://doi.org/10.1029/2004JB003210>
- Merritts, D.J., Vincent, K.R., Wohl, E.E., 1994. Long river profiles, tectonism, and eustasy: A guide to interpreting fluvial terraces. *Journal of Geophysical Research: Solid Earth* 99, 14031–14050. <https://doi.org/10.1029/94JB00857>

- Molin, P., Fubelli, G., Nocentini, M., Sperini, S., Ignat, P., Grecu, F., Dramis, F., 2012. Interaction of mantle dynamics, crustal tectonics, and surface processes in the topography of the Romanian Carpathians: A geomorphological approach. *Global and Planetary Change* 90–91, 58–72. <https://doi.org/10.1016/j.gloplacha.2011.05.005>
- Molnar, P., Brown, E.T., Burchfiel, B.C., Deng, Q., Feng, X., Li, J., Raisbeck, G.M., Shi, J., Zhangming, W., Yiou, F., You, H., 1994. Quaternary climate change and the formation of river terraces across growing anticlines on the north flank of the Tien Shan, China. *The Journal of Geology* 102, 583–602.
- Pan, B., Burbank, D., Wang, Y., Wu, G., Li, J., Guan, Q., 2003. A 900 k.y. record of strath terrace formation during glacial-interglacial transitions in northwest China. *Geology* 31, 957–960. <https://doi.org/10.1130/G19685.1>
- Pan, B., Su, H., Hu, Z., Hu, X., Gao, H., Li, J., Kirby, E., 2009. Evaluating the role of climate and tectonics during non-steady incision of the Yellow River: evidence from a 1.24 Ma terrace record near Lanzhou, China. *Quaternary Science Reviews* 28, 3281–3290. <https://doi.org/10.1016/j.quascirev.2009.09.003>
- Pazzaglia, F.J., Brandon, M.T., 2001. A Fluvial Record of Long-term Steady-state Uplift and Erosion Across the Cascadia Forearc High, Western Washington State. *American Journal of Science* 301, 385–431. <https://doi.org/10.2475/ajs.301.4-5.385>
- Personius, S.F., 1995. Late Quaternary stream incision and uplift in the forearc of the Cascadia subduction zone, western Oregon. *Journal of Geophysical Research: Solid Earth* 100, 20193–20210. <https://doi.org/10.1029/95JB01684>
- Picotti, V., Pazzaglia, F.J., 2008. A new active tectonic model for the construction of the Northern Apennines mountain front near Bologna (Italy). *Journal of Geophysical Research: Solid Earth* 113, B08412. <https://doi.org/10.1029/2007JB005307>
- Prizomwala, S.P., Das, A., Chauhan, G., Solanki, T., Basavaiah, N., Bhatt, N., Thakkar, M.G., Rastogi, B.K., 2016. Late Pleistocene–Holocene uplift driven terrace formation and climate-tectonic interplay from a seismically active intraplate setting: An example from Kachchh, Western India. *Journal of Asian Earth Sciences* 124, 55–67. <https://doi.org/10.1016/j.jseaes.2016.04.013>
- Repka, J.L., Anderson, R.S., Finkel, R.C., 1997. Cosmogenic dating of fluvial terraces, Fremont River, Utah. *Earth and Planetary Science Letters* 152, 59–73. [https://doi.org/10.1016/S0012-821X\(97\)00149-0](https://doi.org/10.1016/S0012-821X(97)00149-0)
- Robinson, A.C., Owen, L.A., Chen, J., Schoenbohm, L.M., Hedrick, K.A., Blisniuk, K., Sharp, W.D., Imrecke, D.B., Li, W., Yuan, Z., Caffee, M.W., Mertz-Kraus, R., 2015. No late Quaternary strike-slip motion along the northern Karakoram fault. *Earth and Planetary Science Letters* 409, 290–298. <https://doi.org/10.1016/j.epsl.2014.11.011>
- Rockwell, T.K., Keller, E.A., Clark, M.N., Johnson, D.L., 1984. Chronology and rates of faulting of Ventura River terraces, California. *Geological Society of America Bulletin* 95, 1466–1474. [https://doi.org/10.1130/0016-7606\(1984\)95<1466:CAROFO>2.0.CO;2](https://doi.org/10.1130/0016-7606(1984)95<1466:CAROFO>2.0.CO;2)
- Ruszkiczay-Rüdiger, Z., Braucher, R., Novothny, Á., Csillag, G., Fodor, L., Molnár, G., Madarász, B., 2016. Tectonic and climatic control on terrace formation: Coupling in situ produced <sup>10</sup>Be depth profiles and luminescence approach, Danube River, Hungary, Central Europe. *Quaternary Science Reviews* 131, Part A, 127–147. <https://doi.org/10.1016/j.quascirev.2015.10.041>
- Schanz, S.A., Montgomery, D.R., 2016. Lithologic controls on valley width and strath terrace formation. *Geomorphology* 258, 58–68. <https://doi.org/10.1016/j.geomorph.2016.01.015>

- Schildgen, T.F., Cosentino, D., Bookhagen, B., Niedermann, S., Yıldırım, C., Echtler, H., Wittmann, H., Strecker, M.R., 2012. Multi-phased uplift of the southern margin of the Central Anatolian plateau, Turkey: A record of tectonic and upper mantle processes. *Earth and Planetary Science Letters* 317–318, 85–95. <https://doi.org/10.1016/j.epsl.2011.12.003>
- Seong, Y.B., Larson, P.H., Dorn, R.I., Yu, B.Y., 2016. Evaluating process domains in small arid granitic watersheds: Case study of Pima Wash, South Mountains, Sonoran Desert, USA. *Geomorphology* 255, 108–124. <https://doi.org/10.1016/j.geomorph.2015.12.014>
- Simoës, M., Avouac, J.P., Chen, Y.-G., 2007. Slip rates on the Chelungpu and Chushiang thrust faults inferred from a deformed strath terrace along the Dungpuna river, west central Taiwan. *Journal of Geophysical Research: Solid Earth* 112, B03S10. <https://doi.org/10.1029/2005JB004200>
- Stock, J.D., Montgomery, D.R., Collins, B.D., Dietrich, W.E., Sklar, L., 2005. Field measurements of incision rates following bedrock exposure: Implications for process controls on the long profiles of valleys cut by rivers and debris flows. *Geological Society of America Bulletin* 117, 174–194. <https://doi.org/10.1130/B25560.1>
- Tyráček, J., Westaway, R., Bridgland, D., 2004. River terraces of the Vltava and Labe (Elbe) system, Czech Republic, and their implications for the uplift history of the Bohemian Massif. *Proceedings of the Geologists' Association* 115, 101–124. [https://doi.org/10.1016/S0016-7878\(04\)80022-1](https://doi.org/10.1016/S0016-7878(04)80022-1)
- Van der Woerd, J., Ryerson, F.J., Tapponnier, P., Gaudemer, Y., Finkel, R., Meriaux, A.S., Caffee, M., Guoguang, Z., Qunlu, H., 1998. Holocene left-slip rate determined by cosmogenic surface dating on the Xidatan segment of the Kunlun fault (Qinghai, China). *Geology* 26, 695–698. [https://doi.org/10.1130/0091-7613\(1998\)026<0695:HLSRDB>2.3.CO;2](https://doi.org/10.1130/0091-7613(1998)026<0695:HLSRDB>2.3.CO;2)
- Van der Woerd, J., Xu, X., Li, H., Tapponnier, P., Meyer, B., Ryerson, F.J., Meriaux, A.-S., Xu, Z., 2001. Rapid active thrusting along the northwestern range front of the Tanghe Nan Shan (western Gansu, China). *Journal of Geophysical Research: Solid Earth* 106, 30475–30504. <https://doi.org/10.1029/2001JB000583>
- Vassallo, R., Mugnier, J.-L., Vignon, V., Malik, M.A., Jayangondaperumal, R., Srivastava, P., Jouanne, F., Carcaillet, J., 2015. Distribution of the Late-Quaternary deformation in Northwestern Himalaya. *Earth and Planetary Science Letters* 411, 241–252. <https://doi.org/10.1016/j.epsl.2014.11.030>
- Vassallo, R., Ritz, J.-F., Braucher, R., Jolivet, M., Carretier, S., Larroque, C., Chauvet, A., Sue, C., Todbileg, M., Bourlès, D., Arzhannikova, A., Arzhannikov, S., 2007. Transpressional tectonics and stream terraces of the Gobi-Altay, Mongolia. *Tectonics* 26, TC5013. <https://doi.org/10.1029/2006TC002081>
- Vignon, V., Mugnier, J.-L., Vassallo, R., Srivastava, P., Malik, M.A., Jayangondaperumal, R., Jouanne, F., Buoncristiani, J.F., Carcaillet, J., Replumaz, A., Jomard, H., 2017. Sedimentation close to the active Medlicott Wadia Thrust (Western Himalaya): How to estimate climatic base level changes and tectonics. *Geomorphology* 284, 175–190. <https://doi.org/10.1016/j.geomorph.2016.07.040>
- von Suchodoletz, H., Menz, M., Kühn, P., Sukhishvili, L., Faust, D., 2015. Fluvial sediments of the Algeti River in southeastern Georgia — An archive of Late Quaternary landscape activity and stability in the Transcaucasian region. *CATENA, Past Hydrological Extreme Events in a Changing Climate* 130, 95–107. <https://doi.org/10.1016/j.catena.2014.06.019>

- Wang, X., Vandenberghe, J., Yi, S., Van Balen, R., Lu, H., 2015. Climate-dependent fluvial architecture and processes on a suborbital timescale in areas of rapid tectonic uplift: An example from the NE Tibetan Plateau. *Global and Planetary Change* 133, 318–329. <https://doi.org/10.1016/j.gloplacha.2015.09.009>
- Wegmann, K.W., Pazzaglia, F.J., 2009. Late Quaternary fluvial terraces of the Romagna and Marche Apennines, Italy: Climatic, lithologic, and tectonic controls on terrace genesis in an active orogen. *Quaternary Science Reviews* 28, 137–165. <https://doi.org/10.1016/j.quascirev.2008.10.006>
- Wegmann, K.W., Pazzaglia, F.J., 2002. Holocene strath terraces, climate change, and active tectonics: The Clearwater River basin, Olympic Peninsula, Washington State. *Geological Society of America Bulletin* 114, 731–744. [https://doi.org/10.1130/0016-7606\(2002\)114<0731:HSTCCA>2.0.CO;2](https://doi.org/10.1130/0016-7606(2002)114<0731:HSTCCA>2.0.CO;2)
- Wesnousky, S.G., Kumar, S., Mohindra, R., Thakur, V.C., 1999. Uplift and convergence along the Himalayan Frontal Thrust of India. *Tectonics* 18, 967–976. <https://doi.org/10.1029/1999TC900026>
- Yanites, B.J., Tucker, G.E., Mueller, K.J., Chen, Y.-G., Wilcox, T., Huang, S.-Y., Shi, K.-W., 2010. Incision and channel morphology across active structures along the Peikang River, central Taiwan: Implications for the importance of channel width. *Geological Society of America Bulletin* 122, 1192–1208. <https://doi.org/10.1130/B30035.1>

## APPENDIX B

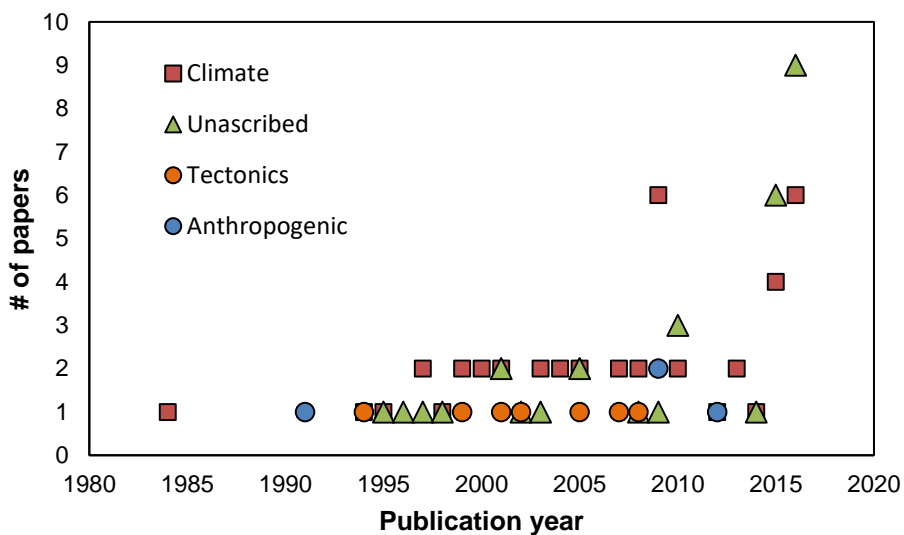


Figure B1. Frequency of each terrace forcing from Chapter 3 is compared against the publications year of the original study. Volcanic forcings are not included because the terraces in our database come from one study published in 2015. Although climate and tectonics are often thought of as the dominant cause of terrace formation, the second oldest study in the database considered anthropogenic forcings, indicating there is not a strong bias towards climate and tectonics with time.

# CURRICULUM VITAE

## SARAH SCHANZ

Department of Earth and Space Sciences  
University of Washington  
4000 15<sup>th</sup> Ave NE, Box 351310  
Seattle, WA 98195  
Phone: 360-304-8665  
E-mail: [schanzs@uw.edu](mailto:schanzs@uw.edu)  
[www.sarahschanz.wix.com/home](http://www.sarahschanz.wix.com/home)

### EDUCATION

- 2018 PhD Earth & Space Sciences, University of Washington  
Thesis advisor: Dave Montgomery: Strath terrace formation: the influence of climate, rock type, and humans.
- 2011 B.S. Geology, Western Washington University  
*Magna cum laude* with University Honors

### PROFESSIONAL EXPERIENCE

- 2018-2019 Postdoctoral Researcher, Department of Earth and Atmospheric Sciences, Indiana University Bloomington. Supervisor: Brian Yanites
- 2017 Lecturer, School of Natural Sciences, California State University Monterey Bay
- 2012-2018 Teaching and Research Assistant, Department of Earth and Space Sciences, University of Washington
- 2012 NAGT Intern and Hydrologist, Oregon Water Science Center, US Geological Survey
- 2008-2011 Engineering Assistant, Lewis County Public Works

### PUBLICATIONS

- Schanz, SA**, Montgomery, DR, Collins, BD, Duvall, A.R., 2018. Multiple paths to straths: A review and reassessment of terrace genesis. *Geomorphology* 312, 12–23.  
<https://doi.org/10.1016/j.geomorph.2018.03.028> \*invited review
- Schanz, SA**, Montgomery, DR, 2016. Lithologic controls on valley width and strath terrace formation. *Geomorphology*, 258, 58-68. Doi:10.1016/j.geomorph.2016.01.015
- Collins, B.D., Montgomery, D.R., **Schanz, S.A.**, Larsen, I.J., 2016. Rates and mechanisms of bedrock incision and strath terrace formation in a forested catchment, Cascade Range, Washington. *Geological Society of America Bulletin*, pp B31340-1. doi:10.1130/B31340.1

### TEACHING

#### Instructor

*California State University Monterey Bay*

GEOL 360: Geomorphic Systems, Fall 2017.

*University of Washington*

ESS 230: Rivers & Beaches, Fall 2015. Co-taught with Chuck Nittrouer.



ESS 400a: Field Geology, Summer 2014. Taught the fluvial geomorphology & neotectonics module.

### **Teaching assistant**

#### ***University of Washington***

ESS 101: Introduction to Geology; ESS 106: Volcanoes; ESS 211: Physical Processes of the Earth; ESS 301: Geology of the Pacific Northwest; ESS 326: Introduction to Geomorphology; ESS400a&b: Field Geology; ESS 418: Geoscience Communication; ESS 426: Fluvial Geomorphology

#### ***Western Washington University***

GEO 101: Introduction to Geology; GEO 210: Physical Geology

### **GRANTS**

NSF Doctoral Dissertation Improvement Award “Investigating the Influence of Deforestation on River Incision and Landscape Change” for \$15,913. Co-PI with Dave Montgomery. One of four proposals ranked “High Priority” of a total of 96 proposals. Aug 2016-Aug 2018.

Quaternary Research Center, University of Washington grant “River incision driven by changes to woody debris and sediment retention” for \$6,980. June 2016-Sept 2017.

Geological Society of America Student Research Grant “Strath terrace formation through changes in sediment retention in the Pacific Northwest” for \$1674. April 2015-2016.

Geological Society of America Student Research Grant “Rock strength controls on strath terrace formation and preservation” for \$1500. April 2014-2015.

### **AWARDS**

- 2017 Joseph A Vance Endowed Fellowship, University of Washington
- 2016 Joseph A Vance Endowed Fellowship, University of Washington  
Jody Bourgeois Graduate Support Fund, University of Washington
- 2015 Howard Coombs Fellowship for Teaching Excellence, University of Washington  
George Edward Goodspeed Geology Scholarship, University of Washington  
Marie Morisawa Award in Geomorphology, Quaternary Geology & Geomorphology Division, GSA  
Best Oral Presentation, ESS Research Gala, University of Washington
- 2014 Exxon Mobile and Peter Misch Fellowship Awards, University of Washington
- 2013 Dorothy G Stephens Graduate Fellowship Award, University of Washington
- 2012 Top Scholar Award, University of Washington
- 2011 Field Scholarship, National Association of Geoscience Teachers  
Scholarship, Mt Baker Rock and Gem Club  
Scholarship, Skagit Rock and Gem Club  
Dennis Rahm Award in Geomorphology, Western Washington University
- 2008 National Merit Scholar

### **PROFESSIONAL SERVICE**

#### **Peer Review**

2017 to present Ad-hoc reviewer for National Science Foundation EAR Postdoctoral Fellowship program

2017 to present Journal peer reviewer for Earth Surface Processes & Landforms, Geology

### **University of Washington**

2015-2017 Graduate peer mentor

2014-2016 Graduate student representative to faculty

2013-2015 Graduate seminar series organizer

2013-2015 Graduate student representative to MESSAGE exams

2013 ESS Open House organizer

### **Outreach**

2013-present Volunteer with UW Rockin' Out

2013-2016 Workshop leader at Seattle Expanding Your Horizons

2010, 2013 Volunteer at the Chehalis Basin Student Congress. Taught middle and elementary school students about riparian zones, macroinvertebrates, and water quality.

### **PROFESSIONAL DEVELOPMENT & WORKSHOPS**

2018 Raising Awareness in the STEM Community, WA Space Grant, University of Washington

2018 Strategies for Cultivating Inclusion in STEM, University of Washington

2017 Science communication workshop, College of the Environment, University of Washington

2016 Preparing for an Academic Career, National Association of Geoscience Teachers

2015 Summer School on Geomorphology, Kaunertal Valley, Austria

### **PROFESSIONAL MEMBERSHIPS**

American Geophysical Union, 2013-present

Geological Society of America, 2014-present

National Association of Geoscience Teachers, 2016-present

Association of American Geographers, 2016-present

### **INVITED TALKS**

2016 Oregon Water Science Center, Portland, OR

### **PRESENTATIONS**

**Schanz, SA**, Montgomery, DR, and Collins, BD, 2018. "River incision along the Middle and West Fork Teanaway Rivers, central Cascade Mountains, caused by wood loss and decreased sediment retention" 2018 ESS Research Gala

**Schanz, SA**, Montgomery, DR, Collins, BD, and Duvall, AR, 2017 "River incision and terrace formation caused by reduced sediment retention and deforestation in the Pacific Northwest, USA." Oral presentation at the 2017 American Geophysical Union Fall Meeting

**Schanz, SA**, Montgomery, DR, Collins, BD, and Duvall, AR, 2017 "Multiple paths to climatic straths: how local conditions and dating methods obscure terrace correlation with climate cycles." Poster presentation at the 2017 Geological Society of America Annual Meeting

**Schanz, SA**, Montgomery, DR, Collins, BD, and Duvall, AR, 2017 "Multiple paths to straths: re-examing strath terrace genesis." Oral presentation at 2017 ESS Research Gala

- Schanz, SA**, Montgomery, DR, Collins, BD, and Duvall, AR, 2016 “Examining alternative hypotheses for Holocene strath terrace formation: the role of sediment retention and woody debris.” Oral presentation at 2016 Geological Society of America Annual Meeting
- Schanz, SA**, Montgomery, DR, Collins, BD, and Duvall, AR, 2016 “Modeling the effects of in-stream sediment retention on rates of river incision and strath terrace formation.” Poster presentation at 2016 Community Surface Dynamics Modeling System (CSDMS) Annual Meeting
- Schanz, SA**, 2016. “Investigating the effect of temporally and spatially variable sediment retention on river incision through numerical modeling.” Oral presentation at the 2016 ESS Research Gala
- Schanz, SA**, Montgomery, DR, Collins, BD, and Duvall, AR, 2015 “River incision and strath terrace formation as a result of shifts in sediment retention.” Poster presentation at 2015 Geological Society of America Annual Meeting
- Schanz, SA** and Montgomery, DR, 2015 “Lithologic controls on valley width and strath terrace formation” Oral presentation at 2015 ESS Research Gala
- Schanz, SA**, 2014 “Strath terrace formation through internal forcing, WF Teanaway River, WA” Oral presentation at 2014 ESS Research Gala
- Schanz, SA** and Montgomery, DR, 2013 “Influence of bedrock lithology on strath terrace formation in the Willapa River watershed, SW Washington, USA” Oral presentation at the 2013 Fall AGU Meeting